DESIGN AND DEVELOPMENT
OF A MULTIFIBER SHIELDED LASER CATHETER SYSTEM
FOR REMOVAL OF ATHEROSCLEROTIC PLAQUE

by
Robert M. Cothren, Jr.

S.B., Massachusetts Institute of Technology
(1981)
M.S., Massachusetts Institute of Technology
(1984)

Submitted in Partial Fulfillment
of the Requirements of the
Degree of

Doctor of Philosophy
in Medical Engineering

at the

Massachusetts Institute of Technology
June, 1987

Signature of Author _____
Division of Health Sciences and Technology
June, 1987

Certified by _____
Michael S. Feld
Thesis Supervisor

Accepted by _____
Roger G. Mark
Co-Director; Division of Health Sciences and Technology

DESIGN AND DEVELOPMENT
OF A MULTIFIBER SHIELDED LASER CATHETER SYSTEM
FOR REMOVAL OF ATHEROSCLEROTIC PLAQUE

by

Robert M. Cothren, Jr.

Submitted to
the Division of Health Sciences and Technology
in June, 1987,
in partial fulfillment of the requirements of the
Degree of Doctor of Philosophy
in Medical Engineering

ABSTRACT

A multifiber laser angiosurgery system was developed which is capable of controlled laser ablation of arterial obstructions in vivo. Development of the system can be broken down into a few important steps.

A laser light delivery scheme employing an optical fiber enclosed in a transparent optical shield was developed to allow for the controlled delivery of laser energy. Characterization of this delivery scheme using argon ion laser light showed that quantitatively predictable tissue ablation could be achieved. Ablation proceeded at a constant rate, with the depth of the ablated crater increasing linearly with time. The crater diameter approached the incident laser spot diameter for sufficiently long exposure times. The ablation

process was also shown to be additive if multiple exposures were used, that is, each successive exposure produced an increase in the crater depth equal to the exposure preceeding it.

This delivery scheme was then extended to a multifiber shielded laser angiosurgery catheter system, which was designed to be capable of controlled laser ablation of arterial obstructions. That system consisted of a multifiber shielded catheter employing the controlled delivery scheme of the transparent optical shield, an optical system which allowed for remote location of the laser source and careful shaping of the catheter's output beam profile, and a sophisticated computer based control system to operate and monitor the ablation process.

Characterization of that system demonstrated that, as before, ablation proceeds at a constant rate, with the depth of the ablated composite hole increasing linearly with time, and, as before, the ablation process was additive if multiple exposures are used. An ablation yield, the volume of tissue removed per unit of energy delivered, was defined, and found to be constant at a value of $0.16mm^3/J$ for many different laser exposure parameter combinations. A threshold laser power of 1W was identified, a minimum power required to overcome the loss of energy through thermal diffusion. A threshold exposure time of 10ms was also identified, corresponding to a minimum energy that must be delivered to raise the tissue's temperature to the ablation temperature and deposit the latent heat of ablation. Histological evaluation of the peripheral damage imposed by laser ablation showed that a layer of 100-200um of vacuolization and hypereosinophilia surrounded each composite hole, a level of damage that should be acceptable.

The successful use of the laser angiosurgery system using the multifiber shielded catheter was also demonstrated in an animal model. Both controlled recanalization of the obstructed artery and evidence of proper healing of the treated site were shown.

A simple theoretical model for laser ablation is also presented which describes the way in which different laser and tissue parameters effect the ablation process. The ablation velocity and ablation efficiency predicted by this model were

in good agreement with results of multifiber device experiments.

Thesis Advisor: Michael S. Feld

Professor of Physics
Director, MIT Spectroscopy Laboratory

ACKNOWLEDGEMENTS

To Professor Michael Feld, advisor and friend, whose support and guidance were instrumental in the successful completion of this work. Throughout my graduate career, he both taught me as a student and listened to me as colleague.

To Dr. John Kramer, cardiologist at the Cleveland Clinic Foundation, whose advise constantly help direct both this work in particular and the Laser Angiosurgery Project in general.

To Carter Kittrell, who was always willing and anxious to assist when things were not working and explain the sometimes puzzling operations of modern optics and detection systems.

To pathologist Dr. Burr Ratliff and surgeons Dr. Floyd Loop and Dr. Bruce Lytle of the Cleveland Clinic Foundation, whose professional advice was freely given and always welcome.

To Gary Hayes, who has, without complaint, been ever willing to build any and every permutation of catheter I could dream up. Without his steady hand, open mind, and desire for perfection, this project would not be where it is today.

To all of the students and colleagues of the MIT Laser Angiosurgery Group, who over the years have made the MIT Spectroscopy Lab an interesting and fun place to be. They provided a constant source of minds with which to share ideas and discuss problems, and friends with which to share good times.

To Carol, Kim, and Sue, who were willing to put up with the constant presence of a graduate student keeping them from thier work with conversation and administrative details.

To my parents, who have supported me throughout my schooling. It was their guidance, support, and love that have kept me going through my entire life at school.

But most importantly, to my wife Daphne, who saw me through many hard times, long days, and sleepless nights. Her patience and love, her understanding and willingness to sacrifice, have made it possible to complete my career at MIT with some spirit, joy, and sanity.

This work was part of an ongoing Laser Angiosurgery Project, a collaboration between the MIT Spectroscopy Laboratory, the Cleveland Clinic Foundation, and American Hospital Supply Corporation.

TABLE OF CONTENTS

LIST OF FIGURES

LIST OF TABLES

SECTION I

INTRODUCTION

I.1 ATHEROSCLEROTIC DISEASE

Arteriosclerosis is the name given to a group of diseases generally characterized by a thickening of the arterial wall and a loss of the wall's elasticity [1]. Of the three major forms of arteriosclerosis, the most common is atherosclerosis [1,2].

Atherosclerosis is a degenerative disease of the large- and medium-sized arteries in which atheromas containing cholesterol, lipoid and fibrous material, cellular debris, and calcium are formed within the intima and inner media [1]. A number of risk factors such as hypercholesterolemia, hypertension, smoking, diabetes, obesity, age, and lack of physical activity have been correlated with the development of atheromatous plaque, though a cause and effect relationship has not been clearly established [1,3,4].

Although the pathogenesis of atherosclerosis has been the subject of intense investigation for many years, the exact steps leading to the formation of atheromatous lesions is still not clear. It is generally thought to be a complex combination of two mechanisms: intimal injury and increased uptake of lipid by the artery wall. Figure I.1 diagrams schematically the steps that may be involved as these two mechanisms proceed. High concentrations of low density lipoproteins (LDL) induce endothelial injury and the adherence and aggregation of platelets; platelet aggregation is prompted further by the injury itself. The endothelial injury, along with hyperlipoproteinemia, leads to an increased rate of LDL penetration into the subendothelial space. Both the increased concentration of LDL in the arterial wall and factors released by the platelets are probably responsible for the stimulation of smooth muscle cell proliferation and the entrapment of LDL in the extracellular fibrous matrix which secreted by them. The continual reiteration of this process eventually gives rise to a space filling atheroma made up of a fibrous region of proliferated smooth muscle cells, collagen, and lipoid material and, eventually, a necrotic center of cellular debris, cholesterol crystals and cholesterol esters, and calcium deposits (see Figure I.2 and Figure I.3) [1,5-9].

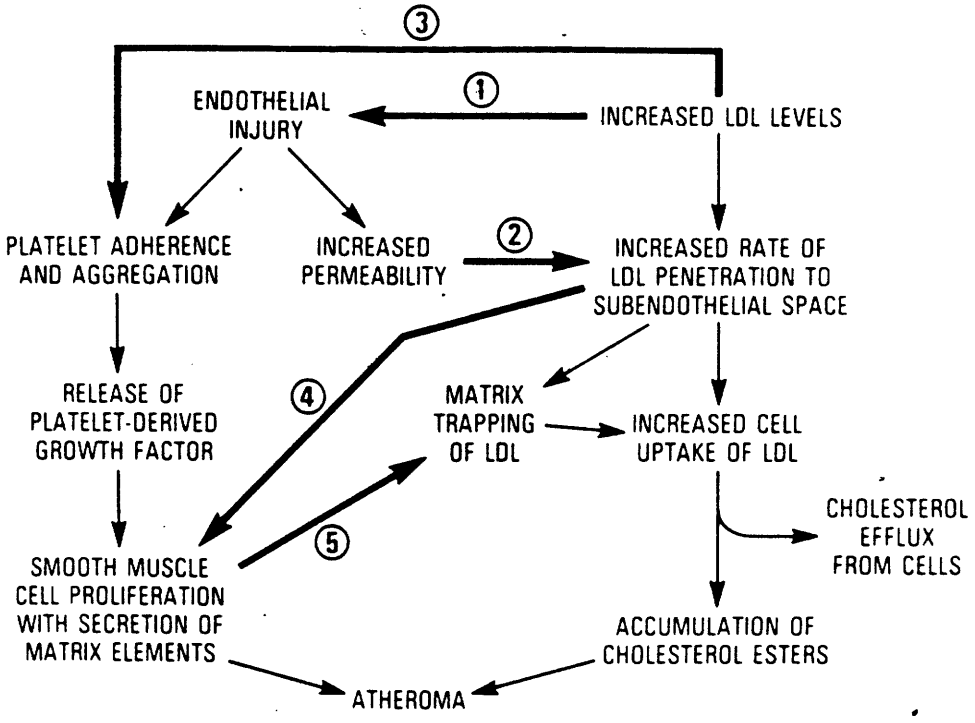

Figure I.1

Schematic diagram of the probable interactions between the two major pathogenic mechanisms of atherogenesis [6].

The process of atheroma formation begins early in life with the appearance of fatty streaks in the intimal lining of the arteries. The disease does not become clinically significant however until at least 75% of the diameter of the vessel's original lumen has been filled by the developing plaque. At this point, blood flow becomes seriously compromised. The disease most commonly manifests itself as ischemic pain (i.e., angina or claudication) resulting from

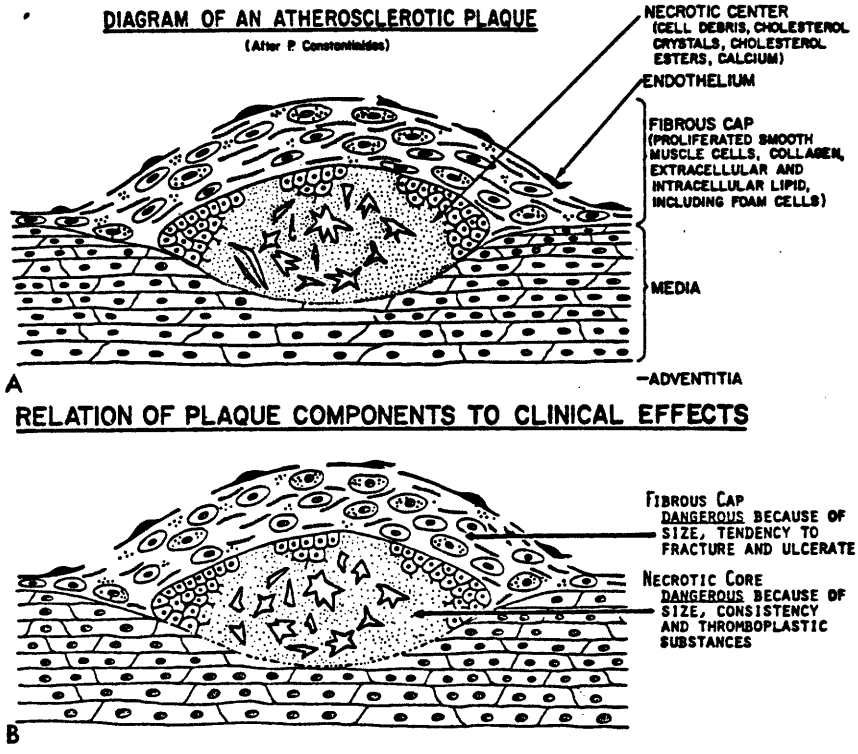

Figure I.2

Major components of the advanced atherosclerotic plaque [1].

inadequate delivery of oxygen, aneurysm formation due to deterioration of the artery, and stroke, heart attack, or infarct of some other tissue due to complete interruption of blood flow (see Figure I.4) [1,10].

Nearly one million Americans die each year as a direct result of cardiovascular disease, making it the cause of almost half of all deaths in this country. Nearly five million Americans are estimated to have significant coronary heart

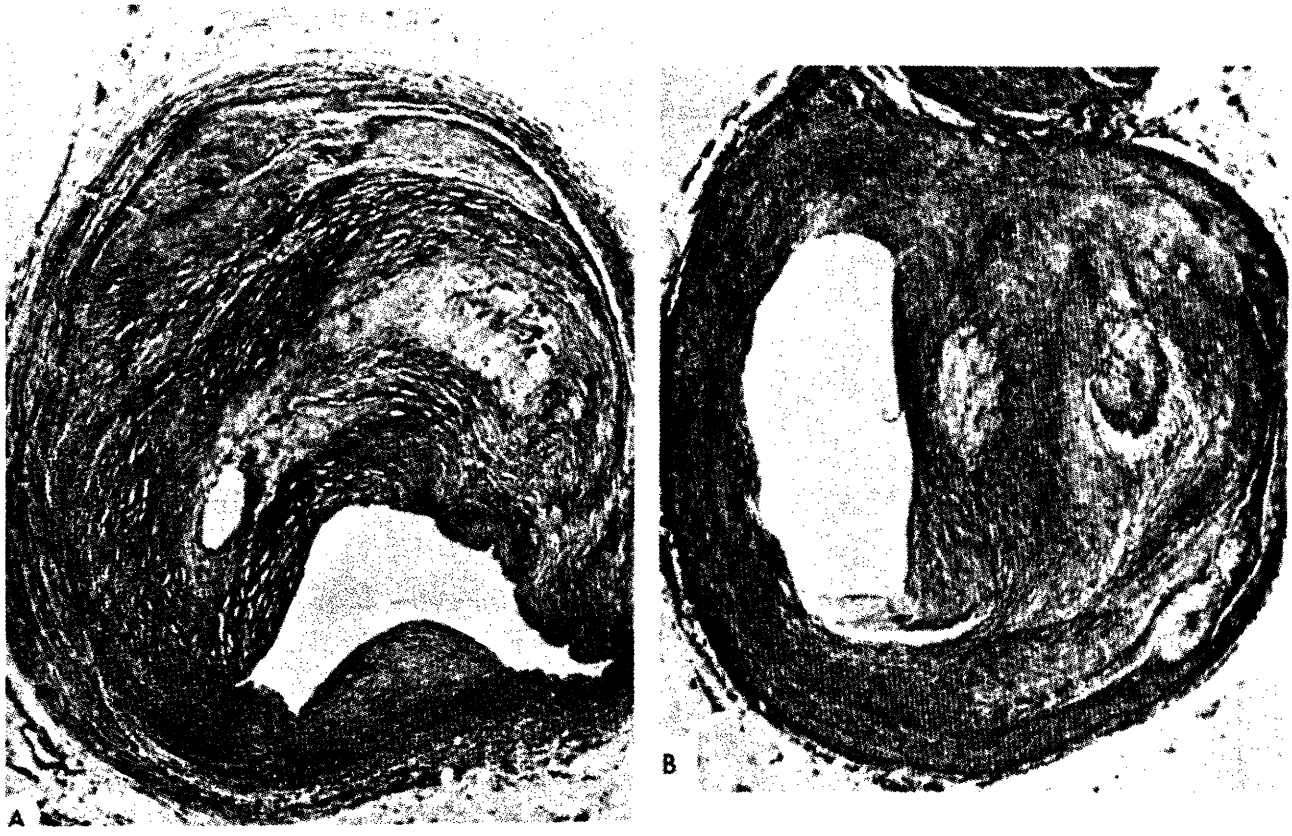

Figure I.3

Histological sections of advanced atherosclerotic plaques in the coronary arteries of two people. Note the principal components of fibrous cap and necrotic core in each [1].

disease, with another two million suffering from strokes, both largely due to atherosclerotic disease [2].

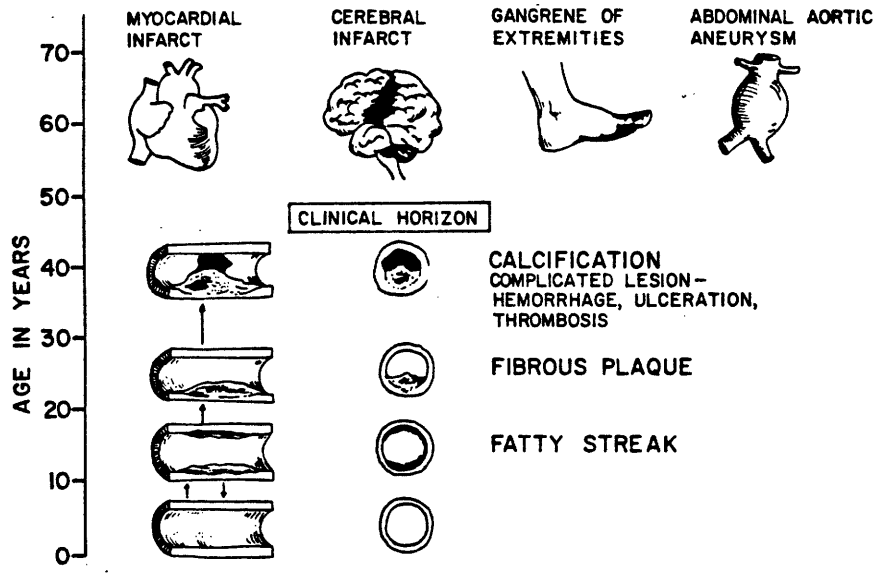

Figure I.4

The natural history of atherosclerosis [1].

I.2 TREATMENT MODALITIES FOR ATHEROSCLEROTIC DISEASE

There are two major corrective treatments for occlusive atherosclerotic lesions in popular use today: surgical bypass and balloon angioplasty. Both of these modalities are designed to restore full blood flow in the artery distal to the obstructive lesion and return perfusion to the target tissue. Although both modalities have enjoyed increasing success over the last several years, each has some serious drawbacks.

I.2.1 Arterial Bypass Surgery

The specifics of the bypass technique vary with the location and size of the diseased artery. In most cases, a segment of vein or artery from elsewhere in the patient's body is grafted to the diseased artery around the site of stenosis to provide an alternate path for blood flow. Over 200,000 coronary bypass operations are performed annually in the United States alone [2]. Success of this technique is very good, with a national operative mortality rate of only 2.3%. Bypass grafts usually provide adequate flow for seven to ten years without complication or obstruction of the graft [1]. When the graft does fail, usually due to plaque formation in the graft, the procedure can often be repeated once.

However, like any surgical technique, arterial bypass has disadvantages. The surgery is very traumatic to the patient. It is expensive; coronary artery bypass usually costs $16,000 or more, with a required hospital stay of seven to ten days. Not all patients are good candidates for bypass surgery. If atheromas are located diffusely throughout the vessel, a significant increase in blood flow may not be realized. Some vessels may be too small to make bypass feasible [1]. Because most grafts occlude in several years and the procedure can

normally only be repeated once, bypass surgery is usually reserved for older patients.

I.2.2 Balloon Angioplasty

A more recently developed alternative is percutaneous transluminal balloon angioplasty. In this technique, a catheter with a small balloon at its distal end is inserted in a peripheral artery and advanced to the point of occlusion. The balloon is placed across the lesion where it is inflated with several atmospheres of pressure. The artery wall and plaque are fractured and displaced, leaving an enlarged lumen.

Because only a small incision is made in the skin, angioplasty is much less traumatic to the patient, less expensive, and requires only a few days of hospitalization. It can also be repeated as many times as is required, making it the procedure of choice for young patients not responding to medical management. The procedure is relatively safe, requiring emergency bypass surgery in about 6% of patients, and with a national mortality rate of less than 1% [1].

However, balloon angioplasty can not be performed in all situations. It is usually used only for single vessel disease (approximately 80% of cases). It cannot be used if the remaining arterial lumen is too small to pass the catheter and

deflated balloon. It can seldom be used near a point of bifurcation where it might crush the branching vessel. Long or diffuse lesions can be treated with only limited success. Perhaps the biggest drawback of balloon angioplasty however is the recurrence of stenosis. From 15% to 20% of lesions treated by balloon angioplasty reocclude to a point requiring repeat treatment within six months, and nearly 60% reocclude within two years [1].

I.3 LASER ANGIOPLASTY

Removal of atheromatous obstructions by ablation using laser energy (so called laser angioplasty) has received a great deal of interest from researchers as an alternative to bypass surgery and balloon angioplasty. Conceptually, laser ablation of atheromas has advantages over both of these techniques. Since optical fibers can be used to carry laser energy to the lesion, percutaneous techniques can be employed making the trauma and cost imposed by surgery unnecessary. It is hoped that removing the obstructive lesion by ablation, rather than merely displacing it with a balloon, will produce a good clinical result without the high restenosis rate which plagues balloon angioplasty. Laser ablation may also be

applicable as a treatment for long or diffuse lesions, and lesions at arterial bifurcations.

Many researchers have demonstrated that many types of tissue, including arterial tissue and atheromatous plaques, can be ablated using laser light [11-13]. Further, Gerrity studied the long term effects of laser ablation of atheromatous tissue in a porcine model in which atherosclerotic lesions were produced by a combination of hypercholesterolemic diet and balloon deendothelialization of the abdominal aorta. Complete intimal healing with reendothelialization was found within two weeks after laser ablation of lesions [14].

I.4 CURRENT APPROACHES TO LASER ANGIOPLASTY

Experimental use of lasers in the vascular system was first reported in the early 1980's. Although research is being conducted at a large number of centers, laser delivery systems designed for use in the vascular system have remained relatively simple and unsophisticated.

I.4.1 Laser Systems

The wide variety of lasers being investigated for ablation of atheromatous plaque can be broadly divided into two

groups, continuous wave (CW) lasers and pulsed lasers, and subdivided by wavelength.

Continuous lasers are characterized by the delivery of up to hundreds or even thousands of watts of continuous power over a broad range of the spectrum. The ablation mechanism of these lasers is most likely to be thermal in nature, brought on by the heating of absorbing material in the tissue and vaporization of the tissue's water. The rapid generation of steam carries away tissue components, which may be further pyrolyzed by the incoming laser light. The three continuous lasers attracting the most attention are neodimium:YAG (Nd:YAG), carbon dioxide (CO_2), and argon ion.

Nd:YAG lasers have proven their usefulness in photocoagulation therapy such as the treatment of ulcers of the stomach, esophagus, and colon, and have further been used in arterial and nervous anastomosis [15]. However, the property that makes this laser well suited for photocoagulation makes it poorly suited for ablation. Nd:YAG radiation at 1.06um or 1.32um is weakly absorbed by most biological tissues [16]. Large zones of moderate tissue heating are easily obtainable, but heating may not be intense enough for clean ablation. Craters produced in arterial tissue with continuous Nd:YAG

lasers are normally surrounded by large zones of thermal necrosis [17].

The 10.6um radiation from CO_2 lasers is strongly absorbed by tissue water and thus penetrates only a few microns into the tissue [18]. This property has made the CO_2 laser a very popular choice for surgical applications, where clean cuts and rapid healing in many types of tissue, including atherosclerotic models in swine, have been demonstrated [14]. However, optical fibers which transmit 10.6um are not commercially available, preventing the use of CO_2 radiation percutaneously.

Argon lasers fill a middle ground between Nd:YAG and CO_2. The 488nm and 514nm radiation from the argon ion laser is absorbed in about 1/3mm of tissue [16], making it capable of removing tissue without extensive thermal damage if the laser intensity and exposure duration are carefully controlled. The visible wavelengths of this laser are readily transmitted by commercial optical fibers used in the communications industry. However, argon ion laser radiation has proved ineffectual in removing calcified plaque [19-21]. The use of the alternate argon ion 356nm radiation may increase that laser's suitability for tissue ablation because of the increased tissue absorption of ultraviolet wavelengths.

Pulsed lasers are characterized by the delivery of short bursts of light with very high peak power, typically in the range of megawatts for a fraction of a microsecond. The ablation mechanism of these lasers is not well understood, but postulated mechanisms range from thermal to photochemical processes, with or without the formation of plasmas. A number of pulsed laser systems, including excimer, pulsed Nd:YAG, pulsed dye, and, to a lesser extent, pulsed CO_2 have been used to create very clean craters in tissues of all types, including calcified atherosclerotic plaque, kidney stones, and even bone [19-21]. Recent studies have shown that erbium:YAG (Er:YAG) and hydrogen fluoride (HF) lasers can produce similar results [22,23]. However, the very high peak powers generated by all of these lasers makes transmission through optical fibers difficult even at visible wavelengths.

laser system	laser type	wavelength	tissue absorber	fiber optics
excimer	UV/pulsed	193nm	protein	no
	UV/pulsed	248nm	protein	difficult
	UV/pulsed	308nm	protein	difficult
	UV/pulsed	351nm	protein	difficult
argon	VIS/CW	488-514nm	*	yes
Nd:YAG	VIS/pulsed	532nm	*	difficult
	IR/pulsed	1064nm	*	difficult
	IR/CW	1.06um	*	yes
CO_2	IR/pulsed	10.4um	water	future
	IR/CW	10.4um	water	future
Nd:YAG	UV/pulsed	355nm	protein	difficult
	IR/CW	1.32um	*	yes
argon	UV/CW	351-364nm	protein	yes
pulsed dye	pulsed	UV-IR	*	difficult
Er:YAG	IR/pulsed	2.9um	water	future
HF	IR/pulsed	2.6-3.1um	water	future
	IR/CW	2.6-3.1um	water	future

Table I.1

Lasers systems currently being explored for ablation of atheromas. Wavelengths range from well into the ultraviolet to well in the infrared. Probable tissue absorbers and the availability of optical fibers are noted.
* Tissue absorbs only weakly at these wavelengths. The specific absorber in the tissue is largely unknown.

I.4.2 Laser Delivery Techniques

A number of schemes have been proposed to deliver laser energy to a lesion in the vascular system. The common use of optical fibers to carry the laser radiation in all of these schemes has largely limited laser ablation systems to continuous visible or near infrared laser radiation. The argon ion laser has largely been the laser of choice.

The earliest delivery systems consisted of a single optical fiber passed through the lumen of a catheter. Others also incorporated a coherent fiber bundle for visualization of the arterial lesion during ablation.

The first successful attempt to recanalize occluded peripheral arteries was performed in 1982 using a device of this type [24]. An argon ion laser was used to treat a thrombus produced in the ligated vessel of a dog. Histological examination showed that initial intimal necrosis was followed by complete intimal healing after five days with no post-treatment thrombus formation. Successful recanalization of human atherosclerotic arteries, which were grafted into the circulation of a dog, has also been demonstrated with a similar device [25]. Nd:YAG lasers have been used to remove model lesions produced in rabbits through the combined use of a hypercholesterolemic diet and deendothelialization with

limited success [26-28]. Unfortunately, results have been plagued by complications due to aneurysm formation and/or arterial perforation.

The first reports of clinical use of laser ablation of atheroma was published in 1984, again using this simple delivery scheme [29]. In five patients undergoing coronary bypass surgery, an argon ion laser was used to recanalize coronary stenoses of 80-90%. Recanalization was initially successful in three of the five cases. Since that time, a number of researchers have reported successful recanalization of femoral arteries and popliteal arteries, using the argon ion laser or the Nd:YAG laser delivered through simple fiber optic systems [30-33]. However, control of the laser light was a consistent problem, and balloon angioplasty was often used after laser treatment, greatly clouding the results of these studies.

In 1985, a different type of delivery scheme was introduced in which the optical fiber was capped with a metal tip which absorbed all of the laser radiation. The laser was simply used to deliver power to heat this, tip which in turn heated the tissue to "melt" or "vaporize" the tissue it contacted.

This technique has been shown to reduce stenotic model lesions induced in rabbits by the use of hypercholesterolemia and deendothelialization [28]. Recently, the first reports of clinical use of this device in a technique termed "laser-assisted angioplasty" were published [34,35]. Eight patients were treated to reduce stenosis of coronary arteries, with one perforation and one acute thrombosis, along with two cases of acute myocardial infarction. The use of "laser-assisted angioplasty" has continued in the treatment of peripheral arteries in a series of 56 patients [36]. Successful treatment was demonstrated in femoral, popliteal, and iliac arteries with only one perforation and two acute occlusions due to thrombosis. However, all successful uses of the metal tip delivery scheme have incorporated the use of balloon angioplasty following treatment with the laser, making it almost impossible to interpret the results of these studies.

Some important modifications to both of these delivery schemes have been proposed. In one, a sapphire ball is fixed to the distal end of a single bare optical fiber carried in a catheter. When used, the sapphire tip is brought into contact with the tissue to be removed and the tissue is exposed to laser light passing through the ball. In a second, a metal tip is placed over the end of an optical fiber similar to the

one described above. However, in this case, a hole is placed in the distal end of the metal tip which lets some fraction of the laser light exit the tip and expose the tissue directly, while the rest heats the tip itself. Results using both of these schemes are largely pending, but the researchers have demonstrated a desire to address the problem of controlled delivery by defining to some extent the geometry of the tissue wvich is irradiated.

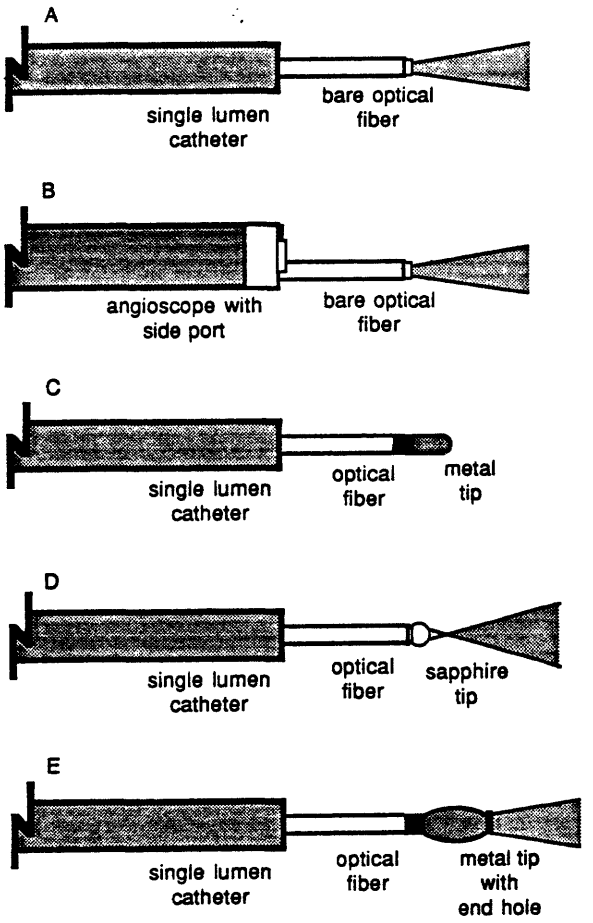

Figure I.5

Schematic diagram showing the five delivery schemes most often used to delivery laser energy to ablate atheroma. A, a single bare optical fiber carried in a simple catheter; B, a single bare optical fiber with a coherent bundle or angioscope for viewing; C, an optical fiber with a laser heated metal cap; D, an optical fiber with a sapphire tip; E, a modified laser heated metal cap.

I.5 LASER ANGIOSURGERY

Although previous studies have clearly demonstrated that laser ablation of atheromatous plaque is possible, limited success of safe, controlled removal of tissue has also clearly demonstrated the need for a more quantitative understanding of the tissue ablation process. A controlled laser light delivery scheme and an integrated ablation system designed specifically for tissue ablation are both essential if controlled ablation is to be realized.

This has prompted the advent of what we term "laser angiosurgery", the precise removal of atherosclerotic arterial obstructions by laser ablation under controlled conditions.

I.6 PURPOSE

The purpose of this study is to develop a successful laser angiosurgery system, and demonstrate precise tissue ablation using the concepts learned in its development. To that end, the study can be divided into several sections. First, a controlled means of laser light delivery will be explored through the investigation of optically shielded single fiber devices. Ablation using this light delivery scheme will be characterized using argon ion laser light. Second, a simple theoretical model will be presented which describes certain

aspects of the ablation process. Although the full development of this model is beyond the scope of this thesis, it can be used as a tool to point out the importance of certain ablation parameters and to predicting the effects of changing those parameters. Third, a multifiber shielded angiosurgery catheter will be described along with the ablation system necessary to support its use. The ablation process using this catheter and system will be characterized through the use of ablation velocity and ablation yield measurements, and histological evaluation of peripheral damage. Last, an example animal experiment taken from a parallel collaboration at the Cleveland Clinic Foundation will be described as a demonstration of the system's performance and workability in vivo.

REFERENCES

1. E. Braunwald, editor, Heart Disease: A Textbook of Cardiovascular Disease, Second Edition, W.B. Saunders Co., Philadelphia, 1984.

2. American Heart Association, "Heart Facts", Dallas, 1986.

3. D.M. Haust and R.H. More, "Development of Modern Theories on the Pathogenesis of Atherosclerosis", The Pathogenesis of Atherosclerosis, The Williams and Wilkins Co., Baltimore, 1972.

4. J.R. Mitchell and C.J. Schwartz, Arterial Disease, F.A. Davis Co., Philadelphia, 1965.

5. P. Constenatinides, Experimental Atherosclerosis, Elsevier Publishing Co., Amsterdam, 1965.

6. D. Steinberg, "Metabolism of Lipoproteins at the Cellular Level in Relation to Atherogenesis", in Lipoproteins, Atherosclerosis and Coronary Heart Disease, Elsevier, Amsterdam, 1981.

7. R. Ross and J.A. Glomset, "The Pathogenesis of Atherosclerosis", N. Engl. J. Med., 295:420 (1976).

8. R.W. Wissler and D. Vesselinovitch, "Animal Models of Regression", in Atherosclerosis IV, Springer-Verlag, Berlin, 1977.

9. W.C. Roberts, "The Coronary Arteries in Coronary Heart Disease: Morphologic Observations", Pathobiol. Annu., 5:249 (1975).

10. H.C. McGill, Jr., "Natural History of Human Atherosclerotic Lesions", in Atherosclerosis and Its Origin, Academic Press, New York, 1963.

11. G.S. Abela, S. Normann, D. Cohen, R.L. Feldman, E.A. Geiser, C.R. Conti, "Effects of Carbon Dioxide, Nd-YAG, and Argon Ion Laser Radiation of Coronary Atheromatous Plaques", Am. J. Cardiol., 50:1199 (1982).

12. D.S.J. Choy, S.H. Stertzer, H.Z. Rotterdam, M.S. Bruno, "Laser Coronary Angioplasty: Experience with 9 Cadaver Hearts", Am. J. Cardiol., 50:1209 (1982).

13. G. Lee, R.M. Ikeda, B.S. Kozina, D.T. Mason, "Laser Dissolution of Coronary Atherosclerotic Obstruction", Am. Heart J., 102:1974 (1981).

14. R.G. Gerrity, F.D. Loop, L.A.R. Golding, L.A. Erhart, Z.B. Argenyi, "Arterial Response to Laser Operation for Removal of Atherosclerotic Plaques", J. Thorac. Cardiovasc. Surg., 85:409 (1983).

15. D.Dew, "Anastomoses of Biological Structurea with Lasers", presentation at the MIT Seminar Series on Lasers and Medicine, March 28, 1984.

16. M.J.C. van Gemert, R. Verdaasdonk, E.G. Stassen, G.A.D.M. Schets, G.H.M. Gijsbers, J.J. Bonnier, "Optical Properties of Human Blood Vessel Wall and Plaque", Las. Surg. Med., 5:235 (1985).

17. W.S. Grunfest, F. Litvack, J.S. Forrester, T. Goldenberg, H.J.C. Swan, L. Morgenstern, M. Fishbein, I.S. McDermid, D.M. Rider, T.J. Pacala, J.B. Laudenschlager, "Laser Ablation of Human Atherosclerotic Plaque Without Adjacent Tissue Injury", J. Am. Coll. Cardiol., 5:929 (1985).

18. M.J.C. van Gemert, G.A.C.M. Schets, E.G. Stassen, J.J. Bonnier, "Modeling of (Coronary) Laser-Angioplasty", Las. Surg. Med., 5:219 (1985).

19. C. Kittrell, J. Tobin, J.R. Kramer, N.B. Rattliff, M.S. Feld "Plasma Ablation of Soft and Hard Tissue", abstract in Las. Surg. Med., 6:267 (1986).

20. J. Tobin, "Laser Induced Plasma Ablation of Biological Tissue", Bachelor's thesis, Massachusetts Institute of Technology, 1985.

21. J.F. Isner, R.H. Clarke, "The Current Status of Lasers in the Treatment of Cardiovascular Disease", IEEE J. of Quan. Electron., QE-20:1406 (1984).

22. R. Bellinger, De-Xiu Shi, E. Gomes, E.M. Mikat, R. Stack, M.L. Wolbarsht, "Radiation of Human Atherosclerotic Plaque with Mid-infrared (3um) and CO_2 (10.6um) Lasers: A Histologic Comparison", abstract in Las. Surg. Med., 7:80 (1987).

23. M.P. Sartori, P.D. Henry, "Laser/Tissue Interactions: CW and Pulsed HF/DF Chemical Laser Interactions with Cardiovascular Tissues", abstract in Las. Surg. Med., 7:81 (1987).

24. D.S.J. Choy, S. Stertzer, H.Z. Rotterdam, N. Sharrock, I.P. Kaminow, "Transluminal Laser Catheter Angioplasty", Am. J. Cardiol., 50:1206 (1982).

25. G.S. Abela, C.R. Conti, S. Normann, R.L. Feldman, C.J. Pepine, "A New Model for Investigation of Transluminal Recanalization: Human Atherosclerotic Coronary Artery Xenografts", Am. J. Cardiol., 54:200 (1984).

26. G.S. Abela, S.J. Normann, D.M. Cohen, D. Franzini, R.L. Feldman, F. Crea, A. Fenech, C.J. Pepine, C.R. Conti, "Laser Recanalization of Occluded Atherosclerotic Arteries In Vivo and In Vitro", Circulation, 71:403 (1985).

27. H.V. Anderson, G.S. Zaatari, G.S. Roubin, P.P. Leimgruber, A.R. Gruentzig, "Steerable Fiberoptic Catheter Delivery of Laser Energy in Atherosclerotic Rabbits", Am. Heart J., 111:1065 (1986).

28. T.A. Sanborn, D.P. Faxon, C.C. Haudenschild, T.J. Ryan, "Experimental Angioplasty: Circumferential Distribution of Laser Thermal Energy with a Laser Probe", J. Am. Coll. Cardiol., 5:934 (1985).

29. D.S.J. Choy, S.H. Stertzer, R.K. Myler, F. Marco, G. Fournial, "Human Coronary Laser Recanalization", Clin. Cardiol., 7:377 (1984).

30. J.M. Isner, R.H. Clarke, N.G. Pandian, R. Fortin-Donaldson, D.N. Salem, M.A. Konstam, D.D. Payne, R.J. Cleveland, "Laser Myoplasty for Hypertrophic Cardiomyopathy. In Vitro Experience in Human Post Mortem Hearts and In Vivo Experience in a Canine Model (Transarterial) and Human Patient (Interoperative)", Am. J. Cardiol., 53:1620 (1984).

31. H. Geschwind, G. Boussignac, B. Teisseire, C. Vieilledent, A. Gaston, J.P. Becquemin, P. Mayiolini, "Percutaneous Transluminal Laser Angioplasty in Man", Lancet, 2:844 (1984).

32. R. Ginsburg, D.S. Kim, D. Guthaner, J. Toth, R.S. Mitchell, "Salvage of an Ischemic Limb by Laser Angioplasty: Description using the coWcepts learned in its development. To that end, the study can be divided into several sections. First, a controransliminal Laser Angioplasty for Treatment of Peripheral Vascular Disease - Clinical Experience with 16 Patients", Radiology, 156:619 (1985).

34. F. Crea, G. Davies, W. McKenna, M. Pashazade, K. Taylor, A. Maseri, "Percutaneous Laser Recanalization of Coronary Arteries", Lancet, 2:214 (1986).

35. D.C. Cumberland, I.R. Starkey, G.D.G. Oakley, J.S. Fleming, G.H. Smith, F.F. Goiti, D.J. Taylor, J. Davis, "Percutaneous Laser-Assisted Coronary Angioplasty", Lancet, 2:214 (1986).

36. D.C. Cumberland, D.J. Tayler, C.L. Welsh, J.K. Guben, T.A. Sanborn, D.J. Moore, A.J. Greenfield, T.J. Ryan, "Percutaneous Laser Thermal Angioplasty: Initial Clinical Results with a Laser Probe in Total Peripheral Artery Occlusions", Lancet, 1:1457 (1986).

SECTION II

CONTROLLED DELIVERY OF LASER ENERGY

II.1 OVERVIEW

Three independent optical parameters which govern the tissue ablation process are defined and a laser light delivery scheme capable of controlling them, the optical shield, is described. The optical shield delivery scheme will be employed in the design of the multifiber catheter ablation system.

II.2 CONTROL OF OPTICAL PARAMETERS: THE OPTICAL SHIELD

During laser irradiation of any type of tissue, the rate and extent of tissue removal is governed by three independent optical parameters: the laser power incident on the tissue (P), the exposure time (t), and the area of tissue irradiated (A). A common design flaw in every laser delivery scheme which directly exposes atheroma to laser energy has been the lack of control of all three of these parameters.

Figure II.1 illustrates the shortcomings of a bare fiber delivery scheme. Laser light that is focused on the proximal input end of an optical fiber emerges in a diverging, conical beam dictated by the fiber's numerical aperture, or NA, which is defined as: $NA = \sin(\Theta)$ (see Figure II.1). The diameter of the projected spot of light (d) and thus the diameter of the irradiated circle of tissue, can be computed to be equal to: $d/2 = [l^2/(1-NA^2)]^{1/2}$, where l is the distance from the distal output end of the optical fiber to the target tissue surface. Unfortunately, experience has shown that even under direct visualization using an angioscope, it is impossible to control the distance l, and thus impossible to control the area of tissue irradiated.

The situation is further complicated by the lack of control over the medium through which the laser light must pass after it leaves the optical fiber. Even if the artery is flushed with saline, the inevitably imperfect purge will leave blood remaining between the fiber's distal output end and the tissue to be irradiated. Even a small amount of blood will strongly absorb many wavelengths and scatter all wavelengths, attenuating the laser light and making it impossible to control how much power actually reaches the tissue surface. Release of ablation products and the formation of bubbles in

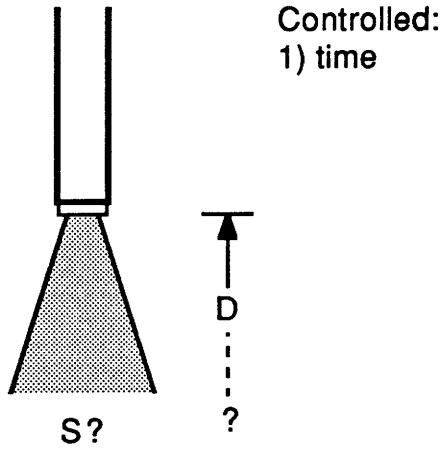

Figure II.1

Diagram illustrating the shortcomings of the bare optical fiber delivery scheme. The incident laser power and area of tissue irradiated cannot be controlled.

the medium surrounding the tissue may further change the amount of light that reaches the tissue.

The laser exposure time, which can be regulated by a shutter in the laser beam proximal to the optical fiber, is the only optical parameter that can be controlled. Hence, controlled tissue removal cannot be achieved.

Figure II.2 illustrates how all of the optical parameters can be controlled by enclosing the distal output end of the

optical fiber in a transparent, protective optical shield. When the output surface of the shield is positioned in contact with the tissue to be irradiated and removed, it locally displaces any blood or other intervening fluid to provide a clear field between the tip of the fiber and the target tissue. All of the laser power emerging from the optical fiber reaches the tissue surface (minus the known reflections at the inner and outer surfaces of the shield). Since the optical fiber can be rigidly fixed inside the shield, the distance between the fiber's output tip and the tissue surface is fixed, fixing the distance l and thus the spot diameter, and defining the area of tissue to be irradiated. With the incorporation of a shutter to control exposure time, all optical parameters are controlled.

To a large extent, it would be possible to insure control over all three laser parameters by bringing the output end of an optical fiber into direct contact with the tissue itself. In this way, the optical fiber plays the role of the optical shield, displacing intervening fluid and defining a treatment area equal in size to the fiber's core. However, it is unlikely that the optical fiber could withstand the violent reaction produced during ablation. In addition, the optical shield allows for greatly increased flexibility in catheter

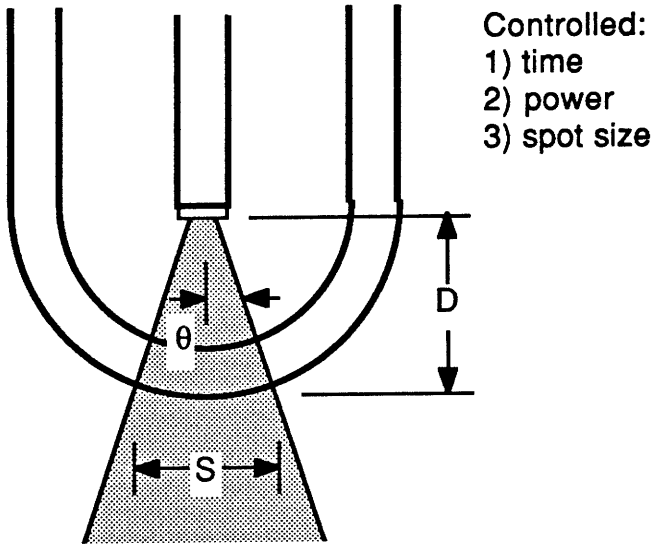

Figure II.2

Diagram illustrating the control allowed by incorporation of a transparent optical shield. The incident laser power and area of tissue irradiated can now be controlled.

design by producing laser spot diameters which greatly exceed the diameter of the optical fiber.

A number of other parameters can be derived from laser power, exposure time, and spot diameter which, although not independent, are useful in describing the laser/tissue interaction and ablation parameters. They include the

delivered laser energy (E) (the product of laser power and exposure time, E = Pt), the incident laser intensity (I) (the ratio of power to spot area, I = P/A), and the fluence (Ø) (the product of laser power and exposure time divided by spot area, Ø = Pt/A).

II.3 OTHER ADVANTAGES OF THE TRANSPARENT OPTICAL SHIELD

Along with providing the required control over all three optical parameters, the optical shield concept provides some other important advantages. During ablation, the reaction at the distal output tip of the optical fiber is violent, leading to char formation, corrosion, and tip damage [1,2]. The optical shield can protect the delicate optical fiber from this potentially harmful environment. Fluid displacement should reduce the unnecessary and undesirable heating of blood by removing it from the light path. The blunt end provided by the optical shield protects the artery from mechanical perforation by the sharp end of an optical fiber. The shield can also be used to house additional optics, lenses, filters, mirrors, etc., if shaping of the laser beam is desired.

It is important to note that, although the optical fiber is fixed within an enclosure, the optical shield differs dramatically from the hot metal tip approach. Since the laser

light passes through the optical shield and irradiates the tissue directly, the tissue is heated by the absorbtion of laser light, and not by a hot surface. The rate of energy transfer to the tissue is thus dictated by the laser power alone, and not by thermal conduction from the shield to the tissue. Thus, it may be possible to deposit energy into an atheroma much more rapidly by direct irradiation using an optical shield than by thermal conduction using a metal tip.

It is also important to note that the optical shield concept is effectual only if the shield is brought into contact with the tissue to be removed. All three optical parameters are controlled only under those circumstances.

II.4 SELECTION OF A LASER SYSTEM

Conceptually, the optical shield delivery scheme can be used with any laser system or laser wavelength for which optical fibers (or an equivalent light guide) and an optical shield material are available. Current commercially available optical fibers transmit well at all visible wavelengths and into the near infrared. Fibers are also available which transmit near ultraviolet with mixed success. Shield materials such as glass or quartz are readily available for all of these wavelengths as well. Unfortunately, the conduction of

the very high peak powers generated by pulsed laser systems and laser wavelengths further in the ultraviolet and infrared by optical fibers pose problems that have attracted a great deal of attention, but are yet largely unsolved.

For this study, the argon ion laser was selected to demonstrate the ability to use the optical shield concept as a controlled laser light delivery scheme and to develop a laser angiosurgery system. The results should be applicable to other laser systems as optical fiber technology improves.

REFERENCES

1. G. Lee, R.M. Ikeda, B.S. Kozina, D.T. Mason, "Laser Dissolution of Coronary Atherosclerotic Obstruction", Am. Heart J., 102:1974 (1981).

2. D.S.J. Choy, S.H. Stertzer, H.Z. Rotterdam, M.S. Bruno, "Laser Coronary Angioplasty: Experience with 9 Cadaver Hearts", Am. J. Cardiol., 50:1209 (1982).

SECTION III

SINGLE FIBER SHIELDED DEVICE BEHAVIOR

III.1 OVERVIEW

A single fiber optically shielded device was constructed to deliver argon ion laser light in a controlled way. It was used to produce craters in atheroma to characterize the rate of tissue ablation, and the size and shape of the craters produced. These experiments demonstrate that the use of the optical shield delivery scheme makes precise, quantifiable ablation possible, and give some insight into how ablation proceeds.

The purpose of this study was to demonstrate the workability of the optical shield concept and gain knowledge necessary to develop an ablation system based on that concept. A larger study designed specifically to investigate ablation thresholds and evaluate the accuracy of the theoretical model using similar single fiber shielded devices is being

undertaken as a collaborative effort at the Cleveland Clinic Foundation [1].

III.2 EXPERIMENTAL METHODS

The optical shield laser catheter constructed for these studies consisted of an optical fiber with a carefully cleaved or polished output tip rigidly centered inside a transparent shield (Figure III.1). The fiber had a 133um core diameter and a numerical aperture of 0.21. The shield was formed by a length of 0.5mm thick quartz tubing of 3mm outer diameter, closed at one end with a torch to form a hemispherical output surface. The spot diameter (measured on the output surface of the shield) was adjusted by choosing the appropriate distance between the tip of the fiber and the output surface. Reticon linear diode array measurements showed the beam profile to be approximately uniform across the spot, falling rapidly to zero at the edges (see Figure III.2). Spot diameter was measured by immersing the device in a bath of water containing a small amount of rhodamine laser dye to permit visualization of the beam (see Figure III.3). The beam was observed perpendicular to the axis of the device with a dissecting microscope, and its diameter measured at the output surface of the shield with

a reticle. Spot diameter determinations were accurate to ±25um.

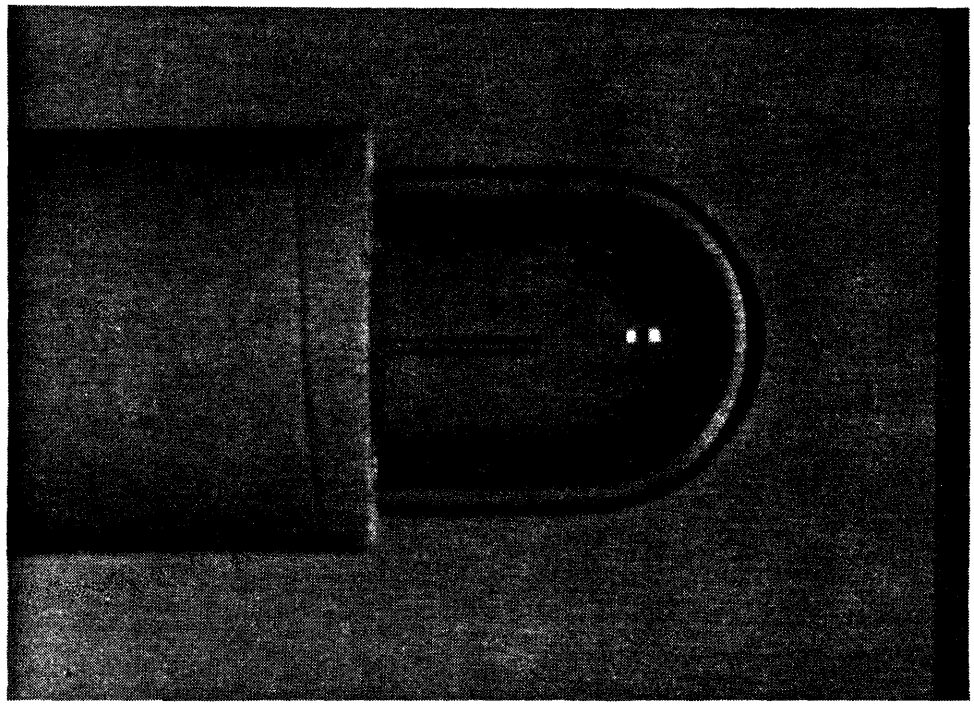

Figure III.1

Optically shielded single fiber device.

Tissue ablation studies were performed using blue-green light (all lines) from a Coherent I-20 argon ion laser. Human atherosclerotic carotid artery obtained at autopsy was cut open lengthwise to expose the luminal surface. Samples, typically 1mm thick, exhibited relatively acellular intimal fibroplasia, often infiltrated by lipid and foam cells,

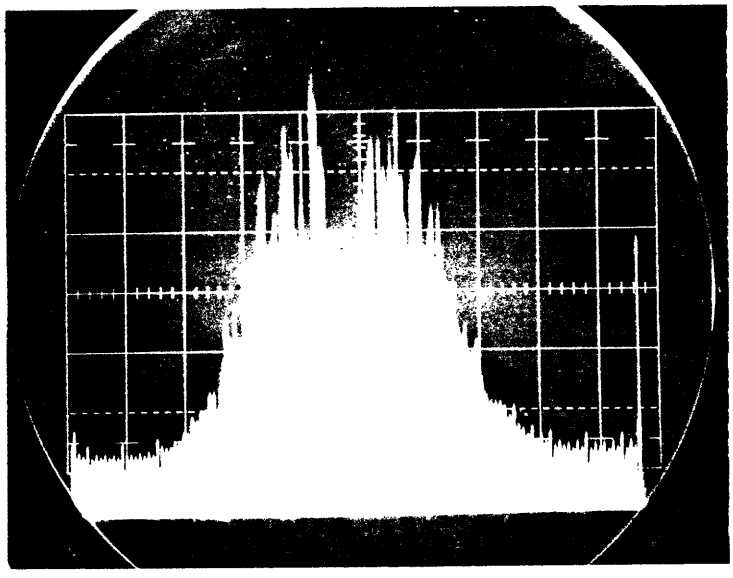

Figure III.2

Single fiber shielded device output profile measured with a Reticon linear diode array.

overlaying media, and were selected for sample to sample uniformity. Each sample was placed in a petri dish and immersed in either blood or saline solution. The tip of the optical shield was brought into perpendicular contact with the luminal surface, displacing the intervening fluid, and pressed against it with a force of one ounce (0.28N). Laser power was measured at the output surface of the device to an accuracy of $\pm$50mW using a thermal power meter. Exposure times, controlled

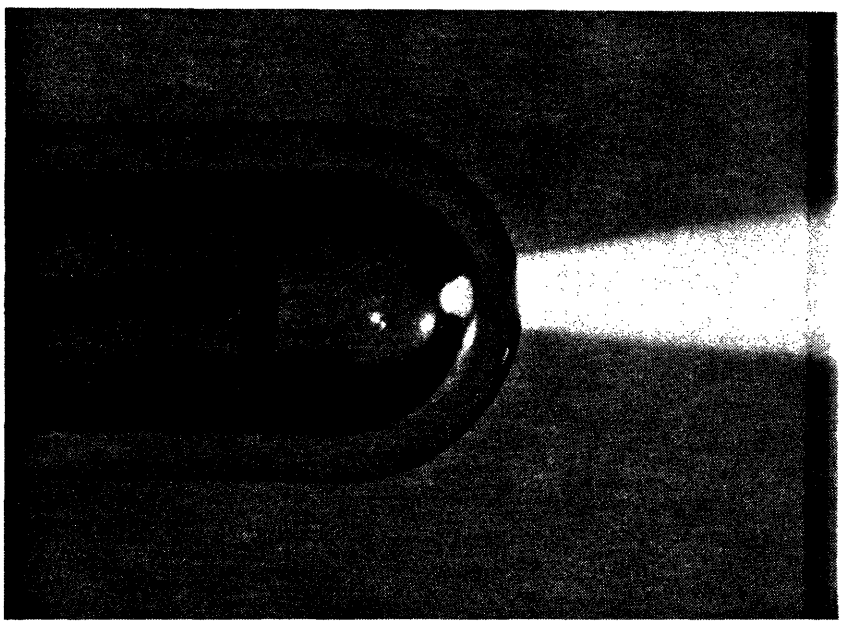

Figure III.3

Single fiber shielded device output as visualized by immersing the device in a bath containing laser dye.

by an electronic shutter placed in the laser beam, were accurate to ±2msec. Saline was used in most studies, since the dimensions of craters produced in blood and saline were found to be the same within experimental variability.

The craters formed by laser ablation were roughly cylindrical with rounded bottoms. Crater diameter (d) was measured at the luminal surface of the tissue using a

dissecting microscope with an eyepiece reticle. Crater depth (l) was measured using a histological microscope with a calibrated fine adjustment focusing knob, bringing first the tissue surface and then crater bottom into focus. Measured crater dimensions were accurate to $\pm$25um.

Craters were randomly selected for histological examination. Each was fixed in formalin, embedded in paraffin, serially sectioned, and hematoxylin and eosin stained to determine the degree of peripheral damage.

For each combination of ablation parameters of laser power (P) and spot diameter, the ablation velocity (v), or the rate of change of crater depth with exposure time (t), was computed as the ratio: $v = \Delta l/\Delta t$.

III.3 RESULTS

Three separate experiments were performed to characterize the ablation process under varying ablation parameters and conditions. In all cases, mean crater depths and diameters were computed from at least six individual craters. The mean values are reported, along with error bars indicating the entire range of values, for each set of ablation parameters.

III.3.1 Variation in Ablation Rate with Varying Power

The existence of a power dependence on the rate of tissue ablation and crater formation was examined by producing craters using single laser exposures through a shielded device with a 750um spot diameter. Craters were made with several different exposure times at 2.5W, 5.0W, 7.5W, and 10.0W.

The craters produced were relatively free of char at all power levels and exposure times, with a slight increase in char production at lower powers and longer times. Histology showed a narrow layer of vacuolation and hypereosinophilia surrounding the crater. A region beyond that showed slight collagen alteration typified by an increase in unstained space without hypereosinophilia. The structure of the arterial wall did not appear to be compromised by this change. A typical histological section is shown in Figure III.4. Occasional splits in the media were observed radiating from the produced crater in many cases. Qualitatively, the thickness of the layers of vacuolation and collagen alteration decreased with decreasing delivered energy, that is, with decreasing power at the same exposure time and with decreasing exposure time at the same power. Almost no vacuolation or collagen alteration was observable for short exposure times at 10.0W power levels.

Figure III.4

Typical histological section through a ablated crater. Photon dose for this crater was 5W/100ms, and a 750um spot diameter was used. Crater diameter is 750um as well.

The resulting crater diameters are plotted versus exposure time in Figure III.5, and thus represent a time history for crater formation. For all laser powers, the crater diameter approached the spot diameter as the exposure time increased, with the spot diameter being reached at shorter exposure times for higher laser powers. The full spot diame-

ter was never reached for laser powers of 2.5W even for the longest time exposure investigated.

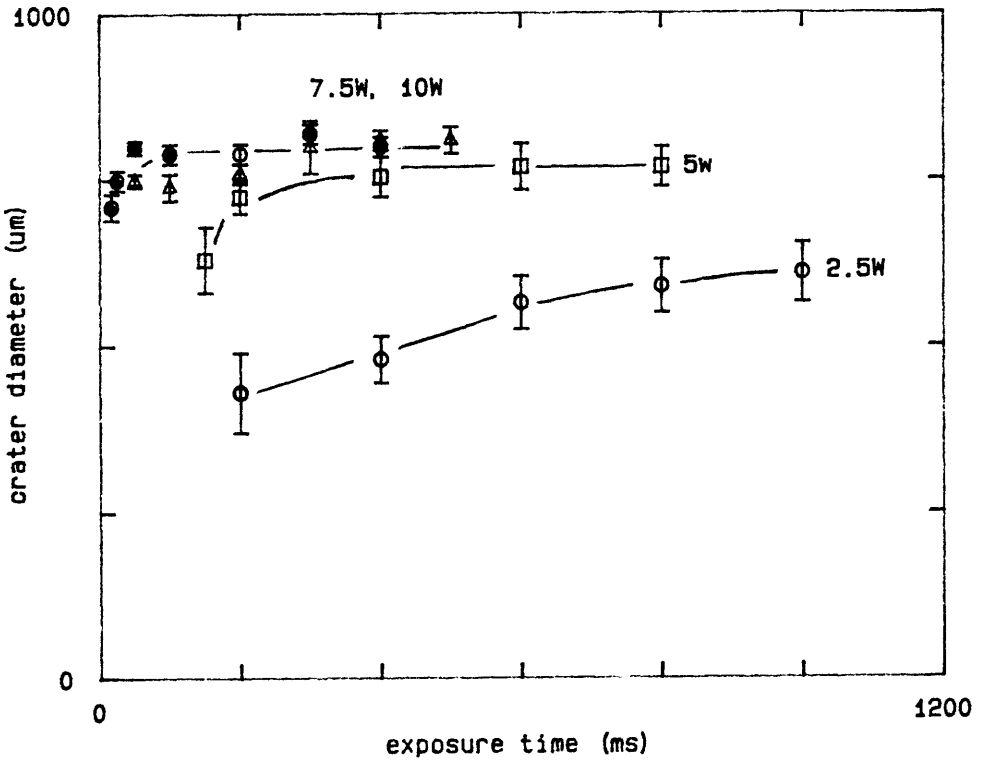

Figure III.5

Crater diameter versus exposure time for single exposures with a 750um spot diameter and various laser powers.

The resulting crater depths are plotted in Figure III.6. For all laser powers, the crater depth increased linearly with exposure time, indicating a constant ablation velocity. In all cases, ablation velocity increased with laser power.

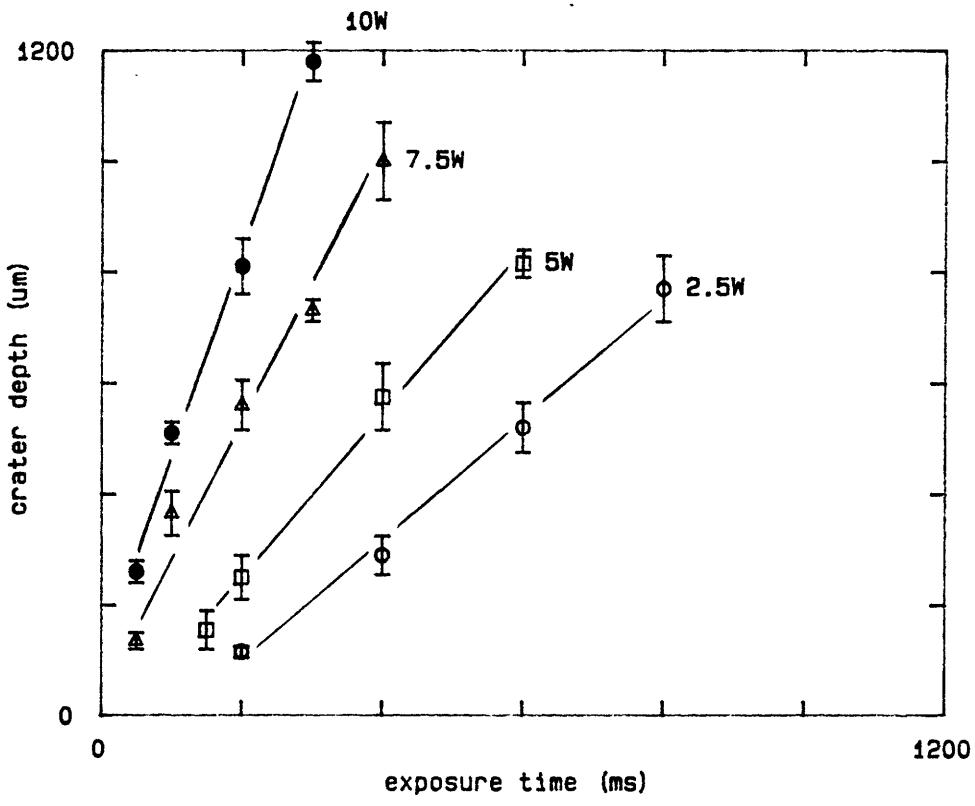

Figure III.6

Crater depth versus exposure time for single exposures with a 750um spot diameter and various laser powers.

III.3.2 Variation in Ablation Rate with Varying Spot Diameters

The existence of a laser spot diameter dependence on the rate of tissue ablation and crater formation was examined by producing craters using single laser exposures at 5.0W. Craters were made with several different exposure times using

shielded devices with spot diameters of 250um, 500um, 750um, and 1000um.

The craters produced were likewise relatively free of char at all spot diameters and exposure times, with some noticeable increase in char production at larger spot diameters and longer times. Histology was similar in appearance of that shown in Figure III.4. Qualitatively, the thickness of the layers of vacuolation and collagen alteration decreased with decreasing spot diameter at the same exposure time and with decreasing exposure time at the same spot diameter.

The resulting crater diameters are plotted versus exposure time in Figure III.7. For all spot diameters, the crater diameter approached the spot diameter as the exposure time increased, with the spot diameter being reached at shorter exposure times for smaller spot diameters.

The resulting crater depths are plotted in Figure III.8. For all spot diameters, the crater depth increased linearly with exposure time, indicating a constant ablation velocity. In all cases, ablation velocity decreased with increasing spot diameter.

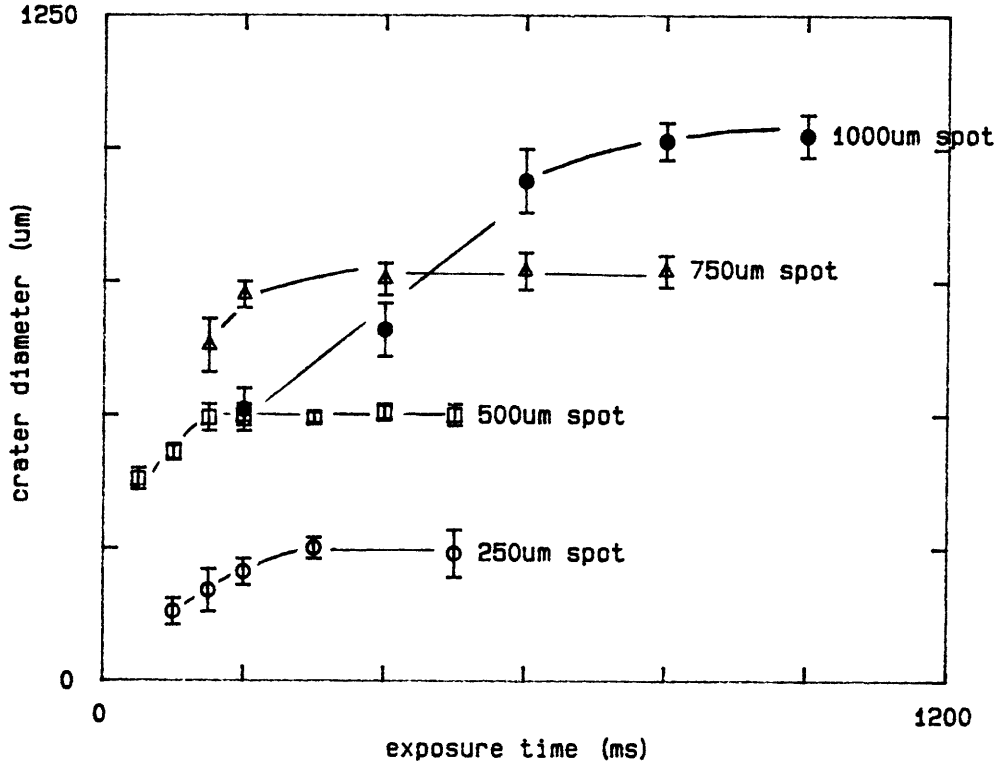

Figure III.7

Crater diameter versus exposure time for single exposures at 5.0W and and various spot diameters.

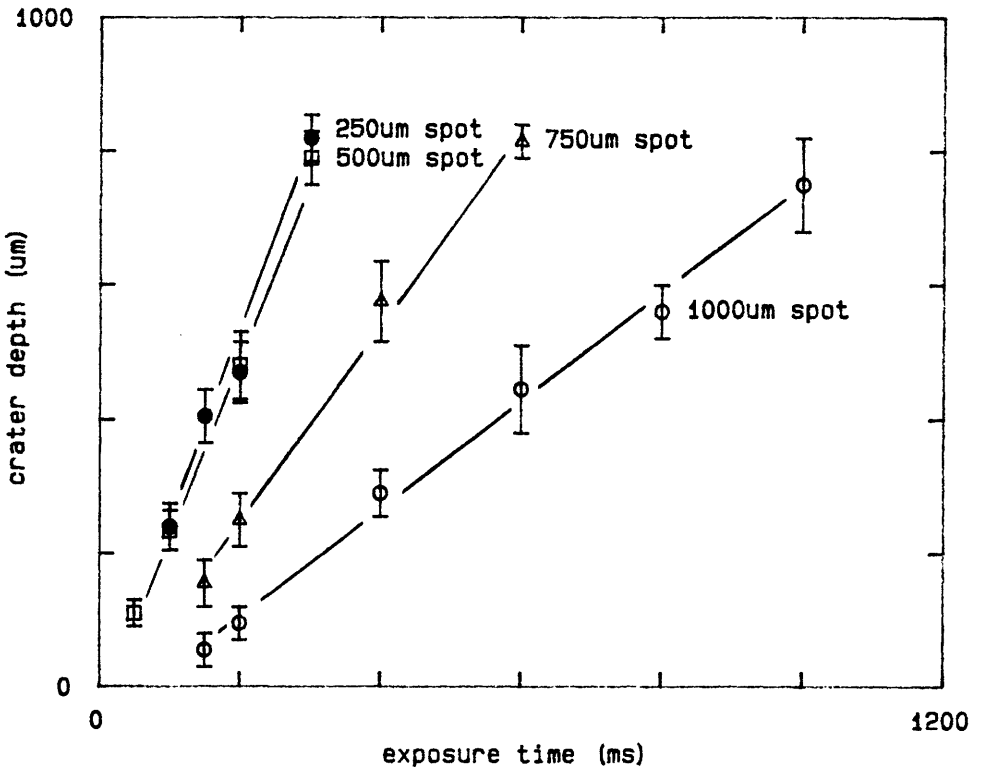

Figure III.8

Crater depth versus exposure time for single exposures at 5.0W and various spot diameters.

III.3.3 Variation in Ablation Rate with Repeated Exposures

The effect of multiple laser exposures at the same tissue site was examined by producing craters using 10W/35ms exposures and 10W/63ms exposures, both using a device with a 500um

spot diameter. Craters were made using from one to five exposures.

All resulting craters were relatively free of char. Histology was similar in appearance of that shown in Figure III.4, with an almost total absence of vacuolation and collagen alteration due to the short exposure times and high laser power. A typical histological section is shown in Figure III.9.

All crater diameters were equal to the spot diameter of 500um. The resulting crater depths are plotted versus the number of exposures in Figure III.10. For both exposure times, the crater depth increased linearly with the number of exposures, again indicating a constant ablation velocity even with multiple exposures.

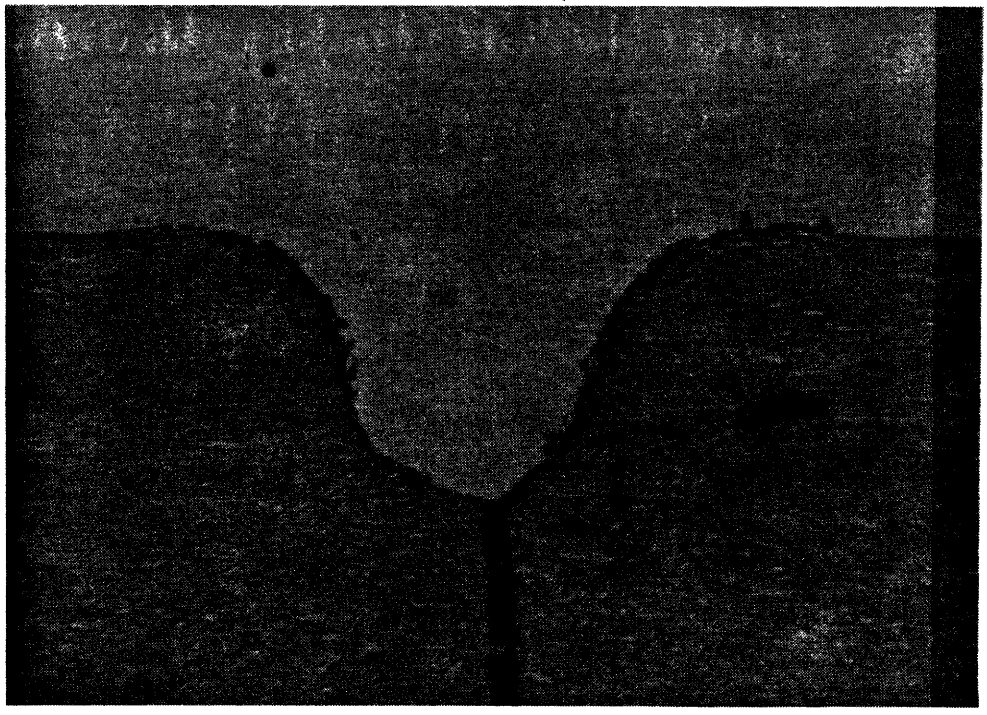

Figure III.9

Typical histological section through an ablated crater. Photon dose for this crater was 10W/63ms, and a 500um spot diameter was used.

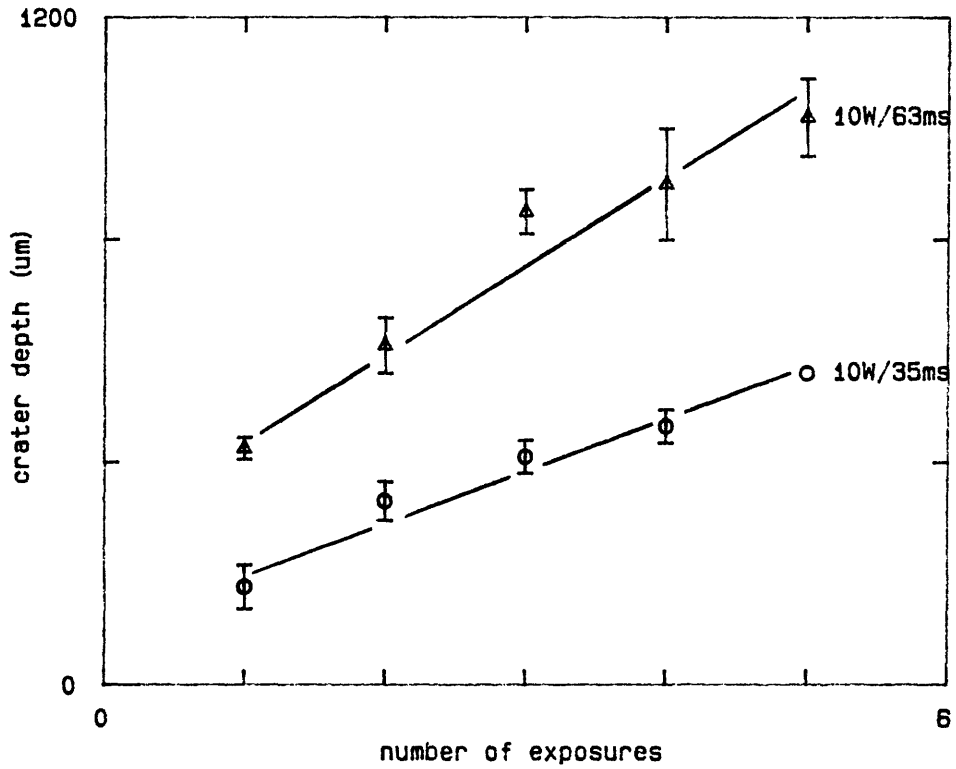

Figure III.10

Crater depth versus number of exposures for photon doses of 10W/35ms and 10W/63ms and a spot diameter of 500um.

III.4 DISCUSSION

The small variability in crater diameter and depth with any given combination of power, time, and spot diameter illustrates the consistency of laser ablation using a scheme capable of precisely controlled delivery of laser light. This

Laser Power (W)	Spot Diameter (um)	Intensity (W/mm^2)	Startup Time (msec)	Ablation Velocity (mm/sec)
5.0	250	102	250	2.80
5.0	500	25.5	200	2.73
5.0	750	11.3	200	1.42
5.0	1000	6.37	600	0.87
2.5	750	5.65	>1000	1.05
5.0	750	11.3	200	1.42
7.5	750	17.0	25	2.43
10.0	750	22.6	25	2.56

Table III.1

Observed practical threshold exposure times, t, and penetration velocities, v.

short exposures can be used to limit tissue removal to small incremental volumes, but the diameter of the craters created will be roughly equal to the spot diameter with a substantial degree of certainty. Exposure times can be increased easily with an increase in the depth of the crater being the only result.

The crater depth measurements shown in Figures III.6 and III.8 show that in each case depth increases linearly with exposure time up to the point of perforation. This indicates that after ablation begins, the process proceeds at a constant rate, with a constant ablation velocity, over the entire time

consistency also indicates that a quantitative understanding of the ablation process is realizable, and it is possible to predict with some degree of accuracy not only how much tissue will be removed by a given laser exposure, but the geometry of the crater that is formed as well.

There are several important trends in the data itself. Consider first the curves of crater diameter versus exposure time for single exposures, shown in Figures III.5 and III.7. As exposure time increased, crater diameter approached the spot diameter. Also, as intensity increased, due to either an increase in laser power or an decrease in spot diameter, crater diameter approached spot diameter more rapidly. Table III.1 gives the exposure times for which the crater diameters reach 90% of spot diameter. The 90% diameter is useful because sample-to-sample crater diameter variations are much reduced at this exposure time. It thus may be thought of as a practical threshold for producing reproducible craters.

Together, the trends in crater diameter indicate that it may be desirable to design a laser catheter system to employ high intensities, by the use of high laser powers and/or the use of small spot sizes, to exploit the reproducibility of crater diameters over the practical threshold. In this way, as long as the time exposure is above the practical threshold,

course of crater formation. It also suggests that the removal rates for fibrous plaque and normal arterial wall are similar, since no change in ablation velocity was noted as the crater progressed from plaque to media. Ablation velocity also increased with increasing intensity, brought about either by an increase in laser power or a decrease in spot diameter. The ablation velocity, calculated as the average slope of each curve, are also listed in Table III.1.

From these results, it is possible to form a picture of the time history of tissue ablation and crater formation (see Figure III.11). Ablation begins at the center of the laser spot, at or near the tissue surface. Immediately, the bottom of the crater moves downward into the tissue at a constant velocity. At the same time, the diameter of the crater rapidly reaches the diameter of the laser spot.

A constant ablation velocity was also indicated when multiple exposures were made at the same tissue site, as shown in Figure III.10. The fact that crater depths in Figure III.10 do not extrapolate to the origin may indicate that the tissue is initially altered (eg, denaturation, dehydration, slight char formation) during first exposure, causing more tissue to be removed during that exposure than those that follow. Likewise, crater depths shown in Figures III.6 and III.8 do

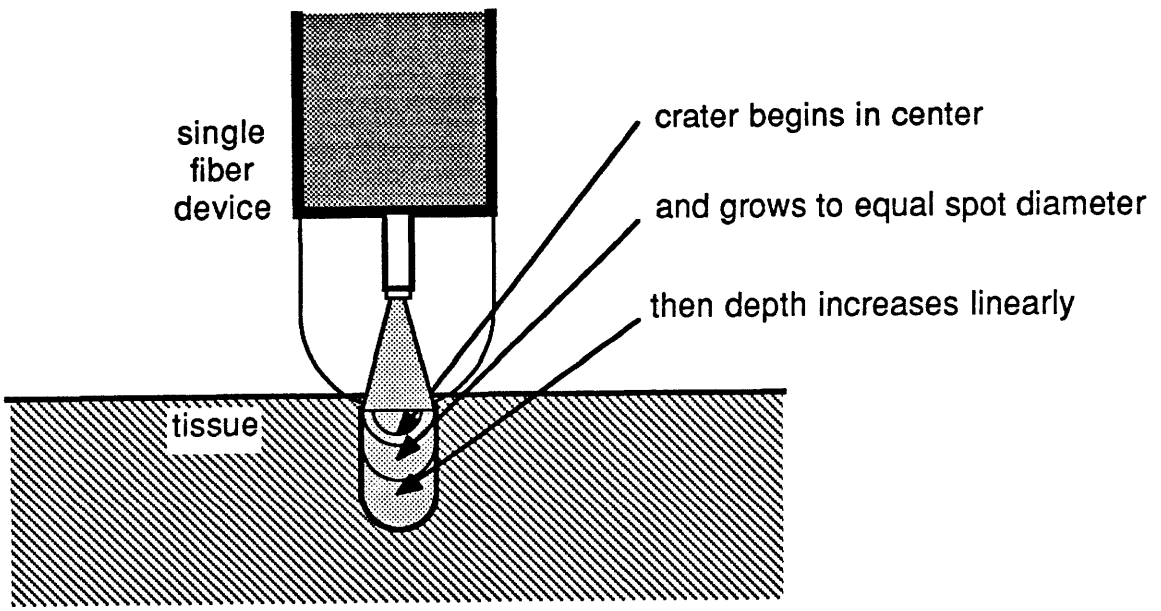

Figure III.11

A schematic visualization of the time course of tissue ablation and crater formation. Ablation begins at the center of the laser spot. As the crater forms, its diameter increases to that of the laser spot, and its depth increases at a constant rate.

not extrapolate to the origin, indicating that this alteration probably takes place at the onset of ablation early in the exposure. However, after the first exposure, the ablation process is purely additive. This consistent, additive nature of ablation makes possible a precise, incremental removal of tissue by the formation of small, shallow nibbles.

Exposure times for which the first perceptible spot of tissue is removed (an "absolute threshold") were found to vary greatly from tissue sample to sample, and are therefore of little clinical value.

The experiments performed here were not designed to give accurate information about the absolute thresholds for tissue ablation. For the successful design of a multifiber catheter system, the practical threshold is a much more important value. They likewise were not designed do give complete information about the peripheral damage produced using a single fiber device. For the purposes of this thesis, that information was obtained from multifiber device experiments presented later. However, absolute threshold determination may be important in fully understanding the laser/tissue interaction as ablation begins. An effort to extend the work presented in this section to investigate the absolute thresholds, and to characterize the peripheral damage and ablation yield using single fiber shielded devices has been undertaken by Sipke Strikwerda in a collaborative effort at the Cleveland Clinic Foundation [1]. Farooz Partovi, a member of the Laser Angiosurgery Group at MIT, is currently investigating the relationship between that data and a theoretical model for tissue ablation.

REFERENCES

1. S. Strikwerda, manuscript in preparation.

SECTION IV

LASER/TISSUE INTERACTION

IV.1 OVERVIEW

A simple model of thermal ablation of tissue using laser irradiation is presented. A relation for the ablation velocity is developed using the heat equation and energy conservation arguments, evaluated as pseudo-steady state in a moving reference frame. Although a complete development of a thermal ablation model is beyond the scope of this thesis, and could be in fact a thesis in and of itself, the relations derived here point out the important parameters that govern the laser/tissue interaction. Ablation velocities predicted by the model are compared with those measured in Section III. A comparison of the theory with multifiber device experiments will be presented in the sections describing those experiments.

An extension of the model presented here is currently under development by members of the MIT Laser Angiosurgery Group [1].

IV.2 REVIEW OF ABLATION MODELS

Although the use of laser radiation is becoming routine in surgery to cut and remove tissue, theoretical modeling of the laser ablation process has until recently received relatively little attention. A quantitative understanding of tissue removal is particularly important when precise ablation and control of the geometry of the ablated volume is necessary, as in laser angiosurgery. The formation of craters which are consistent in size and geometry, demonstrated in the last section, indicates that a quantitative, theoretical description of tissue ablation is possible.

When continuous lasers are used for tissue removal, with intensities on the order of tens to hundreds of watts per square millimeter and exposure times of tens of milliseconds or longer, the ablation process is largely thermal in nature. Tissue removal is largely brought about by vaporization of tissue water. This is distinct from tissue removal by other proposed laser mechanisms, such as excimer laser photodecomposition [2,3], and pulsed laser ablation [4-6] and

explosive fragmentation [7], all of which use light of much shorter pulse widths and much higher peak powers.

A relatively large literature exists on the subject of non-ablative heating of biological materials [8-11]. However, relatively little theoretical information has appeared on thermal ablation. Complications which make thermal ablation difficult to describe theoretically include the abrupt change in thermal behavior of tissue as it is heated to its ablation temperature, the simultaneous occurrence of heat flow and mass removal, and the difficulties associated with describing the distribution of light in a scattering medium. Wolbarsht [12] stressed the importance of using laser wavelengths with large absorption in tissue to minimize the extent of damage in the surrounding tissue. Laufer [13] presents a one-dimensional ablation model, where the heat of ablation is treated artificially by allowing the temperature to rise above the ablation temperature. He does not, however, account for light scattering. Langerholc [14] incorporates vaporization and scattering in the model he describes, but the treatment is again one-dimensional and emphasizes the distribution of light rather than the removal of material. Van Gemert [15] presented a numerical model of thermal ablation, emphasizing the startup of the ablation process. The treatment includes

heat diffusion in three dimensions but restricts the light to the beam cylinder within the tissue.

The literature also includes a limited amount of experimental work aimed at a basic understanding of the ablation process. Welch [16] presents evidence from thermal camera studies that ablation temperature commonly exceed 100^{o}C, and may reach as high as 300^{o}C. Rastegar [17] has demonstrated with agar gel experiments the effects of varying absorption coefficients on the ablation process. The single fiber shielded device experiments described in the last section form a significant addition to the experimental work in this area.

A related literature concerns thermal ablation of metals and other materials for cutting, welding, and materials processing [18]. However, ablation in tissue differs significantly in that light scattering plays a significant role, contrasted to materials processing where scattering is usually negligible compared to absorption. Also, the ratio of specific heat to latent heat of vaporization in water is much higher than those for most industrial materials. Nonetheless, a relevant treatment is presented by Bertolotti [19], where he uses the "heat balance integral method" to study the melting front produced in silicon by an internal heat source. That approach will be used here as well.

A theory of laser ablation which avoids many of the problems discussed in the literature is presented here. First, the complexities of light scattering is avoided by assuming a known light distribution function within the tissue. Second, the chemical changes taking place in the tissue are ignored. The removal process is regarded as being brought about by the evaporation of tissue water. Third, the ablation problem is treated as pseudo-steady state in a reference frame moving with the ablation front.

IV.3 PRINCIPLES OF THE PSEUDO-STEADY STATE APPROACH

The following theoretical analysis is limited to the situation where the ablation process has reached pseudo-steady state, i.e., crater formation progresses at a steady rate governed by the ablation velocity.

The linear increase in crater depth for all incident power levels at all exposure times, found in the single fiber experiments just described, implies that pseudo-steady state is reached early as ablation proceeds. Therefore, a pseudo-steady state approach is likely to describe the bulk of the ablation process without the added complication of describing the transient startup.

Figure IV.1 depicts ablation and crater formation at an arbitrary instant in time after pseudo-steady state has been reached. For simplicity, a collimated beam has been assumed to irradiate the tissue from above, and a cylindrically symmetric geometry has been employed.

As laser light reaches the bottom of the crater, it is distributed within the tissue where it is scattered and absorbed by tissue chromophores. Energy that is deposited by absorption transfers rapidly by thermal conduction to the tissue water. As energy accumulates, the tissue water is heated to its vaporization temperature (T_{vap}). As energy further accumulates, a region forms in the tissue, labelled the T_{vap} region, which has reached the vaporization temperature but has not accumulated the latent heat of vaporization (H_{vap}) necessary to ablate that volume. Energy can be thought of as stored within this volume by the formation of tiny pockets of interstitial steam. Finally, as H_{vap} is accumulated, tissue ablates at the bottom of the crater.

Note that the diameter of the forming crater must be equal to that of the incident laser beam. Since the laser intensity must be most intense in the tissue directly at the crater's bottom, that tissue must receive energy most rapidly and thus must ablate first. Before it is ablated, tissue

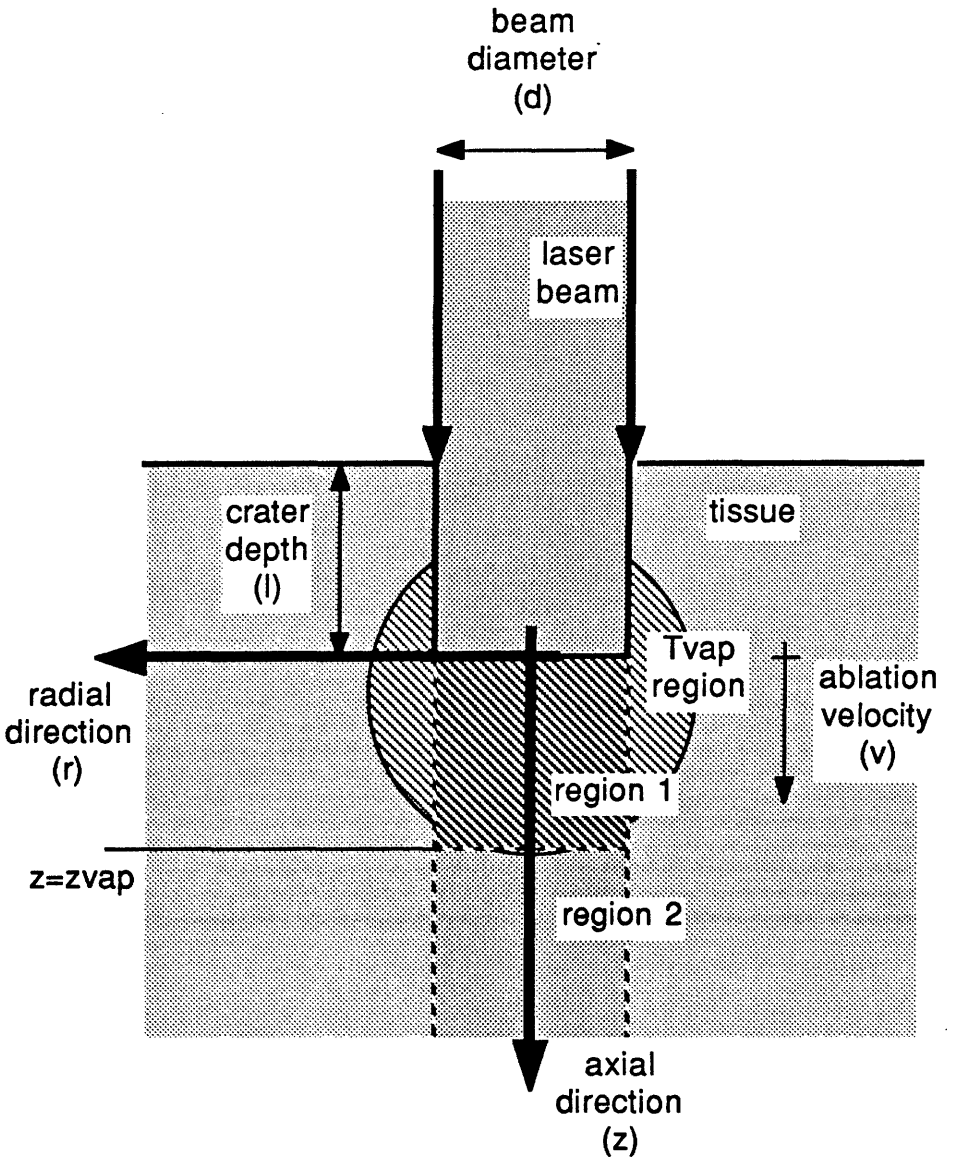

Figure IV.1

Schematic diagram of the pseudo-steady state ablation of tissue. The region of tissue labeled T_{vap} has been heated to the ablation temperature, but has not accumulated the heat of vaporization necessary for ablation.

radially peripheral to it may have accumulated energy scattered into it. However, after it ablates, that tissue no longer receives scattered light and H_{vap} cannot be accumulated. Conversely, if the crater had a diameter smaller than the laser beam, laser light would continue to deposit energy in the remaining tissue until it was vaporized.

This description of the ablation process depends upon the assumption that tissue water with its large heat capacity and heat of vaporization is the primary heat sink for the laser energy, and that ablation is equivalent to vaporizing that water. Once the tissue water has been vaporized, any remaining organic material may continue to absorb heat, rising in temperature above T_{vap} as it undergoes carbonization and pyrolysis. This fact, in addition to the possibility of superheating of the tissue water due to the generation of high pressures within the tissue, may help account for the observed ablation temperatures above $100^{o}C$ which have been reported [16]. The energy involved in this process, however, is probably small compared to that necessary to vaporize the tissue's water.

IV.4 THEORETICAL MODEL

In the arrangement depicted in Figure IV.1, a collimated beam of laser light having a uniform profile and circular cross section and propagating along the z-axis is incident upon a tissue sample. The sample is assumed to be homogeneous and infinite in extent.

The conductive transfer of heat within the tissue is described by the equation of thermal conduction,

$$\frac{d}{dt}T(r,z,t) = k\nabla^2 T(r,z,t) + \frac{1}{\rho C_p}S(r,z,t) \qquad (1)$$

where cylindrical coordinates have been used to exploit the symmetry of the problem. The temperature distribution is represented by the function T(r,z,t), a function of space and time. The heat source term, S(r,z,t), denotes the power density absorbed from the laser beam by the tissue. The tissue's density and thermal parameters are assumed to be constant, and are defined:

ρ = density
C_p = heat capacity
k^p = thermal diffusivity

We shall look at the ablation process from a coordinate system moving with the ablation front, i.e., with the bottom of the crater. This allows us to make some simplifications to

equation (1) to take advantage of the pseudo-steady state assumption. The laboratory coordinate system, (r,z_{lab},t), can be transformed into the moving frame, (r,z,t), by the relations:

$$z = z_{lab} - l(t); \quad v = \frac{dl(t)}{dt} \tag{2}$$

where $l(t)$ is the depth of the ablated crater at time t, and v is the ablation velocity. The heat diffusion equation is transformed into the moving coordinate system by the transforming derivatives:

$$\left(\frac{d}{dz_{lab}}\right)_t = \left(\frac{d}{dz}\right)_t \tag{3a}$$

$$\left(\frac{d}{dt}\right)_{zlab} = \left(\frac{d}{dt}\right)_z - v\left(\frac{d}{dz}\right)_t \tag{3b}$$

After transformation, the heat equation becomes:

$$\frac{d}{dt}T(r,z,t) = v\frac{d}{dz}T(r,z,t) + k\nabla^2 T(r,z,t) + \frac{1}{\rho C_p}S(r,z,t) \tag{4}$$

Also, since the heat flow equation (4) is not effected by adding a constant to T, we will define all temperatures relative to the ambient tissue temperature.

In the pseudo-steady state regime, equation (4) reduces to:

$$0 = v\frac{d}{dz}T(r,z) + k\nabla^2 T(r,z) + \frac{1}{\rho C_p}S(r,z) \qquad (5)$$

where the time derivative has been eliminated, and T(r,z) is now a function of space only. Any changes in the optical tissue parameters with increasing temperature are ignored, resulting in a heat source term, S(r,z), which is likewise space dependent only.

Two regions have been defined within the tissue. The T_{vap} region surrounds the crater and is bounded on the outside by the T_{vap} boundary. All tissue within this region is at the ablation temperature. The rest of the tissue outside of this region is at a temperature less than T_{vap}. The temperature distribution in the T_{vap} region is the trivial one:

$$T(r,z) = T_{vap} \qquad (6)$$

To find the solution outside, the heat equation (5) must be solved, subject to the unusual boundary condition that both the temperature (equal to T_{vap}) and its gradient (equal to zero) be specified at the unknown, moving T_{vap} boundary. In the pseudo-steady state regime, the energy source term, the location of the T_{vap} boundary, and the temperature distribution are all time independent, fixed relative to the

coordinate system which is moving at a constant velocity equal to the ablation velocity. There still exists the unconventional boundary condition: "find a boundary surface such that if the temperature on it is assigned to be T_{vap}, then the temperature gradient on it will come out zero". The other boundary condition is at the far away points where T = 0 (where T has been defined relative to the ambient body temperature).

The solution of equation (5) will be a function of the ablation velocity (v), which appears in that equation. As we shall see later, the requirement of energy conservation can then be used to fix v.

Equation (5) can be solved numerically to find the temperature distribution in the tissue surrounding the forming crater. At this time, however, we will use energy conservation arguments and plausible approximation to estimate the ablation velocity. This will in turn furnish information on the fraction of laser energy that is lost to the surrounding tissue.

Let us focus our attention on the ablation cylinder (shown in Figure IV.1 bounded by dotted lines). This is an infinite cylinder of tissue, of the same radius as the incident laser beam, that would eventually be ablated, an imaginary extension of the laser beam into the tissue. The

top of the cylinder, bounded by the crater bottom at z = 0 and the T_{vap} boundary at $z = z_{vap}$, will be referred to as region 1. The rest of the ablation cylinder, $z > z_{vap}$, will be called region 2. Note that the crater bottom and the section of the T_{vap} boundary making off region 1 are assumed flat.

The source function, S(r,z), represents the power absorbed from the laser beam by a unit volume of the tissue at the point (r,z). Its integral over the volume of the tissue will yield the total power delivered to the tissue:

$$2\pi \int_0^{\infty} r\, dr \int_{-\infty}^{\infty} dz\, S(r,z) = P \qquad (7)$$

This "P" is the total power in the incident laser beam, corrected for the power loss from the surface due to reflection. With a beam diameter (d) and uniform beam profile:

$$P = \frac{\pi d^2}{4} I \qquad (8)$$

where I is the beam intensity.

The source function is in general a complicated function of the beam diameter and the absorption and scattering coefficients of the tissue. It may also depend on the relative index of refraction at the tissue surface. Its correct

functional form is the subject of many theoretical as well as experimental investigations [14-16].

We will not be concerned with finding a rigorous source function, S(r,z), in this work. Instead, we will use the following sample function to demonstrate how it can be used to calculate the quantities of interest. This function assumes that a fraction of the light within the ablation cylinder is deposited within the tissue, and that the beam intensity decreases exponentially in z:

$$S(r,z) = \alpha' \; I \; \exp(-\frac{z}{D}); \quad r < \frac{d}{2} \tag{9a}$$

where α' is the effective absorption coefficient, and D is the penetration depth, i.e., the characteristic depth over at which light is reduced in intensity by 1/e due to the interplay of scattering and absorption. Likewise, a fraction of the light outside of the ablation cylinder is also deposited within the tissue, but in this case the beam intensity falls off exponentially in z and in r as the penetration depth, and falls of as 1/r due to the cylindrical geometry:

$$S(r,z) = \alpha' \; I \; \frac{1}{r} \exp(-\frac{z}{D}) \; \frac{d}{2} \exp(\frac{d/2}{D}) \; \exp(-\frac{r}{D}); \quad r > \frac{d}{2} \tag{9b}$$

A more sophisticated function can always be substituted,

although this may make the following integrals more difficult to evaluate.

Note that the penetration depth is strongly wavelength dependent because light absorption is tissue is a highly varying function of wavelength.

Equations (8) and (9), taken together, can be thought of as a normalization condition that requires that:

$$\alpha' = \frac{f(d)}{D}; \quad f(d) = \frac{d}{d + 4D} \tag{10}$$

relating the effective absorption coefficient to the penetration depth and the beam diameter. The parameter f(d) is the fraction of light contained within the cylinder of tissue, of diameter d, which will be ablated. The rest of the light is lost to the surrounding tissue through scattering.

To get an energy balance equation for region 2, equation (5) is integrated using the source function described in equations (9) and (10). This yields:

$$0 = -Q + -\frac{\pi d^2}{4} v h_0 + \frac{\pi d^2}{4} f(d) \; I \exp(-\frac{z_{vap}}{D}) \tag{11}$$

where Q is the total heat diffusing out of region 2 per unit time, and h_0 is the energy required to raise a unit volume of tissue from the ambient body temperature to T_{vap}:

$$h_0 = \rho C_p T_{vap} \qquad (12)$$

This result can easily be interpreted physically. In the pseudo-steady state regime, the accumulation of energy (equal to zero) is equal to the loss of energy through the boundaries of region 2 by thermal diffusion, plus the loss of energy due to heated tissue crossing the z_{vap} boundary into region 1, plus the energy gained through absorption of energy from the laser beam.

Likewise, a similar energy balance holds for region 1:

$$0 = -\frac{\pi d^2}{4} v H_{vap} + \frac{\pi d^2}{4} v h_0 + \frac{\pi d^2}{4} I \left(1-\exp\left(-\frac{z_{vap}}{D}\right)\right) \qquad (13)$$

Note that no heat escapes this region by diffusion because there is no thermal gradient; no Q term appears in equation (13). The physical explanation of this equation is similar to that of equation (11). The accumulation of energy (equal to zero) is equal to the loss of energy due to tissue ablation leaving region 1 ($-vH_{vap}$), plus the energy gained due to hot tissue entering region 1 (vh_0) and through absorption of energy from the laser beam.

Equations (11) and (13) can be solved to yield the steady state ablation velocity (v):

$$v = \frac{f(d)}{h_0+H_{vap}} \left(I - \frac{4Q}{f(d)\pi d^2}\right) \tag{14}$$

and the depth of the T_{vap} region (z_{vap}):

$$z_{vap} = D \ln\left(\frac{1 + \frac{H_{vap}}{h_0}}{1 + \frac{H_{vap}}{h_0}\frac{4Q}{f(d)\pi d^2 I}}\right) \tag{15}$$

The quantity Q appearing in these equations, although time independent, is an unknown function of I, that will be known only if the pseudo-steady state heat equation (5) is solved and the temperature distribution is used to calculate the heat flux leaving region 2. To get an approximate value for Q, we expand it in a Taylor series about $I = I_0$, the threshold intensity for tissue ablation, and keep only the first term:

$$Q = Q(I) = Q(I_0) \tag{16}$$

This is a reasonable approximation, because roughly speaking, heat flux out of region 2 depends on the temperature distribution in this region relatively to the ambient tissue temperature. The highest temperature in this region is T_{vap}, no matter what the intensity. Hence, greater intensities should

result in greater ablation velocities but not appreciably different temperature distributions in region 2.

With the assumption (16), Q can be calculated from either equation (14) or (15), setting v or z_{vap} to zero:

$$Q = \frac{\pi d^2}{4} f(d) I_0 \tag{17}$$

Equations (14) and (15) can be combined with equation (17) to give the final relations:

$$v = \frac{f(d)}{h_0+H_{vap}} (I-I_0) \tag{18}$$

$$z_{vap} = D \ln\left(\frac{1 + \frac{H_{vap}}{h_0}}{1 + \frac{H_{vap}}{h_0}\frac{I_0}{I}}\right) \tag{19}$$

To calculate the crater depth (l) produced by a given exposure, we need to make the approximation that the pseudo-steady state ablation velocity is reached immediately after ablation begins, and that ablation begins after a short startup time t_0:

$$l = v(t-t_0) = \frac{f(d)}{h_0+H_{vap}} (I-I_0) (t-t_0) \tag{20}$$

An ablation efficiency can be calculated from the above results, to gain insight into the most efficient combination of ablation parameters. The ablation efficiency ( ) is equal to the ratio of the energy used to ablate tissue to the energy absorbed by all the tissue:

$$= \frac{\frac{\pi d^2}{4} l (h_0+H_{vap})}{\frac{\pi d^2}{4} It} = f(d) (1 - \frac{I_0}{I}) (1 - \frac{t_0}{t}) \quad (21)$$

The above theoretical model of the ablation process has been extended [1] to include calculation of the startup parameters. The undetermined parameters I_0 and t_0 in the above relations were estimated in that work to be:

$$I_0 = \frac{2 \rho C_p k T_{vap}}{f(d) d} \quad (22)$$

$$t_0 = \frac{(H_{vap}+h_0) D}{f(x) I} \quad (23)$$

IV.5 DISCUSSION

For the purposes of illustration, physical constants present in the above equations will be taken to be equal to those of water, and are listed in Table IV.1. In particular,

T_{vap} will be taken to be the boiling point of water minus normal body temperature, $T_{vap} = 100-37 = 63^{o}C$. The penetration depth of argon ion laser light in tissue will be taken to be D = 1/3mm, consistent with the findings of van Gemert for the absorption and scattering coefficients for human aorta [20].

Symbol	Definition	Value
ρC_p	heat capacity per unit volume	$0.00396 J/^{o}C mm^3$
k	thermal diffusivity	$0.106 mm^2/s$
T_{vap}	boiling point relative to ambient	$63^{o}C$
D	penetration depth for argon ion laser	1/3mm
$h_o = C_p T_{vap}$	energy needed to heat unit volume to T_{vap}	$0.25 J/mm^3$
H_{vap}	latent heat of vaporization	$2.25 J/mm^3$

Table IV.1

Definitions and values of the physical parameters used.

A characteristic time over which thermal diffusion (τ) takes place can be estimated using the thermal diffusivity of water (k) and taking the characteristic length of the thermal

gradient to be the penetration depth of laser light (D) in the relation:

$$\tau = \frac{D^2}{k} = \frac{(1/3)^2}{0.106} = 1.1s \qquad (24)$$

Equation (24) suggests that thermal diffusion may not play an important role in the ablation process for exposure times much less than one second. In equation (18), the loss of energy due to thermal diffusion is accounted for by subtracting the threshold intensity (I_0) from the incident intensity (I). In the absence of thermal diffusion, or in the limit where thermal diffusion is unimportant because of high intensities and high ablation velocities, equation (18) would simplify to:

$$v = \frac{f(d)}{h_0+H_{vap}} I \qquad (25)$$

In equation (25), the ablation velocity (v) is equal to the incident intensity (I) divided by the total energy necessary to raise a unit volume of tissue to the vaporization temperature (h_0) plus the latent heat of ablation (H_{vap}). This same result can be obtained through a simple energy balance on the volume of tissue ablated.

The single fiber ablation experiments described in Section III measured ablation velocity as a function of incident laser power and spot diameter. The results of those experiments are reproduced in Table IV.2.

Experiment Number	Laser Power (W)	Spot Diameter (um)	Intensity (W/mm^2)	Ablation Velocity (mm/sec)
1	5.0	250	102	2.80
2	5.0	500	25.5	2.73
3	5.0	750	11.3	1.42
4	5.0	1000	6.37	0.87
5	2.5	750	5.65	1.05
6	5.0	750	11.3	1.42
7	7.5	750	17.0	2.43
8	10.0	750	22.6	2.56

Table IV.2

Observed ablation velocities, v, reproduced from the single fiber ablation experiments in Section III.

Equation (25) predicts that the ablation velocity (v) should proportional to the laser intensity (I) for $I > I_0$, with the proportionality constant equal to $f(d)/(h_0+H_{vap})$. If the quantity v/I is computed for each experimental value of v in Table IV.2, an experimental value for the proportionality constant can be obtained. Then taking h_0+H_{vap} to be equal to

$2.5J/mm^3$, an experimental value for f(d) can be computed. The results of those computations are shown in Table IV.3.

Experiment Number	Intensity (W/mm^2)	Ablation Velocity (mm/sec)	$\frac{f(d)}{h_0+H_{vap}}$	f(d)
1	102	2.80	0.028	0.07
2	25.5	2.73	0.107	0.27
3	11.3	1.42	0.126	0.32
4	6.37	0.87	0.137	0.34
5	5.65	1.05	0.186	0.47
6	11.3	1.42	0.126	0.32
7	17.0	2.43	0.143	0.36
8	22.6	2.56	0.113	0.28

Table IV.3

Computed values for $f(d)/h_0+H_{vap}$ and f(d) from the intensities used and ablation velocities observed in the single fiber ablation experiments in Section III.

The average value for f(0.75) (experiments 5-8) can be calculated to be 0.36. Taking the form of f(d) to be given by equation (10), with d = 0.75mm, the value for the penetration depth, D, can be calculated to be 0.33mm, which is in good agreement with the 1/3mm, consistent with the findings of van Gemert for the absorption and scattering coefficients for human aorta [20].

Table IV.4 shows the predicted ablation velocities using equation (25) and the values listed in Table IV.1.

Experiment Number	Experimental Ablation Velocity (mm/sec)	Predicted Ablation Velocity (mm/sec)
1	2.80	6.52
2	2.73	2.75
3	1.42	1.63
4	0.87	1.10
5	1.05	0.82
6	1.42	1.63
7	2.43	2.45
8	2.56	3.25

Table IV.4

Observed and predicted ablation velocities.

Predicted ablation velocities are in relatively good agreement with those observed in the single fiber ablation experiments, with the obvious exception of experiment 1 using a 250um spot diameter. It is quite possible that our simplistic form of f(d) does not give a good results for very small spot diameters.

The single fiber ablation experiments of Section III were not designed to provide information about absolute threshold

times or threshold intensities. Comparison of practical thresholds and theory would be of limited value, since it is not clear how practical threshold times relate to the t_0 threshold time defined in equation (23). However, since equation (23) defines the time required before any ablation takes place, we would expect practical thresholds to be longer than that time. In fact, the practical thresholds are longer by a factor of two to five for all but the experiments where 7.5W or 10W were used. In this case, the practical threshold was much less than t_0.

Some preliminary experiments performed in this lab have indicated that the penetration depth, D, may change dramatically with tissue heating and the onset of ablation, tending towards a value much less than 1/3mm. This may be due to creation of a thin layer of char on the tissue surface or as a result of tissue dehydration or heating directly. It is quite possible that such a dramatic change in the penetration depth reduces the threshold times for ablation dramatically as well, since t_0 is such a strong function of D.

Equation (19) gives the depth (z_{vap}) of the the T_{vap} region below the crater. After the laser beam has been turned off, a thickness of z_{vap} of tissue at the bottom of the crater has been heated to T_{vap}. This region has been heated to a

temperature capable of damaging the tissue through the formation of pockets of steam and coagulation of tissue proteins. In addition, it may be the source of energy which may damage surrounding tissue as the energy in the T_{vap} region dissipates. The maximum value for z_{vap} is:

$$z_{vap} = D \ln(1 + \frac{H_{vap}}{h_0}) = 1/3 \ln(1 + \frac{2.25}{0.25}) = 0.76mm \quad (26)$$

The zones of vacuolation damage found to surround the craters created in the single fiber experiments were actually much smaller than that. This would indicate that the T_{vap} region may not extend as deep as predicted. Again, this may be due to changes in the penetration depth, D, as ablation proceeds, causing the laser light to penetrate less deeply in the tissue and producing a smaller damage region.

Equation (21) describes the efficiency (η) of the ablation process as a function of the beam diameter (d), the incident intensity (I), and the exposure time (t). Note that the efficiency increases with increasing intensity and with increasing exposure time. The production of deep craters (long exposure times and/or high ablation velocities) is more efficient than shallow craters. However, as pointed out above, I_0 is expected to be small. The production of craters at very short exposure times, found in the single fiber ex-

periments, indicates that the threshold time (t_0) is small as well. Equation (21) can be approximated by:

$$\eta = f(d) = \frac{d}{d + 4D} \tag{27}$$

Note that as the penetration depth (D) decreases, i.e., as the tissue absorption for the laser wavelength used increases, the efficiency increases, approaching a limiting value of unity. Likewise, as the beam diameter increases, scatter becomes less and less important, and again the efficiency approaches unity.

Although the ablation efficiency can be thought of as a measure of the fraction of energy that goes into ablation verses the fraction that simply damages the peripheral tissue, it is important to note that this definition is somewhat misleading. As ablation proceeds at steady state, the size of the T_{vap} region surrounding the bottom of the hole is determined by the tissue properties, and not by the exposure time or laser intensity, as shown in equation (19). When the laser is turned off, the region of peripheral damage is likely to be related to the size of this T_{vap} region.

In summary, the simple model described here points out the important parameters that define the ablation process, namely laser intensity, laser exposure time, laser spot diameter, penetration depth, and the specific heat and heat of

ablation of the tissue. The model predicted ablation velocities relatively well using the properties of water and a value of the penetration depth reported in the literature. However, the model also points out some definite short comings. It is clear that a better understanding of the penetration depth and how it changes is necessary before a more accurate model can be developed. A better understanding of the light distribution within the tissue both before and during ablation may allow the formulation of a better relation for f(d). This model has made no attempt to account for the spreading of the incident laser beam inherent in optical fiber delivery. Further refinement of the model to address some of these problems is being undertaken by members of the Laser Angiosurgery Group with the addition of a large body of single fiber device data provided by collaborators at the Cleveland Clinic Foundation.

REFERENCES

1. F. Partovi, J.A. Izatt, R.M. Cothren, C. Kittrell, J.E. Thomas, S. Strikwerda, J.R. Kramer, M.S. Feld, "A Model for Thermal Ablation of Biological Tissue Using Laser Radiation", Las. Surg. Med., accepted for publication.

2. R. Srinivasan, W. Seigh, "Ablative Photodecomposition: Action of Far-Unltraviolet (193nm) Laser Radiation on Poly(ethylene terephthalate) Films", J. Am. Chem. Soc., 104:6784 (1982).

3. W.S. Grundfest, F. Litvak, F.S. Forrester, T. Goldenberg, H.J.C. Swan, L. Morgenstern, M. Fishbein, I.S. McDermid, D.M. Rider, T.J. Pacala, J.B. Laudenslager, "Laser Ablation of Human Atherosclerotic Plaque Without Adjacent Tissue Injury", J. Am. Coll. Cardiol., 6:929 (1985).

4. O.N. Khrokhin, "Generation of High-Temperature Vapors and Plasmas by Laser Radiation", in Laser Handbook, Vol. 2, North Holland, Amsterdam, 1982, p.1372.

5. P.H. Gibson, D. Holten, S.C. Smith, B.R. Chaitman, H.L. Kennedy, "Absence of Thermal Tissue Injury Using a Pulsed Mode Nd:YAG Laser", abstract in Circulation, 72:III-402 (1985).

6. C. Kittrell, J. Tobin, J. Rulnick, M.S. Feld, "Plasma Ablation of Tissue", abstract in Las. Surg. Med., 6:267 (1986).

7. P. Teng, N.S. Nishioka, R.R. Anderson, T.F. Deutsch, "Optical Studies of Pulsed Laser Fragmentation of Biliary Calculi", Appl. Phys. B., 42:73 (1987).

8. F.C. Henriques, "Studies of Thermal Injury", Arch. Pathol., 43:489 (1947).

9. M.A. Mainster, T.J. White, J.H. Tips, P.W. Wilson, "Transient Thermal Behaviour in Biological Systems", Bull. Math. Biophys., 32:303 (1970).

10. A.M. Stoll, M.A. Chianta, "Heat Transfer Through Fabrics as Related to Thermal Infury", Trans. N.Y. Acad. Sci., Series II, 33:649 (1971).

11. L.A. Priebe, A.J. Welch, "A Dimensionless Model for the Calculation of Temperature Increase in Biological Tissues Exposed to Nonionizing Radiation", IEEE Trans. Bio. Eng., 26:244 (1979).

12. M.L. Wolbarsht, "Laser Surgery: CO_2 or HF", IEEE J. Quant. Elect., 20:1427 (1984).

13. G. Laufer, "Primary and Secondary Damage to Biological Tissue Induced by Laser Radiation", Appl. Opt., 22:676 (1983).

14. J. Langerholc, "Moving Phase Transitions in Laser-Irradiated Biological Tissue", Appl. Opt., 18:2286 (1979).

15. M.J.C. van Gemert, G.A.C.M. Schets, E.G. Stassen, J.J. Bonnier, "Modeling of (Coronary) Laser-Angioplasty", Las. Surg. Med., 5:219 (1985).

16. A.J. Welch, J.W. Valvano, J.A. Pearce, L.M. Hayes, M. Motamedi, "Effects of Laser Radiation on Tissue During Laser Angioplasty", 5:251 (1985).

17. S. Rastegar, M.J.C. van Gemert, A.J. Welch, L.J. Hayes, "Laser Ablation in Absorbing Disks of Agar Gel", to be published.

18. W.W. Duley, Laser Processing and Analysis for Materials, Plenum, New York, 1983.

19. M. Bertolotti, C. Sibilia, "Depth and Velocity of the Laser-Melted Front from an Analytical Solution of the Heat-Conduction Equation", IEEE J. Quant. Elect., 17:1980 (1981).

20. M.J.C. van Gemert, R. Verdaasdonk, E.G. Stassen, G.A.C.M. Schets, G.H.M. Gijsbers, J.J. Bonnier, "Optical

Properties of Human Blood Vessel Wall and Plaque", Las. Surg. Med., 5:235 (1985).

SECTION V

MULTIFIBER LASER ANGIOSURGERY SYSTEM DESIGN

V.1 OVERVIEW

Based on the results of the single fiber shielded device experiments presented in Section III, the important concepts and considerations in the design of a multifiber shielded laser catheter are presented. The catheter design, and the optical system and computer based control system which support it are described in full. Experiments which fully characterize the ablation process using this system will be presented in the following two sections.

V.2 MULTIFIBER SHIELDED CATHETER DESIGN CONCEPTS

Successful recanalization of obstructed arteries requires that ablation proceed in a controlled and predictable way, that the catheter open a lumen of sufficient diameter to restore normal blood flow through the artery, and that the artery is not damaged by the ablation process in such a way

that it does not provide a good conduit for blood flow. Through the use of controlled laser light delivery afforded by a transparent optical shield, controlled and consistent ablation of atheromatous plaque and artery tissue was demonstrated using a single fiber shielded device in Section III. The same concepts employed in the design of that single fiber device can be extended to produce a catheter capable of save recanalization of arteries in vivo.

The strategy used to design the angiosurgery catheter was to combine many small craters, all produced by single independently targeted optical fibers, to produce a single large composite hole. This can be accomplished by including an array of fibers together inside an optical shield, and firing them one at a time, in rapid succession.

It is absolutely necessary that the individual craters produced by individual fiber exposures overlap with their nearest neighbors to insure that all of the tissue in the catheter's field of view can be vaporized. It is also necessary to completely cover the forward surface of the optical shield, since a lumen as large as the shield diameter must be created into which the catheter can advance. This allows the shield to remain in contact with the tissue to be vaporized, maintaining controlled light delivery.

Although the multifiber design adds to the complexity of the angiosurgery system and catheter, it contributes some important advantages as well. First, a large lumen can be created in an obstructed vessel using modest powers readily available using argon ion lasers or other continuous laser systems (5W to 10W), while keeping the intensity very high (kilowatts per square centimeter) and allowing for short exposures. The single fiber experiments of Section III indicated that high intensities produced less charring of the tissue lining a crater, and allowed for very short time exposures while remaining above the practical threshold for consistent ablation. Second, sequential firing of the fibers in the array allows a low average power to be used (5W to 10W, reduced by the time the laser is off in between exposures). Since all energy delivered to a lesion must be dissipated by the surrounding tissue, this reduction in average power may be important to reduce thermal damage to the tissue not ablated.

This design also adds the possibility of selective removal of diseased tissue, without unnecessary exposure of blood or undesirable ablation of media underlying an atheroma.

Prototype 8F (2.5mm) multifiber shielded catheters were designed and characterized to demonstrate these design concepts. The findings of those studies will be presented in

the following sections. In addition, a smaller 4.5F (1.5mm) catheter has also been developed for use in smaller vessels [1]. This device employed the same design concepts demonstrated by the larger catheter.

V.3 DESCRIPTION OF THE MULTIFIBER CATHETER

Several 8F (2.5mm outer diameter) multifiber shielded catheters were constructed for use in the following experiments. The distal end consisted of a transparent, rounded quartz shield encasing 19 Spectraguide 422 optical fibers, with core diameters of 105um and a numerical aperture of 0.29.

The quartz shield was formed from a short length quartz tubing with a 3.0mm outer diameter and a 2.0mm inner diameter, closed at one end with a torch to form a hemispherical end. The outer diameter of the shield was then reduced to 2.5mm by grinding and polishing (see Figure V.1).

The output ends of the fibers were polished and mounted rigidly inside the shield in a hexagonal close-packed array consisting of a central, axial fiber, surrounded by inner and outer rings of six and twelve fibers, respectively. The fibers were positioned so that the 19 spots of light exiting the distal output surface of the shield formed an overlapping pattern which completely covered that surface. This required

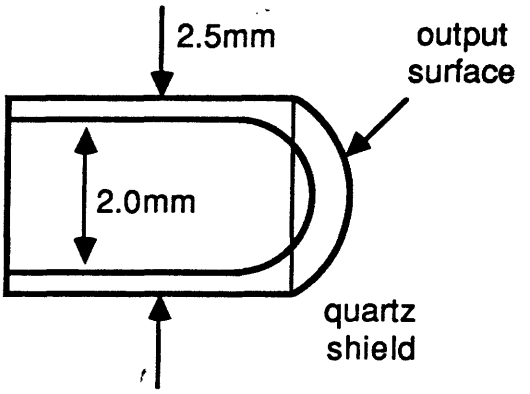

Figure V.1

Schematic diagram of the rounded shield used in the 8F multifiber catheter.

that the fibers be angled, with the inner ring of fibers oriented approximately 7^{o} and the outer ring fibers approximately 15^{o} to the axis of the shield, and spaced approximately 2.0mm from the shield's output surface (see Figure V.2).

Light was coupled into each fiber in such a way that its output beam fully filled the fiber's numerical aperture. Diameters of the light spots created by the exiting laser beam as it intersected the outer shield surface ranged from 800um to 900um in diameter, with the twelve outer ring spots generally being slightly larger than those in the center. A map of the laser spots showing their overlapping pattern was

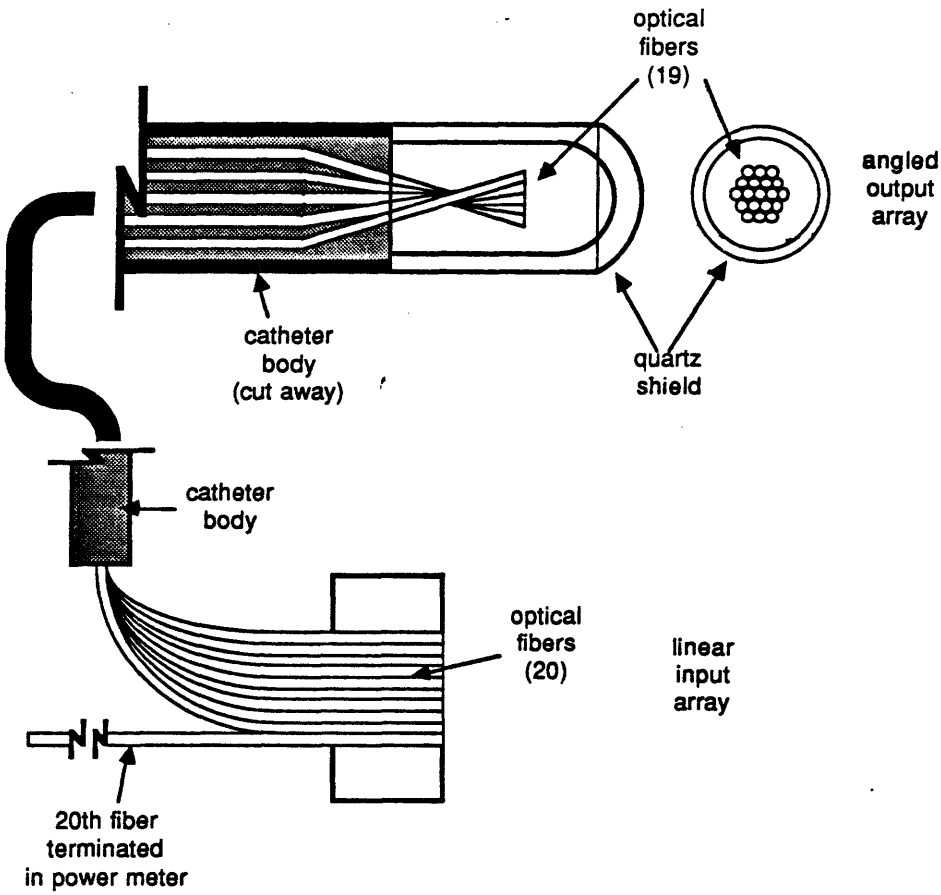

Figure V.2

Schematic diagram of the multifiber shielded catheter, showing the angled orientation of optical fibers inside the optical shield and the linear alignment of the input ends of all optical fibers. The output ends of the fibers are angled, with the inner and outer ring fibers oriented 7^{o} and 15^{o} to the axis of the shield, respectively. Note that an extra twentieth optical fiber is also included in the linear input array to be used to monitor laser power.

produced by imaging the catheter through a dissecting microscope, and is shown in Figure V.3.

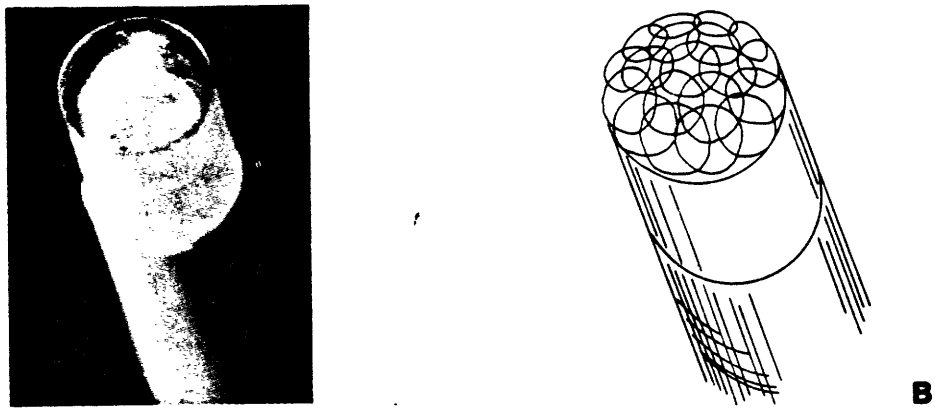

Figure V.3

8F multifiber shielded catheter. A, Photograph; B, Light spot pattern produced by the 19 optical fibers as imaged through a dissecting microscope. Note full coverage of the optical shield.

The input ends of the optical fibers were polished and mounted rigidly in a linear array to allow rapid sequential alignment with a linear translator under computer control (see Figure V.3). A twentieth calibration fiber was also mounted in the array, but terminated outside the shield, to use in measuring delivered power. The body of the catheter was formed by a 3m length of 2.5mm diameter PVC tubing.

V.4 THE LASER ANGIOSURGERY SYSTEM

The entire ablation system can be thought of as divided into three components: the multifiber laser catheter, the optical components of the system, and the control components of the system. Integrated together, they form an reliable and flexible environment for the controlled ablation of tissue.

V.4.1 Optical Subsystem

Figure V.4 diagrams the optical path of the laser angiosurgery system.

Blue-green light from a Coherent Innova 20 or Coherent Innova 100 argon ion laser was used as the laser source for all experiments. When running all lines, these lasers are capable of 20W maximum output, TEM_{00} lowest order Gaussian mode, with most of the power at 488nm and 514nm.

The output of the laser was first focused into a 20m length of 50um core, graded index optical fiber cable with a numerical aperture of 0.21. Its output was collimated and focused sequentially onto each input end of the catheter's fibers with a lens system matching their numerical aperture of 2.9. This coupling scheme helped excite high order modes in the optical fibers to produce maximally diverging output beams with fairly uniform intensity profiles. A typical optical

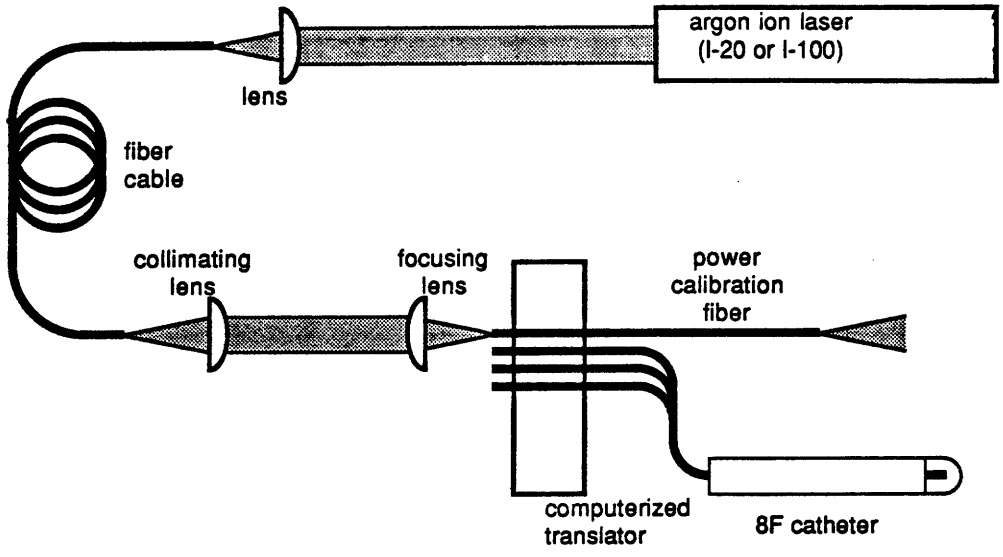

Figure V.4

Schematic diagram of the laser angiosurgery optical path. The intermediate fiber cable is used to help excite high order modes in the optical fibers of the catheter, producing maximally diverging beams.

fiber output is shown in Figure V.5, as measured by a Reticon linear diode array. In addition, the fiber cable provided a means for locating the laser outside of the room in which the procedure was taking place, thus isolating the operators from the noise produced by the laser, freeing the space in the procedure room for other uses, and making it possible for the

same laser to be used in multiple procedure rooms without the need to move it.

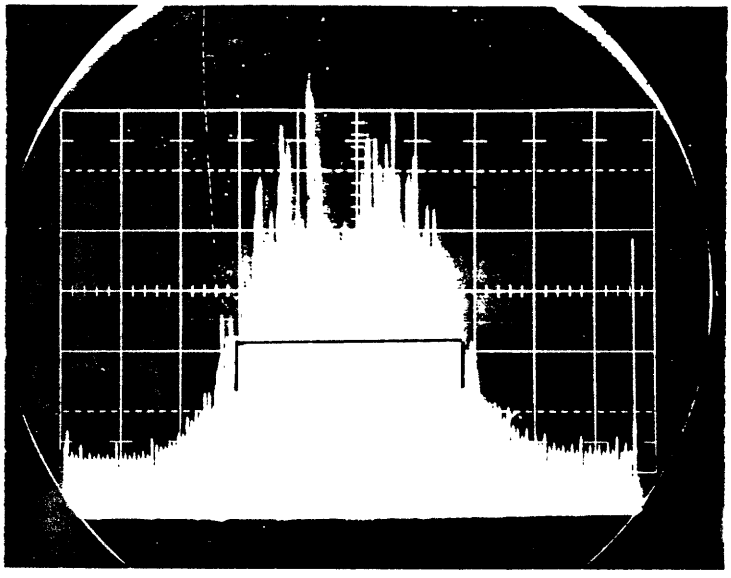

Figure V.5

Reticon linear diode array map of the intensity profile of the center fiber of a 8F multifiber shielded catheter. A diameter of 900um is indicated at the 1/e point. Approximately 85% of the laser's energy will be inside this diameter.

V.4.2 Control Subsystem

Figure V.6 diagrams the control components of the laser angiosurgery system.

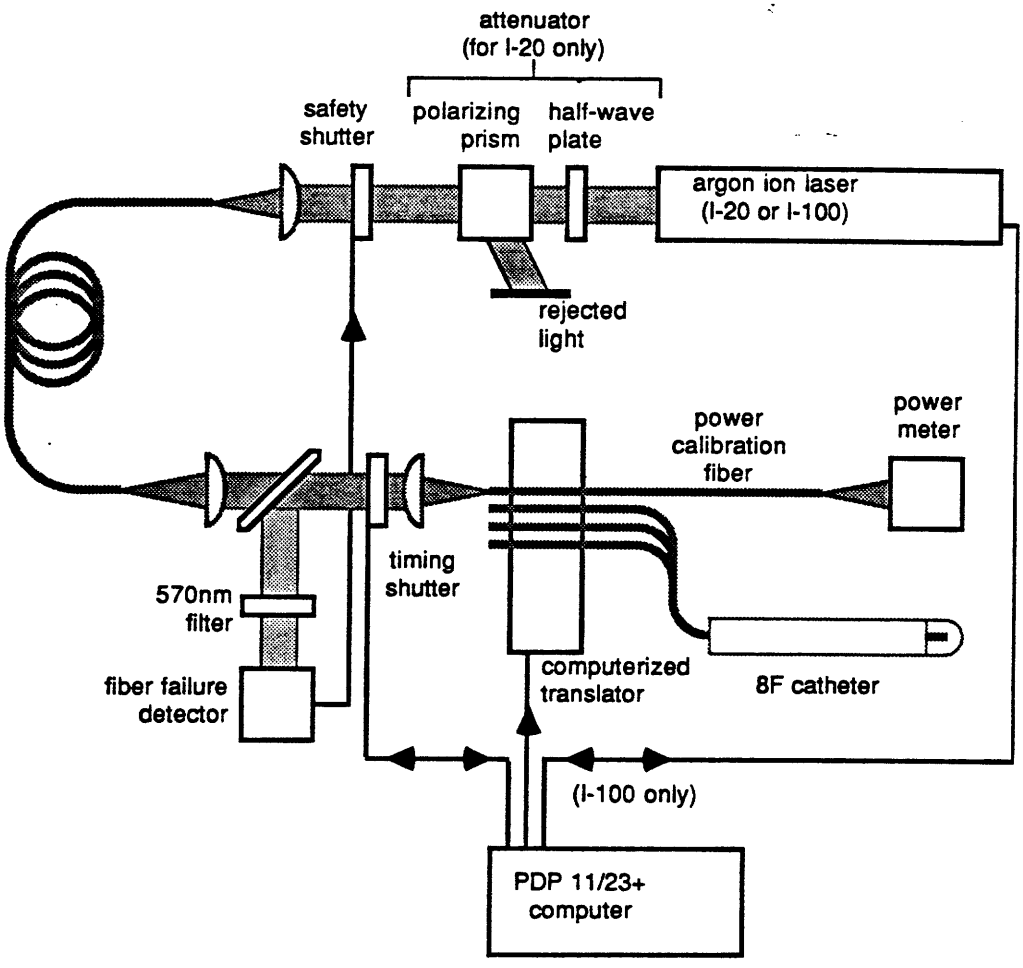

Figure V.6

Schematic diagram of the control components of the laser angiosurgery system.

When using the Innova 20, the light was first passed through an attenuator consisting of a halfwave plate and a polarizing prism. By rotating the halfwave plate, the polarization of the laser beam passing through it could be varied, thereby changing the fraction of the light rejected by the po-

larizing prism. The laser power could be adjusted in this way from nearly 100% transmission of the laser output to a few tens of milliwatts, without deviation or degradation of the laser beam which might compromise optical alignment.

The Innova 100 laser has the means of regulating its output power from 0.1W to 20.0W without the need for an attenuator. In this case, the computer communicated directly with the laser to set and monitor its output power.

Laser power transmitted to the output face of the optical shield was measured using a calibration fiber aligned with the other 19 fibers at the proximal end of the catheter but terminated in a thermal power meter accurate to $\pm$0.1W. The power striking the tissue was about 8% lower due to reflections at the shield surfaces.

Exposure times were controlled by a computer activated Uniblitz SD-1000 shutter placed in the light path before the proximal end of the catheter. Exposure times were accurate to $\pm$2ms. Individual fibers were sequentially aligned by a Unidex II linear translator under computer control. This translator can accurately locate the input end of a fiber with 4um resolution and $\pm$2um accuracy, with a maximum travel rate of 20cm/s. During operation, the computer instructed the translator to align a particular fiber by translating to a

stored location and then activated the shutter to expose, or "fire", the fiber. Unless otherwise noted, there was an interval of approximately 170ms between successive fiber exposures. Normally, all 19 fibers were fired sequentially to form a "round".

A failure detection system was designed to detect the unlikely failure of fibers due to breaks, misalignment, or contamination of the output end inside the optical shield. Such failures may endanger the operator or patient by allowing uncontrolled laser light escape from the catheter or by producing pressures within the shield sufficient to fracture it.

When an optical fiber fails, the laser light reaching the site of the failure generates incandescent light at wavelengths other than the 488nm and 514nm wavelengths of the argon ion laser. A certain percentage of this light is trapped within the optical fiber and conducted back to the input end where it is collimated. A fraction of this light is picked off by a glass plate acting as a beam splitter and directed through a 570nm long pass filter to a detector. A fiber failure such a break generates enough light at the detector to produce a signal approximately ten times the background. The failure detection circuit has been designed to close a safety shutter placed directly in front of the laser

any time the signal is more than twice background. Time response of the system has been measured at 15-20ms, limited by the response of the mechanical shutter. This response time is adequate to discontinue the firing of a single fiber under most conditions, and will always prevent the firing of any fiber after a failure.

The entire ablation system was controlled by a PDP 11/23+ microcomputer running Digital Equipment Corporation's RSX-11M multitasking, multiuser, real-time operating system. A highly optimized, highly flexible pushbutton program, called WILBUR, was written specifically to run the ablation system. It was designed to be "friendly" and robust enough to be used by medical or research personnel with a minimum of computer experience, flexible enough to adapt to the changing demands that experiments demanded, yet fast to use to allow the operator to operate the system in an in vivo environment where quick response is required. Figure V.8 shows the WILBUR screen at top level and during the firing of a round.

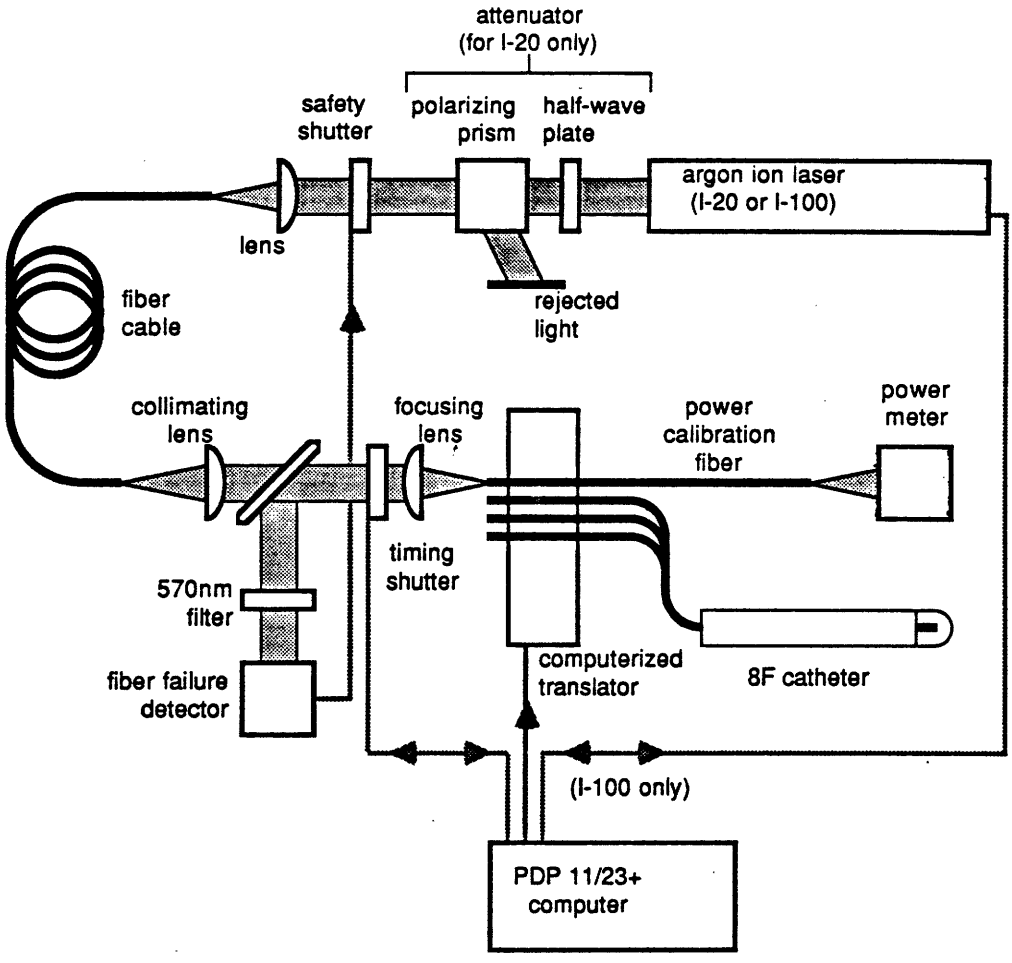

Figure V.7

Schematic diagram of the full laser angiosurgery system.

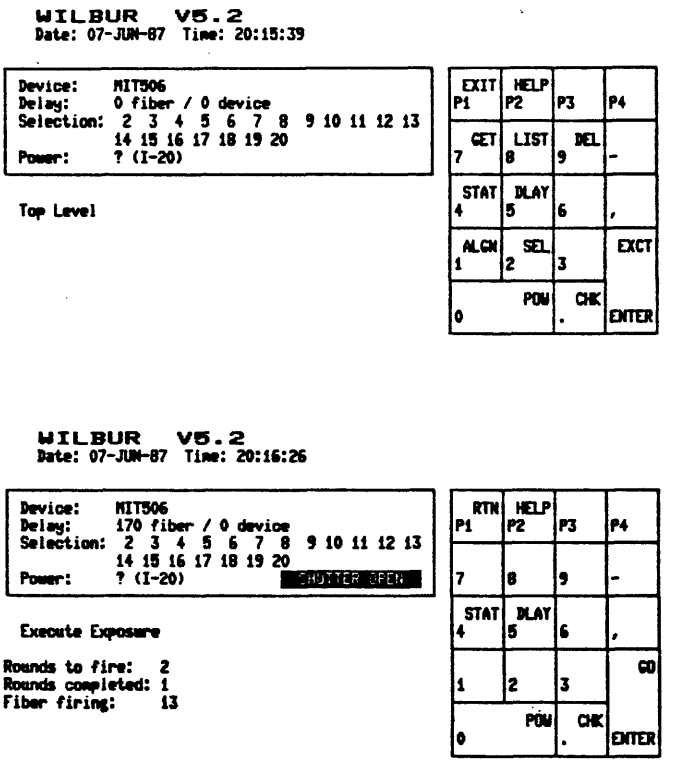

Figure V.8

Screen dump images of the WILBUR laser angiosurgery control program at top level and during firing. Note that all important operating parameters are displayed continuously, except laser power which unavailable when using an I-20 laser. Program functions are accessed through the keypad of a VT100 terminal, which is drawn on the right had side of the screen.

REFERENCES

1. B.J. Costello, "Engineering of a Multifiber Catheter for Coronary Laser Angiosurgery", Bachelor's thesis, Massachusetts Institute of Technology, 1986.

SECTION VI

MULTIFIBER SHIELDED CATHETER BEHAVIOR

VI.1 OVERVIEW

A multifiber optically shielded catheter of the type described in Section V was constructed and used to produce composite holes in atheroma to confirm that the design concepts are valid, and to characterize the rate of tissue ablation, and the size and shape of composite holes in a way similar to that used in the single fiber experiments. A more detailed study of the ablation yields, peripheral damage produced by tissue ablation, and thresholds for ablation are presented in the next section.

VI.2 EXPERIMENTAL METHODS

The catheter used in the following experiments was an 8F (2.5mm outer diameter) multifiber shielded catheter and laser angiosurgery system described in Section V.

The performance of the catheter was evaluated by firing each of the 19 fibers in succession one or more times to produce composite holes in opened samples of fresh postmortem fibrous atherosclerotic aorta immersed in saline or blood with blue-green (all lines) argon ion laser light. At least three composite holes were produced in a single tissue sample for each combination of ablation parameters of laser power, exposure time, and number of rounds. In all cases, the shield was brought into contact with the intimal surface with a constant force of 2 ounces (0.6N) to displace the fluid between the shield and the sample. The optical shield was cleaned after the production of each composite hole.

Composite hole diameters were measured using a dissecting microscope with an eyepiece reticle. Composite hole depths were measured using a histological microscope which could be focused first at the tissue surface and then at the hole bottom, and the travel of the microscope stage measured. Measured hole diameters and depths are accurate to $\pm$25um.

As in the single fiber study, an ablation velocity (v) was computed from measured values of composite hole depth (l) and exposure time (t) by the ratio: $v = \Delta l/\Delta t$. In addition, for composite holes produced with multiple rounds, an incremental advancement (i), or the incremental increase in

composite hole depth with the number of rounds (n), was computed as the ratio: $i = \Delta l/\Delta n$.

VI.3 RESULTS

Three separate experiments were performed to characterize the ablation process under varying ablation parameters and conditions. In all cases, mean composite hole depths were computed and reported along with typical standard deviations for each set of ablation parameters.

VI.3.1 Variation in Ablation Rate with Varying Power

The existence of a power dependence on the rate of tissue ablation and composite hole formation in a single round was examined by producing composite holes with single rounds from the multifiber shielded catheter. Composite holes were made with laser powers of 5.0W, 7.5W, and 10.0W using a number or different exposure times.

With appropriately long exposure times, 2.5mm composite holes with good crater overlap could be produced at 5.0W, 7.5W, and 10.0W. The structure of the composite hole depended on the sequence in which the individual fibers were fired. If the firing order was random, the resulting composite hole had a very uneven bottom surface. If the sequence was outer ring

first, then inner ring, then center fiber, the result was a deep hole approximately 2mm in diameter surrounded by a shallow annular ring extending out to the 2.5mm shield diameter. If the sequence was center fiber first, then inner ring, then outer ring, the resulting hole had a smooth, uniform bottom with a constant depth. Typical composite holes are shown in Figure VI.1. All composite hole measurements reported were made using the latter firing sequence.

The composite holes produced were relatively free of char. Generally, cleaner composite holes with less char were produced when using higher powers and shorter exposure times.

The resulting composite hole depths are plotted versus exposure time in Figure VI.2, and thus represent a time history for composite hole formation. For all laser powers, the composite hole increased linearly with exposure time, indicating a constant ablation velocity. In all cases, ablation velocity increased with laser power. Ablation velocities for all laser powers are listed in Table VI.1.

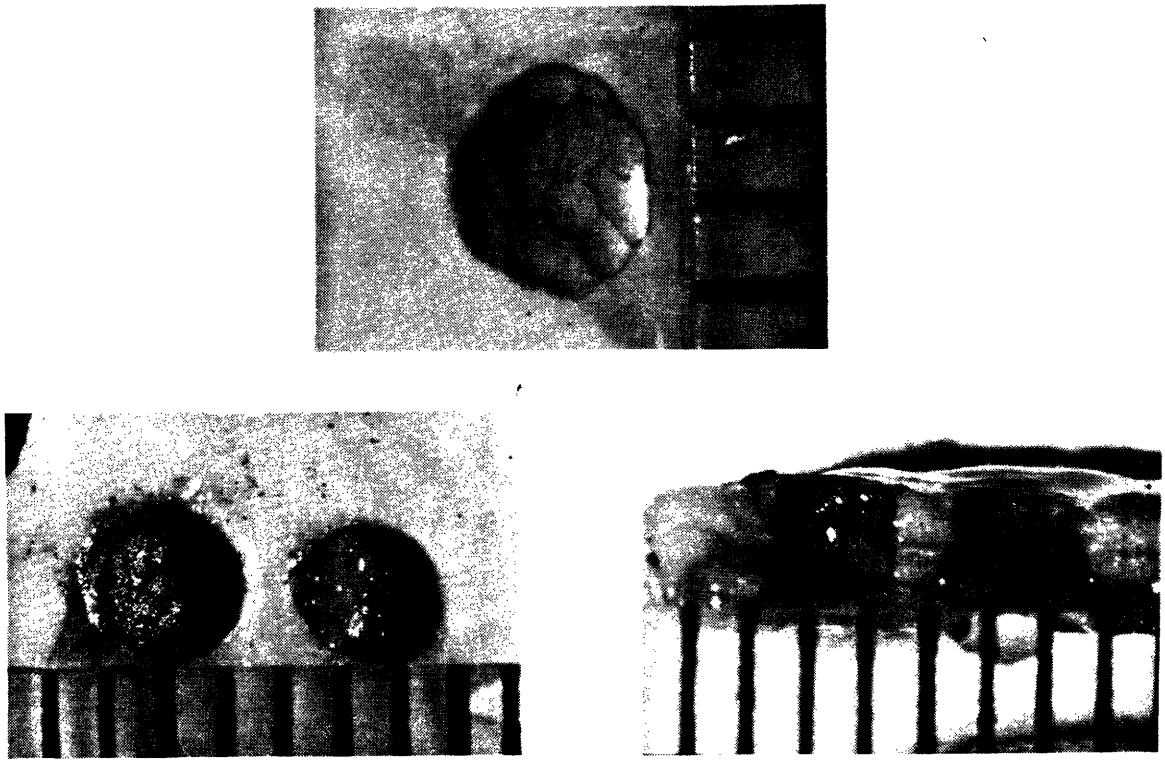

Figure VI.1

Composite holes produced using the multi-fiber catheter. A, 14W/50ms/1round in a blood field; 10W/100ms/4rounds and 14W/72ms/4rounds (left and right) in a saline field looking, B, down on the luminal surface and, C, in cross section. Scale divisions are in millimeters.

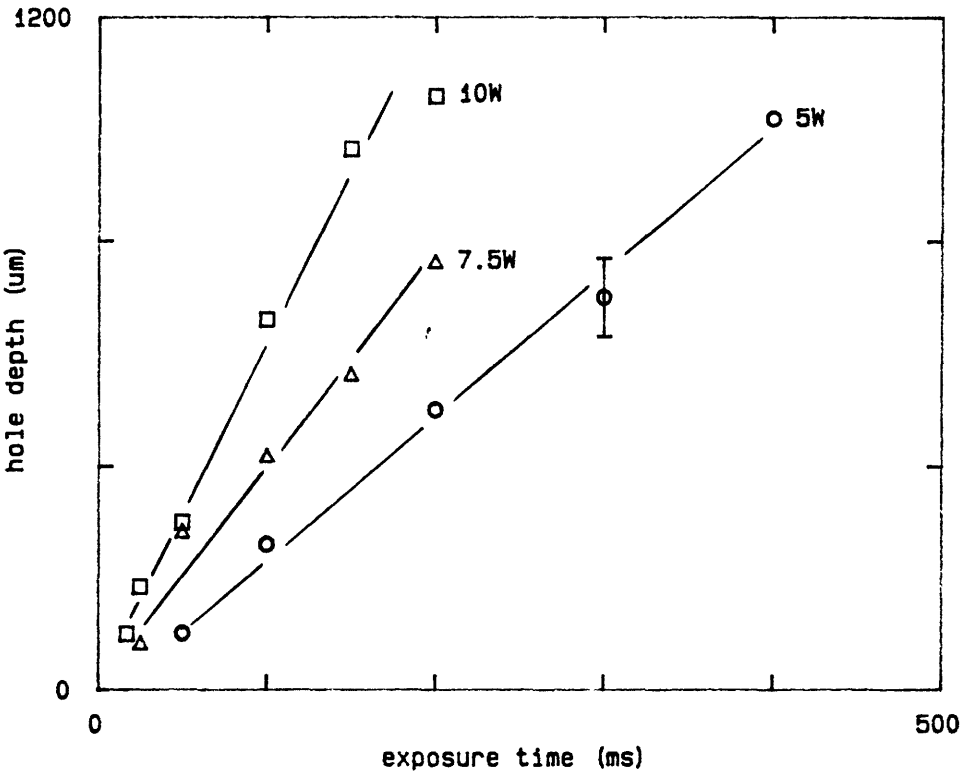

Figure VI.2

Composite hole depth versus exposure time for single rounds with various laser powers. A typical error bar is shown.

laser power (W)	ablation velocity (mm/sec)
5.0	2.5
7.5	3.8
10.0	6.4

Table VI.1

Ablation velocities for three laser powers using the multifiber catheter.

VI.3.2 Variation in Ablation Rate with Repeated Exposures

The second set of experiments was designed to evaluate the advancement of the catheter when successive rounds are fired, which is the intended mode of operation. Composite holes were produced using 7.5W/25ms, 7.5W/50ms, 10W/12ms, and 10W/25ms exposures for varying numbers of rounds. The higher powers and shorter exposure times were selected since the previous experiment showed that shallow composite holes with less char were produced at these values.

The resulting composite hole depths are plotted versus the number of exposures in Figure VI.3. For all combinations of laser power and exposure time, the catheter was found to advance into the sample under two ounces of force as tissue was removed. Composite hole depth increased linearly with the

number of rounds. Incremental advancement per round for each combination of power and time is listed in Table VI.2.

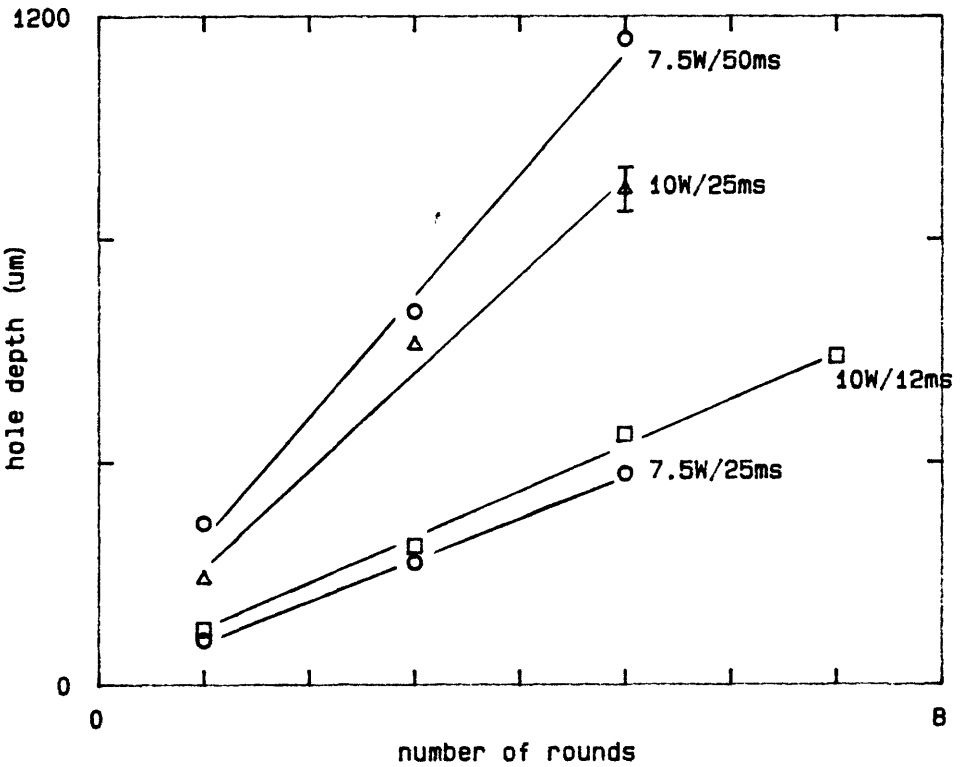

Figure VI.3

Crater depth versus number of exposures for photon doses of 10W/35ms and 10W/63ms and a spot size of 500um. A typical error bar is shown.

laser power and exposure time (W/ms)	incremental advancement (um/round)
7.5/25	75
7.5/50	226
10.0/12	84
10.0/25	190

Table VI.2

Incremental advancement values for several laser power and exposure time combinations using the multifiber catheter.

VI.3.3 Selective Removal of Tissue with a Multifiber Catheter

As a final experiment, the ability of the multifiber catheter to selectively remove portions of tissue in its field of view was investigated by firing various groups of fibers in the array in a single round. Examples of the removal patterns obtained are shown in Figure VI.4.

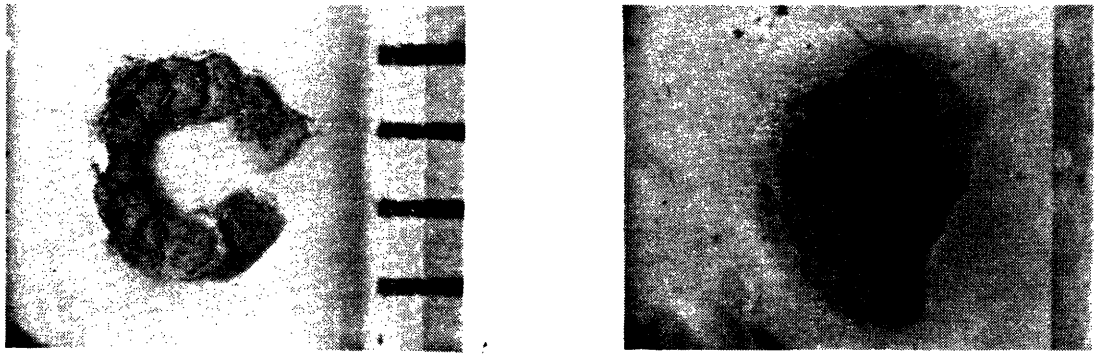

Figure VI.4

Selective removal of plaque using the multifiber catheter. Composite holes were produced by firing selected fibers in the 19 fiber array. A, annulus; B, semicircle. Scale divisions are in millimeters.

VI.4 DISCUSSION

As long as exposure times were longer than the practical thresholds found in the single fiber experiments, complete overlap of the individual craters formed relative clean composite holes, indicating that the design concepts proposed for multifiber shielded catheters are valid. The small variability in composite hole depth shows that controlled, predictable ablation is possible with the multifiber catheter, and that safe restoration of a large lumen is possible.

Composite hole depth as a function of exposure time (Figure VI.2) again shows that in each case, depth increased

linearly with exposure time up to the point of perforation. A constant ablation velocity was indicated, as it was in the single fiber experiments. The velocities are higher by approximately a factor of two than those measured for single fiber exposure. This increase is primarily due to the overlap of the laser light spot of each optical fiber with those of its nearest neighbors (approximately 61% on average), producing an overall larger photon dose at a given tissue site. The volume of tissue removed by a given laser power and spot size were about the same in both single and multifiber devices.

The linear increase in composite hole depth as a function of the number or rounds (Figure VI.3) indicates that the ablation process is additive, as it was for single fiber exposures, and that catheter advancement is constant with the number of rounds.

The final experiments showed that the multifiber catheter is capable of irradiating and removing only a fraction of the tissue in its field of view, demonstrating the ability to selectively remove only tissue deemed to be atheroma. This ability can be combined with a diagnostic system to provide a further safeguard against perforation, even at the bend in a vessel, and to avoid irradiation of blood when treating a vessel that is not totally occluded.

SECTION VII

MULTIFIBER CATHETER ABLATION EFFICIENCY

VII.1 OVERVIEW

A multifiber optically shielded catheter of the type described in Section V was used to produce composite holes in atheroma to investigate how the efficiency of the ablation process (through a defined "ablation yield") varies with ablation parameters and conditions. Both power and exposure time thresholds for ablation were identified. The extent and character of peripheral damage was examined histologically under varying conditions as well.

Results of these experiments give insight into the laser/tissue interaction. The consequences of results are discussed along with a comparison of the single fiber and multifiber ablation characteristics and comparison of the multifiber ablation results to our ablation model.

VII.2 EXPERIMENTAL METHODS

The catheter used in the following experiments was an 8F (2.5mm outer diameter) multifiber shielded catheter and laser angiosurgery system described in Section V.

The performance of the catheter was evaluated by firing each of the 19 fibers in succession one or more times to produce composite holes in opened samples of fresh postmortem fibrous atherosclerotic aorta immersed in saline or blood with blue-green (all lines) argon ion laser light. Except where indicated, three composite holes were produced for each combination of ablation parameters of laser power (P), exposure time (t), and number of rounds (n). The results of the previous section established that a firing sequence of center fiber followed by successive fibers in the inner ring and outer ring, in order, produced the most uniform composite holes. That sequence was used for each round in this study as well. Unless otherwise stated, the shield was brought into contact with the intimal surface with a constant force of 2 ounces (0.6N) to displace the fluid between the shield and the sample. Unless otherwise noted, the optical shield was cleaned after the production of each composite hole.

Composite hole diameters (d) were measured using a dissecting microscope with an eyepiece reticle. Composite hole

depths (l) were measured using a histological microscope which could be focused first at the tissue surface and then at the hole bottom, and the travel of the microscope stage measured. Measured hole diameters and depths are accurate to ±25um.

For each combination of ablation parameters, two composite holes were randomly selected for histological evaluation. Each was fixed in formalin, embedded in paraffin, serially sectioned, and hematoxylin and eosin stained to determine the degree of peripheral damage. The extent of damage was measured with an eyepiece reticle at 40x or 100x magnification to ±10um accuracy.

To compare tissue removal with different ablation parameters, an ablation yield (Y), was computed by dividing the volume of tissue removed by the total laser energy delivered: $Y = \pi(d^2/4)l/(19Ptn)$. From a knowledge of the ablation yield, the tissue volume removed with a prescribed photon dose can be calculated.

VII.3 RESULTS

Five separate experiments were performed to evaluate the variation in ablation yield and extent of peripheral damage with varying tissue samples, ablation parameters, and ablation conditions. In all cases, mean composite hole diameters, depths, and/or ablation yields were computed and reported

along with standard deviations for each set of ablation parameters.

VII.3.1 Variation in Ablation Yield in Different Tissue Samples

The reproducibility of ablation yield was examined by producing composite holes using a photon dose of 10W/50ms/3rounds (28.5J) in a number of different arterial tissue samples. Table VII.1 lists the mean composite hole diameters, depths, and ablation yields for each of seven samples ranging from relatively normal arterial wall to severely complicated atherosclerotic lesions. Calcified plaque was not included because argon ion laser light is not effective in removing calcified lesions [1].

For all tissue samples, the composite hole diameter was 2.50 ± 0.09mm. This equality of composite hole diameter and catheter diameter was born out throughout all experiments, which indicates that a composite hole diameter of 2.50mm can be assumed and the ablation yield can be used to specify composite hole depth by the relation: $l = Y(19Ptn)/(\pi d^2/4) = (3.87)YPtn$ for l in millimeters.

A total of 10 composite holes were produced in sample 1, a fibrous plaque of the type used in all subsequent experiments. The standard deviation of ablation yield in this

MULTIFIBER CATHETER ABLATION EFFICIENCY RESULTS

tissue type	hole diameter (mm)	hole depth (um)	ablation yield (mm^3/J)
fibrous	2.51±0.11	895±70	0.155±0.012
normal	2.48±0.10	926±50	0.158±0.009
normal	2.45±0.18	1013±100	0.167±0.017
fibrous	2.50±0.09	943±64	0.161±0.015
complicated	2.48±0.07	1000±72	0.167±0.010
complicated	2.55±0.18	841±67	0.152±0.015
fatty	2.53±0.19	1333±231	0.233±0.040

Table VII.1

Mean composite hole diameters, depths, and ablation yields for seven tissue samples. Variations are plus or minus one standard deviation. All exposures were delivered at a photon dose of 10W/50ms/3rounds.

sample was ±8%, indicating the variation to be expected within a single fibrous tissue sample. The standard deviation of yield in all tissue types collectively was ±16%, indicating the variation to be expected across many tissue samples, even if no knowledge of the tissue type is available. Note that most of larger variation across tissue samples is due to an increased ablation yield in fatty samples.

VII.3.2 Variation in Ablation Yield and Damage with Varying Power

The existence of a power dependence on ablation yield and extent of damage was examined by producing composite holes using a constant energy of 47.5J delivered in 5 rounds. The laser power was varied from 1W to 14.7W, and the exposure time was varied from 500ms to 34ms to compensate for varying power.

The composite holes produced were relatively free of char at all power levels, with some noticeable increase in char production at lower powers (less than 3.5W). Histology showed a 100-200um layer of vacuolation and hypereosinophilia surrounding the hole (Figure VII.1). A region beyond that with an average thickness of 950um showed collagen alteration typified by an increase in unstained space without hypereosinophilia. The stained material was more fibrous in appearance, aligning itself with the vessel surface. The structure of the arterial wall did not appear to be compromised by this change. Occasional splits in the media were observed up to several millimeters from the hole.

The resulting ablation yields are plotted in Figure VII.2. For powers of 3.5W and above, the ablation yield was constant at $0.156mm^3/J$. The yield fell off rapidly for laser powers less than 3.5W, falling to zero at 1W. Histology also

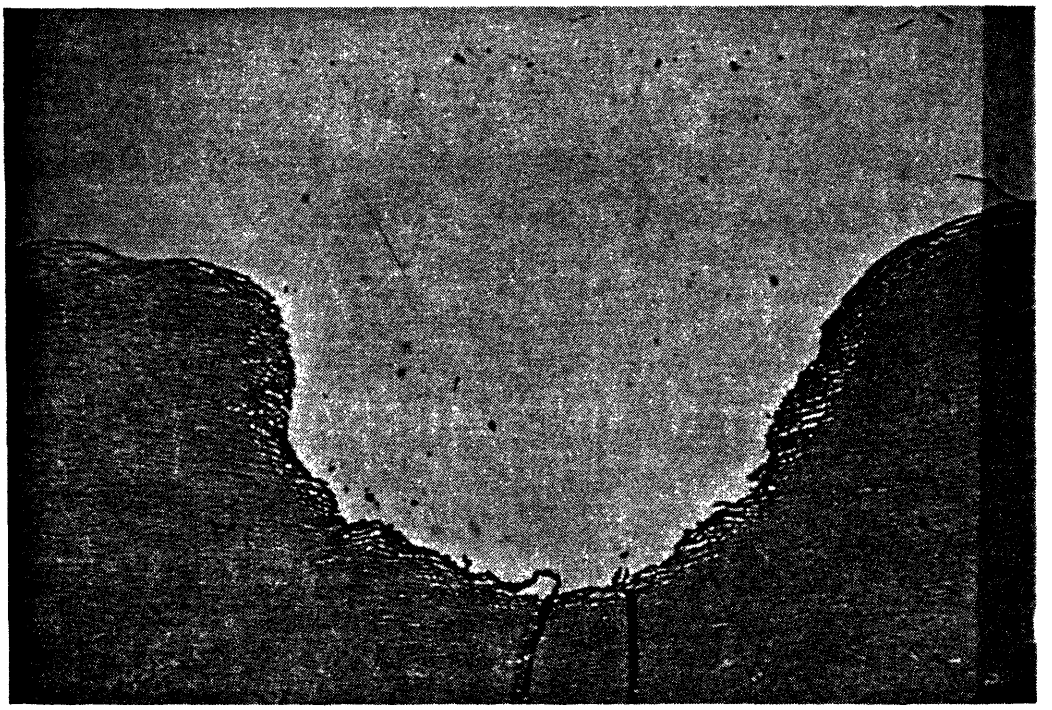

Figure VII.1a

Low magnification of a typical histological section through a 2.5mm diameter composite hole. Photon dose for this hole was 8W/72ms/5rounds.

showed that there was little difference in the amount of peripheral damage produced with laser powers over 3.5W. The volume of tissue involved by vacuolation, as well as the degree of hypereosinophilia and collagen alteration, remained roughly constant throughout the experiments.

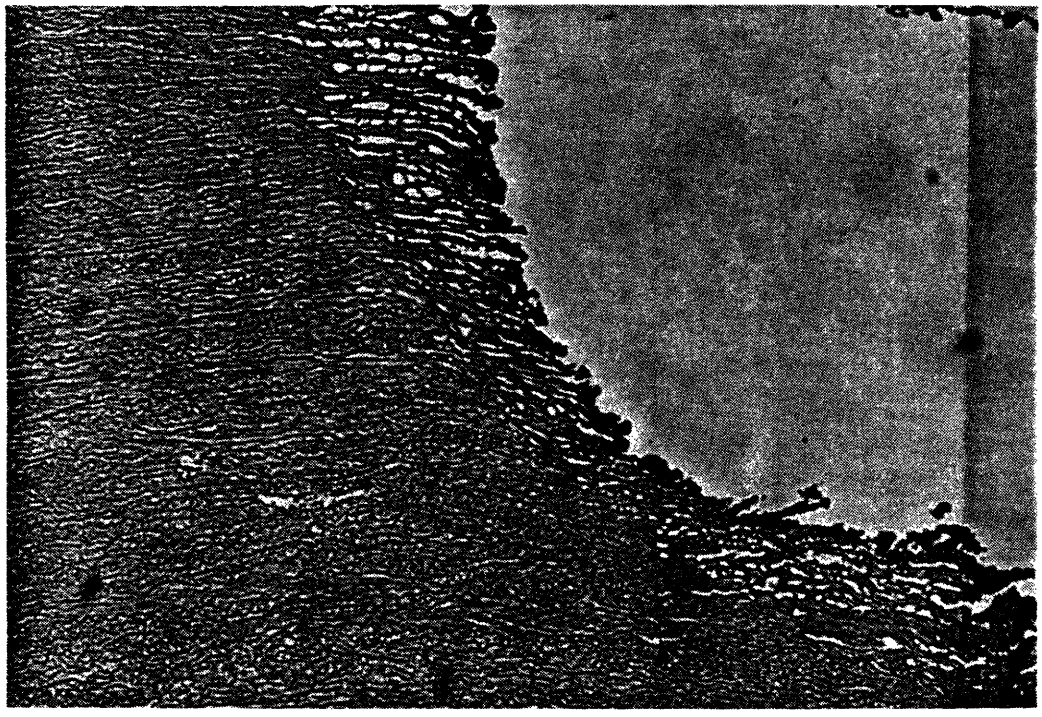

Figure VII.1b

High magnification of a section of the hole shown in Figure VII.1a.

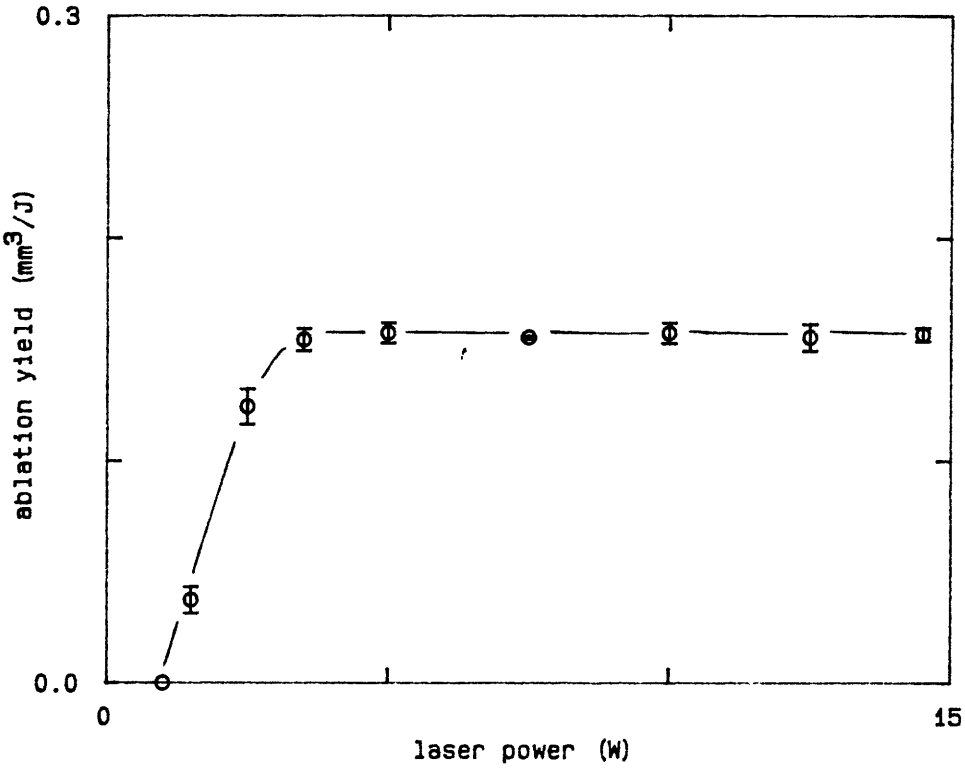

Figure VII.2

Ablation yield versus laser power. All photon doses were delivered at an energy of 47.5J. Number of rounds was constant at 5.

VII.3.3 Variation in Ablation Yield and Damage with Varying Exposure Time

The existence of an energy dependence on ablation yield and extent of damage was examined by producing composite holes using a constant energy of 28.5J delivered at 10W. The

exposure time was adjusted from 9ms to 150ms to vary the energy per round (or likewise, per crater), and the number of rounds ranged from 1 to 17 to compensate for varying exposure time.

The resulting ablation yields are plotted in Figure VII.3. For exposure times of 17ms and above, ablation yield was constant at $0.157mm^3/J$. The yield fell off rapidly for exposure time less than 17ms, falling to zero at 10ms. No significant variation in damage could be detected on histological analysis of composite holes produced with exposure times over 17ms.

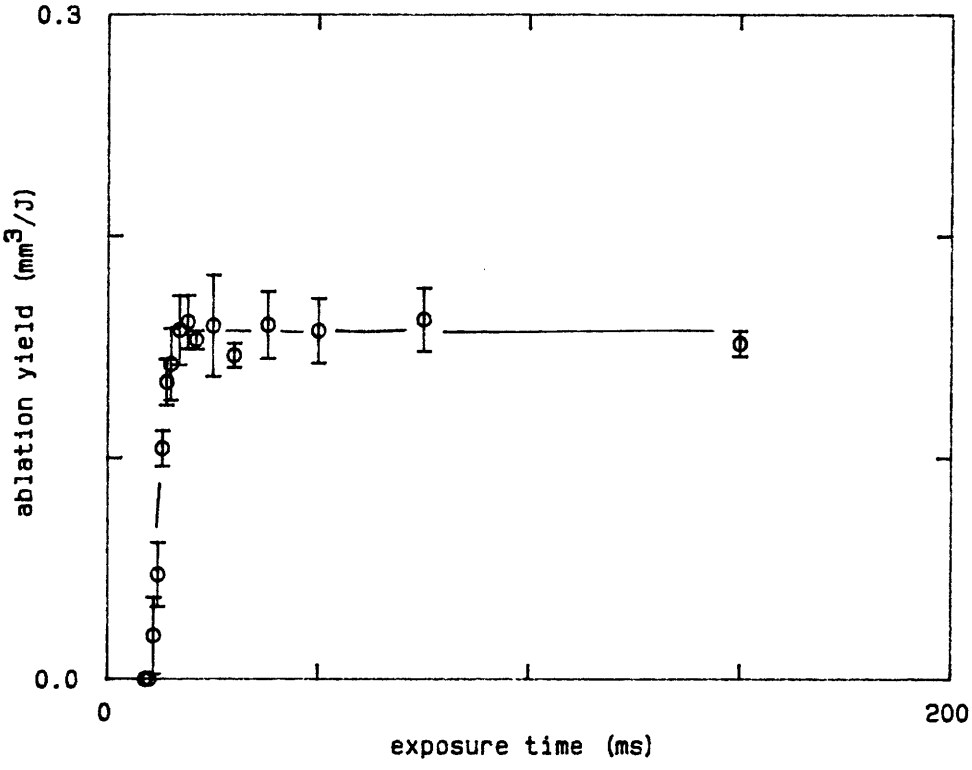

Figure VII.3

Ablation yield versus exposure time. All photon doses were delivered at an energy of 28.5J. Laser power was constant at 10W.

VII.3.4 Variation in Ablation Yield with Varying Advancing Force

To investigate the effect of varying the force used to advance the catheter into the forming composite hole, composite holes were produced using a photon dose of 10W/50ms/3rounds (47.5J). The advancing force was varied from

0.14N (equivalent to 0.5 ounces) to 0.83N (equivalent to 3.0 ounces).

The resulting ablation yields are plotted in Figure VII.4. The ablation yield increased linearly with increasing advancing force from a value of $0.101mm^3/J$ at 0.14N to $0.205mm^3/J$ at 0.83N.

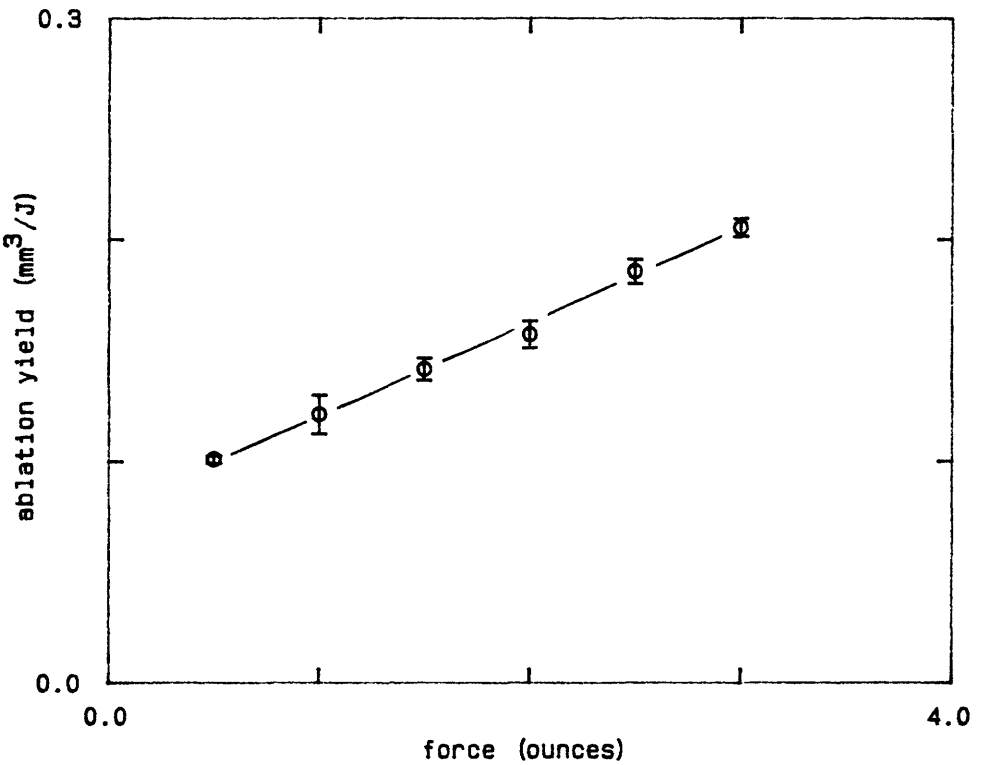

Figure VII.4

Ablation yield versus advancing force. All exposures were delivered at a photon dose of 10W/50ms/5rounds.

VII.3.5 Variation in Ablation Yield and Damage with Varying Delay Times

The effect of varying inter-fiber delay times on the ablation process was investigated by pausing between the firing of each fiber to allow the tissue to cool. Composite holes were produced using using a photon dose of 10W/50ms/3rounds (47.5J), with inter-fiber delays from 170ms to 4.2s.

The resulting ablation yields are plotted in Figure VII.5, and the thickness of the layers of vacuolation and collagen alteration are plotted in Figure VII.6. The ablation yield was constant at $0.154mm^3/J$ for all delay times, and the thickness of the vacuolation layer remained constant at 150um for all delay times. The thickness of the layer of collagen alteration remained constant at 1045um for delay times less than 1.4s, but decreased gradually for delay times of 1.4s and above.

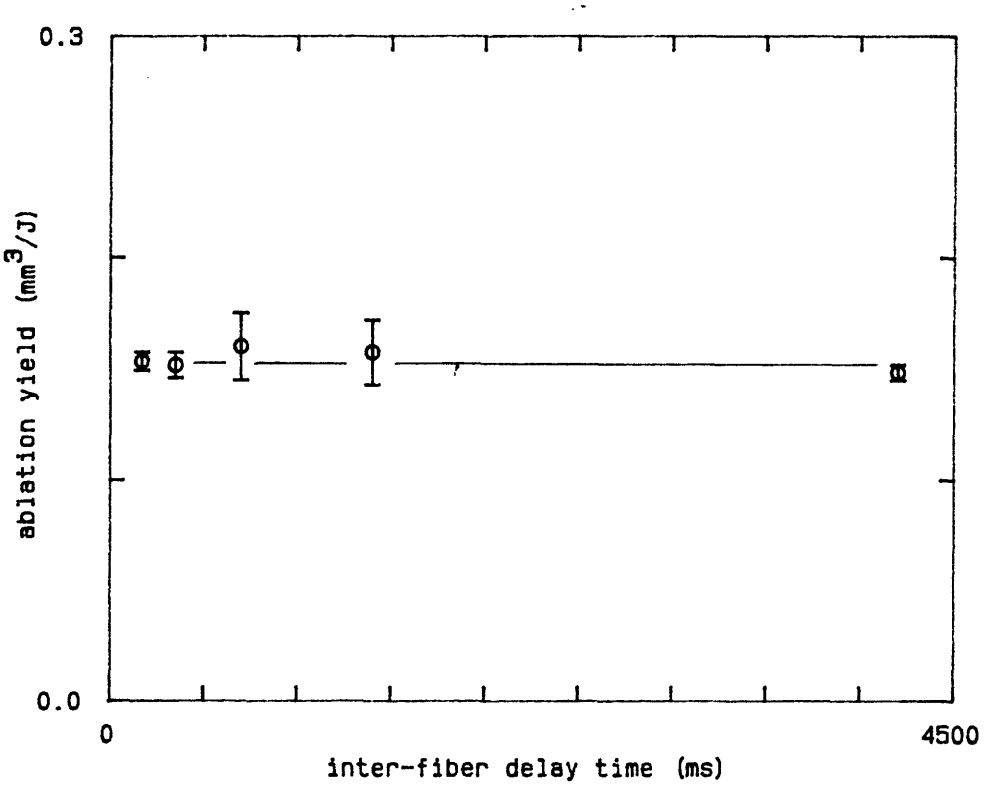

Figure VII.5

Ablation yield versus delay time. All exposures were delivered at a photon dose of 10W/50ms/5rounds.

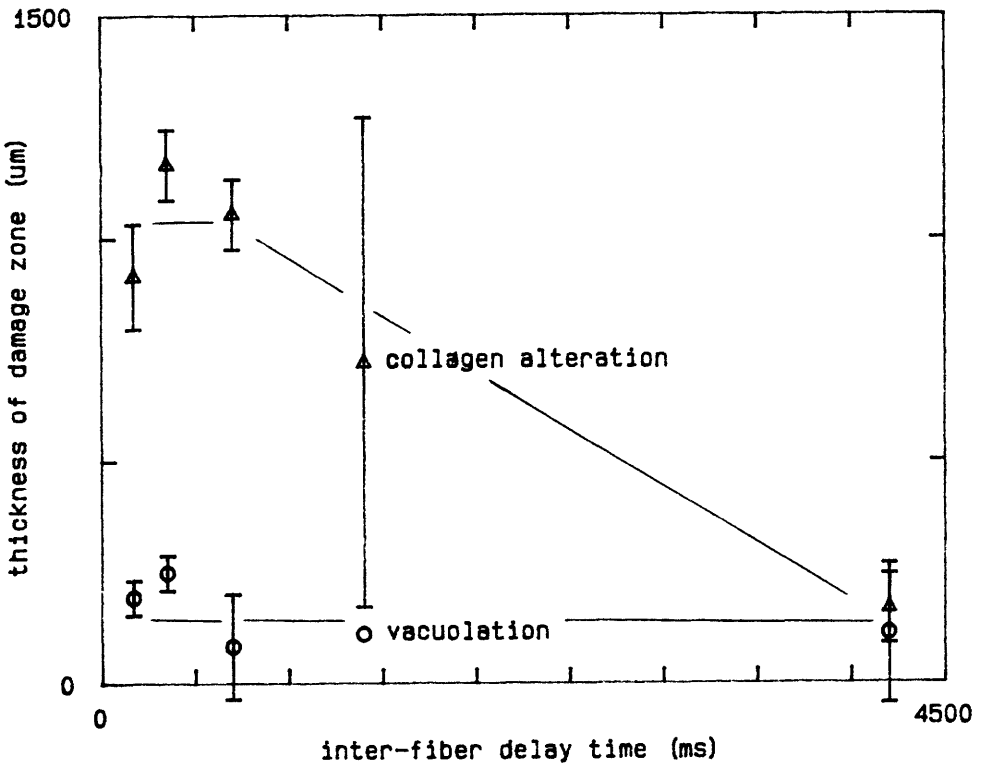

Figure VII.6

Thickness of vacuolation and collagen alteration layers versus delay time. All exposures were at a photon dose of 10W/50ms/5rounds.

VII.3.6 Variation in Ablation Yield with Catheter Usage

The consistency of ablation yield and the effect of repeated catheter use was examined by repeatedly delivering photon doses of 10W/30ms/2rounds (11.4J) to produce many composite holes. A single, newly constructed catheter was

used for the entire study, with no cleaning of the shield between firings.

The resulting ablation yields are plotted in Figure VII.7. Ablation yield was constant at $0.160mm^3/J$ over the entire experiment, essentially equal to the average yield of the previous experiments. After the experiment was completed, the output surface of the shield appear frosted or ptted, with small points of char embedded slightly below the shield's surface.

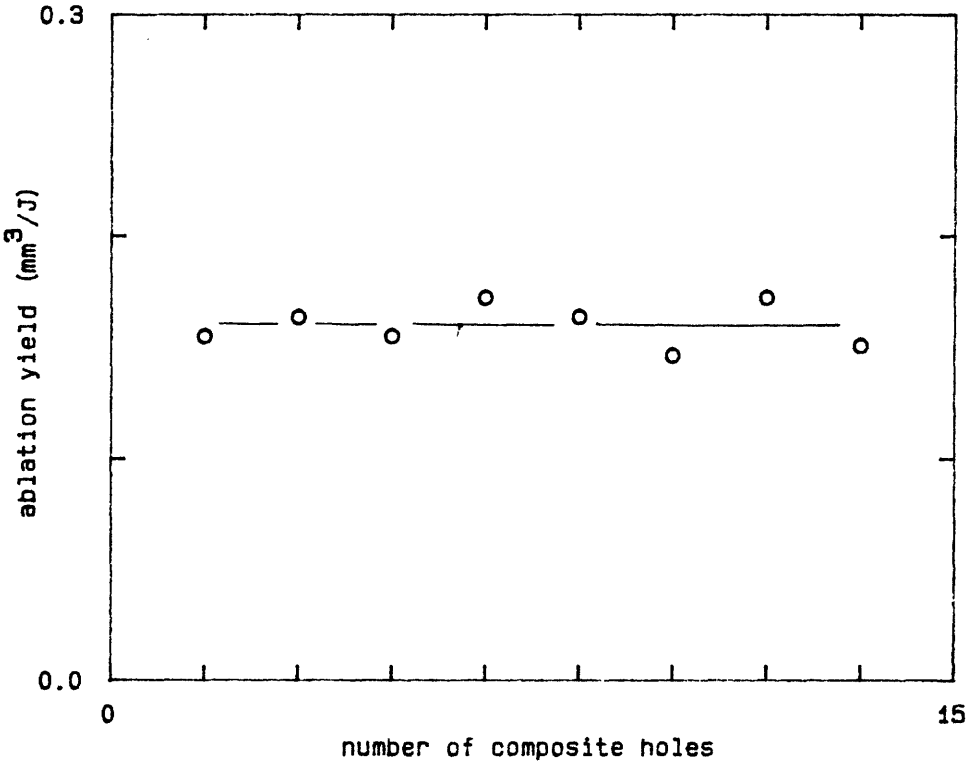

Figure VII.7

Ablation yield versus number of exposures. All exposures were delivered at a photon dose of 10W/30ms/2rounds.

VII.4 DISCUSSION

The small variability in composite hole depth and ablation yield over different tissue types illustrates the consistency of laser ablation using a precisely controlled photon dose. This precise dosimetry could not be possible without

the controlled light delivery provided by the optical shield concept. This consistency also reinforces the validity of subsequent results, and their applicability to a variety of arterial lesions. Even if the exact composition of the target lesion is not known, the volume of tissue removed by a specific amount of delivered energy can be accurately predicted.

The results of the experiment which varied laser power (Figure VII.2) illustrate the existence of a power threshold for tissue ablation. For powers less than 1W, energy was not delivered to the tissue as fast as thermal diffusion took it away. The tissue may have been heated, but the energy required for phase change could not accumulate and no ablation took place. For powers greater than 1W, the rate of energy deposition was greater than thermal diffusion, energy was allowed to accumulate, and ablation began. The ablation yield increased from zero to a constant value at 3.5W as a decreasing fraction of the laser power was thermally conducted away. For laser powers greater than 3.5W, the ablation yield was constant at $0.16 mm^3/J$, indicating that the fraction of energy lost to thermal conduction was small enough to be insignificant. At this point, only the energy delivered, and not the rate of delivery, is important.

The results of the experiment which varied exposure time (Figure VII.3) illustrate the existence of an energy threshold for the ablation process as well. All exposures in this experiment were made at 10W, well above the power threshold for ablation. However, for exposure times less than 10ms, enough energy could not be deposited to raise the tissue to its ablation temperature and accumulate the energy necessary to begin phase change. This energy necessary for ablation to begin could be thought of as a startup energy, and is equal to approximately (10W)x(10ms) = 0.10J per fiber. Note that since all photon dos s were delivered with more than one round, the startup energy must have been deposited each time the tissue was irradiated, and did not accumulate over multiple exposures. For exposure times greater than 10ms, more than the startup energy was deposited, and ablation began. The ablation yield increased from zero to a constant value at 17ms (0.17J) as the startup energy became a decreasing fraction of the total energy delivered. For exposure times greater than 17ms, the ablation yield was again constant at $0.16mm^3/J$, indicating that the fraction of energy lost to the startup process was small enough to be insignificant. At this point, only the energy delivered, and not the startup energy delivery, is important.

It is important to note that the threshold time for ablation using the multifiber catheter, 10ms to 17ms, is of the same order as the thresholds for ablation using the single fiber shielded device with spot diameter of 750um, 17ms for an absolute threshold and 25ms for a practical threshold, described in Section III. It is not clear how adjacent, overlapping fibers in the multifiber catheter may effect each other, but dehydration of the tissue exposed by adjacent fibers may contribute to the slight lowering of this threshold. Note that the absolute threshold predicted by the model described in Section IV, $t_0 = (h_0+H_{vap})D/f(d)I$, is of the order of 100ms, using the properties of water and D = 1/3mm. As suggested in that section, it is likely that high power laser irradiation of tissue and the onset of ablation greatly alter the penetration depth making $D << 1/3mm$. This may well account for the inaccuracy of this prediction.

The change in ablation yield with varying advancing force (see Figure VII.4) illustrates the effect of user variation in the pressure exerted when recanalizing a vessel. Increasing the advancing force produced a predictable increase in the ablation yield, which rose linearly from $0.101mm^3/J$ at 0.5 ounces force to $0.205mm^3/J$ at 3.0 ounces force. It is unlikely that this increase is due to compression of the

tissue, and not actually an increase in the volume of tissue ablated, since histological examination did not show signs of permanent tissue compression. It may be possible that the optical properties of the tissue change as the tissue is reversibly compressed, although a significant change in the optical properties would not be expected. It is more likely that the shield forces interstitial water from the tissue, and thus reduces the amount of energy that is needed to ablate a volume of tissue by reducing its effective heat of ablation. Although the variation is non-zero, it is relatively small with a factor of two increase in ablation yield for a factor of six increase in advancing force. Note that the variability in ablation yield did not change with force.

The lack of change in the ablation yield with increasing delay time (Figure VII.4) indicates that, if exposures from neighboring optical fibers in the fiber array have any effect on the ablation yield, either increasing or decreasing it, the effect is not time dependent on a time scale of 170ms to 4.2s. The characteristic time for thermal relaxation (τ) can be estimated using the thermal diffusivity of water (k) and taking the characteristic length of the thermal gradient to be the penetration depth of laser light (D) in the relation $\tau = D^2/k$. For blue-green argon ion laser light on fibrous

plaque, the penetration depth is approximately 1/3mm [2,3]. This gives a thermal relaxation time of $\tau = (1/3mm)^2/(0.1mm^2/s) = 1.1s$. Since delay times bracketed this relaxation time well, it is not likely that exposures from neighboring optical fibers effect the ablation yield in any way in which the accumulation of heat which can be conducted away by thermal diffusion (such as temperature elevation) plays a role.

Likewise, the thickness of the layer of vacuolation was constant at approximately 150um for all delay times (Figure VII.5), indicating that vacuolation formation may not be governed by thermal processes effected by thermal diffusion. Instead, vacuolation may be a direct consequence of ablation itself.

However, the change in the thickness of the layer of collagen alteration with varying delay time (Figure VII.5) indicates that thermal diffusion may play a role in this type of peripheral damage. For delay times less than 1s, not enough time elapsed between the exposures of neighboring fibers to allow the tissue to cool through thermal diffusion. The thickness of the layer of collagen alteration was approximately constant at 1050um. For delay times greater than 1s, the tissue cooled between exposures and the thickness of this

layer decreased to nearly zero at 4.2s. The elimination of collagen alteration for long delay times indicates that this layer corresponds to a thermally heated zone that may be reduced or eliminated by delays longer than the thermal relaxation time.

Note that this total amount of peripheral damage, even at the shortest delay times, is much less than has been reported earlier by other investigators [4,5]. This is probably due to the careful control of photon dose, using higher laser intensities for very short exposure times.

The lack of change in ablation yield after multiple exposures without cleaning (Figure VII.6) illustrates that the ablation efficiency of a single device is not effected significantly by use, or by char or debris on the shield surface. Extended use of a single device produces some pitting of the outer surface of the shield. However, even when severe pitting had been caused by several hundred exposures, device efficiency was not effected. Extended use of a single device is possible without the need to clean the shield.

As described in Section IV, the efficiency of the ablation process (η) is expected to be equal to:

$$\eta = f(d)\ (1 - \frac{I_0}{I})\ (1 - \frac{t_0}{t})$$

For high intensities (high powers at a fixed spot diameter), and at long exposure times, the efficiency should be approximately constant:

$$\eta = f(d) = \frac{d}{d + 4D} = \frac{850}{850 + (4)(1/3)} = 0.39$$

The expected ablation yield for water would be $1/(2.50J/mm^3)$, or $0.40mm^3/J$. The ablation yield for water multiplied by the expected efficiency, $(0.39)(0.40) = 0.16mm^3/J$, agrees remarkably well with the values measured in this set of experiments.

An ablation yield can be computed for the single fiber device with a spot diameter of 750um, described in Section III. In this case, $Y = Av/P = 0.11mm^3/J$. Note that this yield is lower than that measured for the multifiber catheter. Again, it is unclear what effect exposures for adjacent, overlapping fibers may have, but the effect appears to be to both lower the threshold time and increase the ablation yield, or the efficiency of the ablation process. Alteration of the tissue properties such as dehydration or char formation to decrease D is the probable explanation for this increased yield, although it is also possible that some of the energy deposited in the T_{vap} region surrounding the bottom of a

crater is "recovered" by the adjacent fibers through tissue dehydration or preheating.

It should be noted that, because all of the experiments used a catheter with a constant light spot diameter of 800-900um, they could only show the effects of power and energy thresholds. The important parameters are more likely to be intensity (power per unit area) and fluence (energy per unit area). In these terms, the intensity threshold would be $(1W)/ (0.085cm/2)^2/4 = 180W/cm^2$, and the fluence threshold would be $(0.10J)/ (0.085/2)^2/4 = 18J/cm^2$. The characteristic time for thermal relaxation, however, is not dependent upon the catheter, but the tissue properties and laser wavelength. Therefore, delay time results may be applicable to other catheter configurations using the argon ion laser.

REFERENCES

1. D.J. Dries, P.F. Lawrence, J. Syverud, F. Moatemed, and J. Dixon, "Responses of Atherosclerotic Aorta to Argon Laser", Las. Surg. Med., 5:321 (1985).

2. M.J.C. van Gemert, G.A.C.M. Schets, E.G. Stassen, and J.J. Bonnier, "Modeling of (Coronary) Laser-Angioplasty", Las. Surg. Med., 5:219 (1985).

3. M.J.C. van Gemert, R. Verdaasdonk, E.G. Stassen, G.A.C.M. Schets, G.H.M. Gijsbers, and F.F. Bonnier, "Optical Properties of Human Blood Vessel Wall and Plaque", Las. Surg. Med., 5:235 (1985).

4. W.S. Grundfest, F. Litvack, J.S. Forrester, T. Goldenbert, H.J.C Swan, L. Morgenstern, M. Fishbein, I.S. McDermid, D.M. Rider, T.J. Pacala, and J.B. Loudenslager, "Laser Ablation of Human Atherosclerotic Plaque Without Adjacent Tissue Injury", J. Am. Coll. Cardiol., 5:929 (1985).

5. G. Lee, R. Ikeda, I. Herman, R.M. Dwyer, M. Bass, H. Hussein, J. Kozina, and D.T. Mason, "The Qualitative Effects of Laser Irradiation on Human Atherosclerotic Disease", Am. Heart J., 150:885 (1983).

SECTION VIII

LASER ANGIOSURGERY IN AN ANIMAL MODEL

VIII.1 OVERVIEW

The behavior of the multifiber laser angiosurgery system has been well characterized in vitro using human artery samples obtained at autopsy. As a collaborative effort in conjuction with the Cleveland Clinic Foundation, experiments are currently underway to characterize the behavior of the multifiber laser catheter and the ablation system in an animal model in vivo. Although those studies are far from completion, it is illustrative to briefly describe the results of one such experiment here to demonstrate the success of the system.

The following section describes a typical animal experiment in which a surgically induced obstructive lesion in a dog's carotid artery was ablated using the multifiber laser catheter and ablation system described in Section V. The animal was followed for up to two months angiographically

without complication. This experiment demonstrates that the controlled light delivery concepts of the optical shield, the design and careful characterization of the multifiber catheter, and the integrated ablation system can be used to successfully treat obstructive lesions in vivo.

VIII.2 THE ANIMAL MODEL

A number of animal models have been described for use as a testing ground for laser ablation of atheroma [1-5], including the combined use of a hypercholesterolemic diet and deendothelialization in rabbits and swine, arterial ligation models in dogs, and human xenografts in the arterial circulation of dogs. Unfortunately, it may always remain difficult to find a good model, since humans are nearly unique in their development of this atherosclerosis. Spontaneous regression of the lesions that are produced, and the unknown rate of reformation of lesions after laser treatment may always cloud results. However, success of the ablation system, and healing of the laser treated site (i.e., reendothelialization, thrombus formation, etc.) can be investigated.

In a study ongoing at the Cleveland Clinic Foundation, fibrous arterial lesions have been induced in the common carotid artery of a dog by exposing the artery surgically and

placing crossed cat-gut sutures through the intima and media, into the vessels lumen, to form an "X" shape (see Figure VIII.1). In most cases, a total of two or four pairs of crossed sutures are placed in several locations along the artery. The wound is closed and allowed to heal. Over the next six weeks, the animal generally develops a proliferative/fibrous reaction to the induced injury somewhat similar to early atherosclerotic plaques.

In the case of the animal presented in this example, the severity of the lesion produced by this procedure was evaluated by angiography at six weeks to be approximately 80% (less than 1mm diameter lumen in a vessel with a previous diameter of about 4mm), and is shown in Figure VIII.2. Note that a second, less severe lesion appears approximately 1cm distal to the 80% stenosis where a second set of crossed sutures were placed in the vessel.

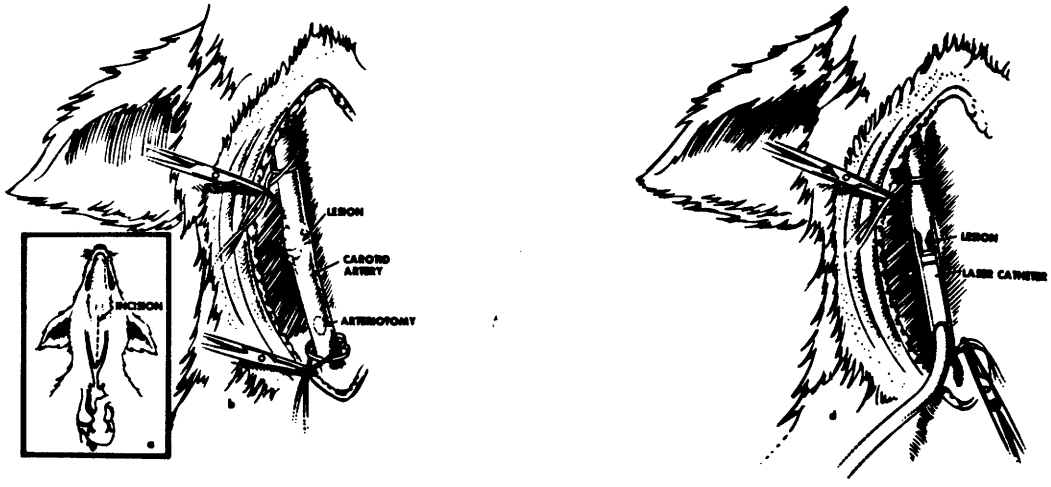

Figure VIII.1

Diagram of the induction of fibrous lesions in the dog model used in these experiments, and of the intraoperative approach that was used to treat it.

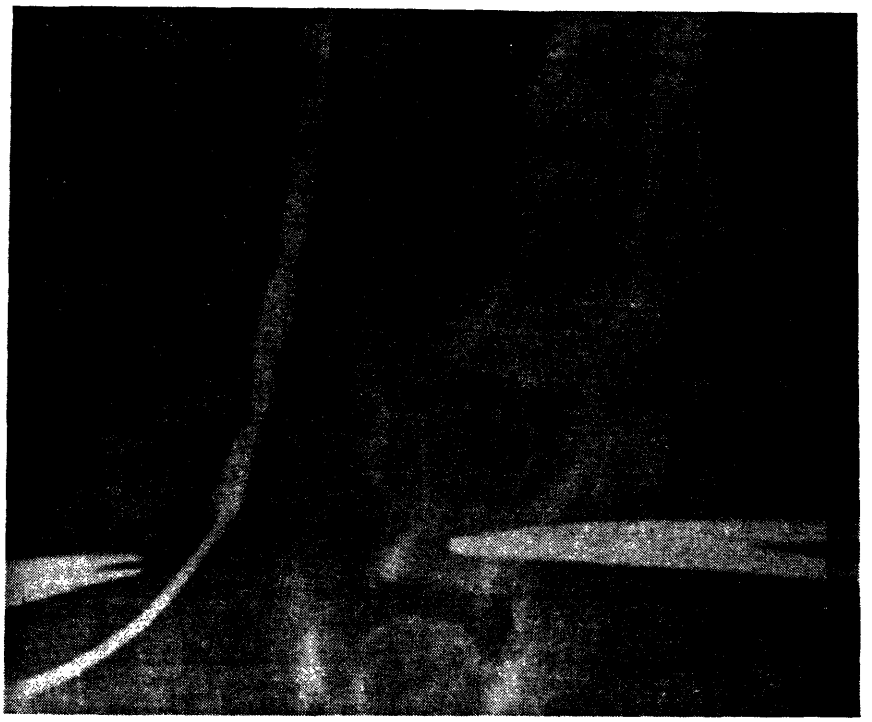

Figure VIII.2

Angiogram showing the extent of obstruction in the right carotid of a dog. Note two lesions, a proximal obstruction of approximately 80%, and a more distal obstruction of much less severity. A metal marker indicates the lesion to be removed. The apparent "obstruction" several centimeters distal to the lesions is due to a surgical tie and will appear in certain subsequent angiograms as well.

VIII.3 EXPERIMENTAL PROCEDURE

The lesions were approached surgically by incision and blunt dissection to isolate the artery to be treated. An

arteriotomy was made approximately 5cm proximal to the first lesion, through which an 8F (2.5mm) multifiber shielded catheter was introduced. The catheter was advanced antegrade until it contacted the first lesion and met with resistance to forward pressure. The lesion could not be crossed mechanically with added advancing force.

The lesion was ablated, using 7W/50ms/2round exposures (a total of 13.3J), which were repeated until the catheter could be advanced past the site of the lesion. The second lesion was not severe enough to impair catheter advancement and was not treated. After treatment, the arteriotomy was closed and the progress of the dog followed by angiography until sacrifice.

VIII.4 RESULTS

A total of five exposures (66.5J) were required to relieve the lesion and create a new lumen 2.5mm in diameter through which the catheter could easily pass. The post-procedure angiogram is shown is Figure VIII.3, clearly demonstrating that the degree of obstruction has been reduced from the 80% lesion shown in Figure VIII.2 to approximately 35% (a 2.5mm diameter lumen in a 4mm diameter vessel).

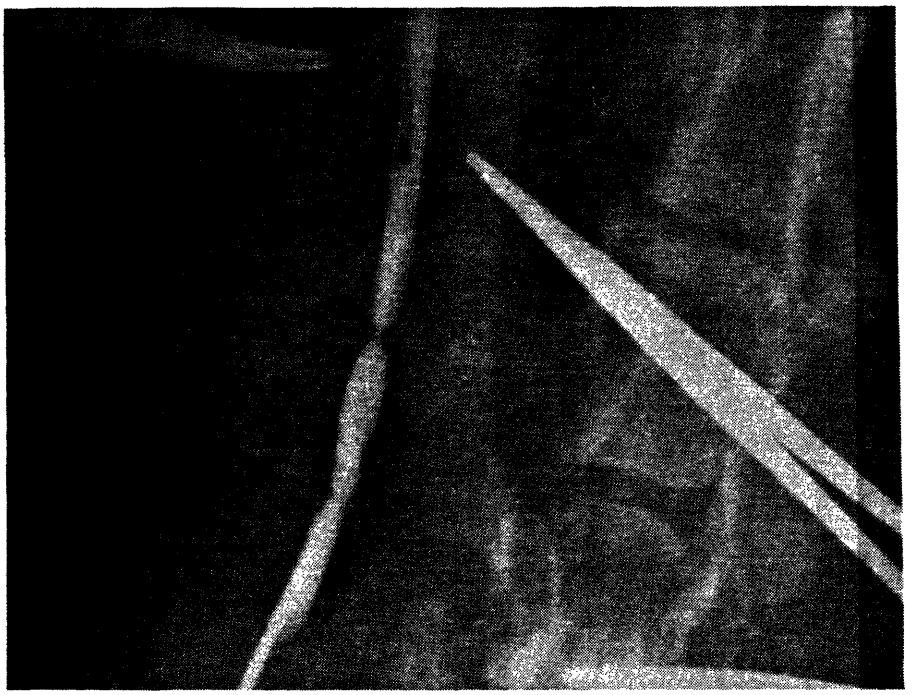

Figure VIII.3

Angiogram of the right carotid of the same dog immediately after laser treatment. The treated site is marked with a metal pointer. The apparent "high grade obstruction" distal to the treated site is due to a vascular tie.

Angiography at two days, one week, and three weeks was essentially indistinguishable from the postprocedure angiography shown in Figure VIII.3. Figure VIII.4 shows an angiogram two weeks after treatment.

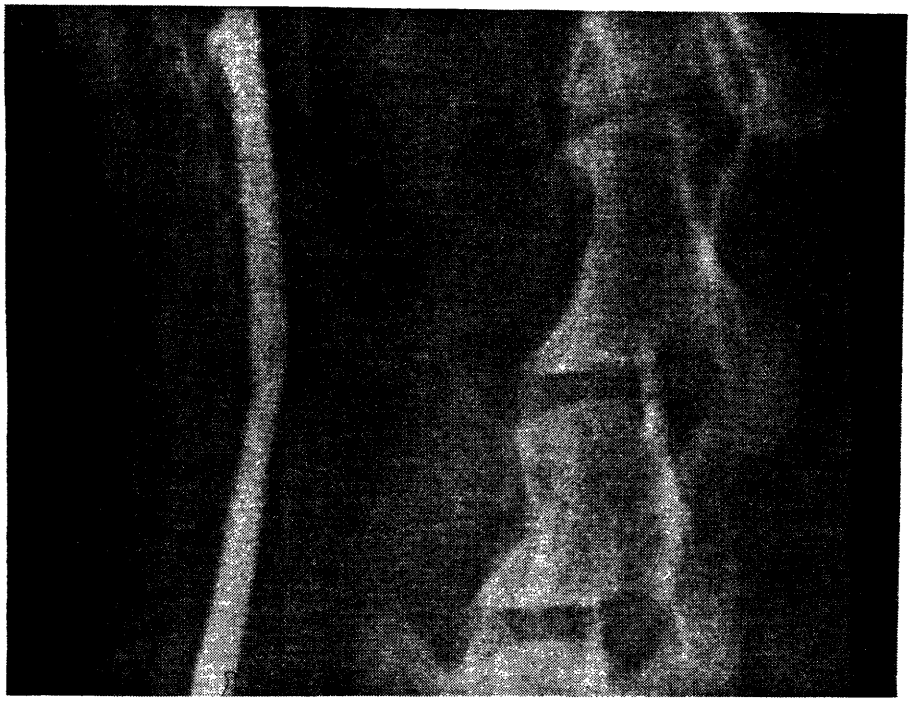

Figure VIII.3

Angiogram of the right carotid of the same dog two weeks after laser treatment.

VIII.5 DISCUSSION

This example clearly demonstrated the success of the multifiber catheter and angiosurgery system in vivo. The procedure was not complicated by acute perforation or thrombus formation. The vessel remained patent with normal healing of the intimal surface and reendothelialization.

Characterization of the multifiber catheter *in vitro* in cadaver artery samples indicated that ablation proceeded with a constant ablation yield of $0.16mm^3/J$, independent of the type of tissue ablated. Based on this result, the 66.5J delivered to treat the lesion in this animal should have removed $10.6mm^3$ of tissue, or a cylinder 2.5mm in diameter and approximately 2mm long. This agrees well with the estimated length of the treated lesion, indicating that the system performs *in vivo* as it did *in vitro*.

Animal studies are continuing at the Cleveland Clinic Foundation in an attempt to gain more information on the behavior of the catheter and ablation system, the host response to laser ablation, and advancements in catheter design necessary to proceed to percutaneous use.

Preliminary results of treatment of surgically induced focal fibrous plaques in the carotid arteries of 22 similarly prepared dogs using 8F (2.5mm diameter) shielded multifiber catheters and the 4.5F (1.5mm diameter) shielded multifiber catheters also developed in our laboratory [6] have recently been reported [7]. Laser treatment was carried out in an open surgical field via an arteriotomy proximal to the lesion in 11 dogs and via femoral artery cannulation in the other 11 using fluoroscopic guidance. Lesion removal, vessel patency, and

healing was examined by angiography, histology, and electron microscopy up to eight weeks post-treatment. The results showed that the lesion could be removed without peripheral arterial damage under the controlled delivery conditions afforded by the multifiber laser angiosurgery system. No perforations or aneurysms occurred. Thrombosis, when present, was seen only in dogs treated intra-operatively and was associated with the arteriotomy site proximal to the laser treated site. Reendothelialization was complete within three weeks and vessels remained patent up to eight weeks.

REFERENCES

1. D.S.J. Choy, S. Stertzer, H.Z. Rotterdam, N. Sharrock, I.P. Kaminow, "Transluminal Laser Catheter Angioplasty", Am. J. Cardiol., 50:1206 (1982).

2. G.S. Abela, C.R. Conti, S. Normann, R.L. Feldman, C.J. Pepine, "A New Model for Investigation of Transluminal Recanalization: Human Atherosclerotic Coronary Artery Xenografts", Am. J. Cardiol., 54:200 (1984).

3. G.S. Abela, S.J. Normann, D.M. Cohen, D. Franzini, R.L. Feldman, F. Crea, A. Fenech, C.J. Pepine, C.R. Conti, "Laser Recanalization of Occluded Atherosclerotic Arteries In Vivo and In Vitro", Circulation, 71:403 (1985).

4. H.V. Anderson, G.S. Zaatari, G.S. Roubin, P.P. Leimgruber, A.R. Gruentzig, "Steerable Fiberoptic Catheter Delivery of Laser Energy in Atherosclerotic Rabbits", Am. Heart J., 111:1065 (1986).

5. T.A. Sanborn, D.P. Faxon, C.C. Haudenschild, T.J. Ryan, "Experimental Angioplasty: Circumferential Distribution of Laser Thermal Energy with a Laser Probe", J. Am. Coll. Cardiol., 5:934 (1985).

6. B.J. Costello, "Engineering of a Multifiber Catheter for Coronary Laser Angiosurgery", Bachelor's thesis, Massachusetts Institute of Technology, 1986.

7. C. Bott-Silverman, A.L. Bylock, T. Kjellstrom, G. Engelman, J.R. Kramer, M.S. Feld, "Removal of Experimental Fibrous Plaques in Dogs Using Laser Angiosurgery: Short and Long Term Follow Up", abstract in Las. Surg. Med., 7:85 (1987).

SECTION IX

CONCLUSION

IX.1 CONCLUSIONS FROM THIS STUDY

Many researchers have demonstrated the ability to remove arterial tissue using laser energy. However, successful laser treatment of atheromatous plaque has been limited by complications including acute perforation, aneurysm formation, and thrombosis of the treated site. Many of these complications are likely to be due to incomplete control of the delivery of laser energy.

A single fiber shielded delivery scheme was shown to allow control of the tissue ablation process, through the control of laser light delivery. This scheme also has several practical features. The shield isolates and protects the fragile output tip of the optical fiber, the site of highest laser intensity, from the corrosive environment of the intravascular contents and ablation products. Char and debris cannot accumulate on the fiber tip, greatly decreasing the

probability of fiber failure. If failure should occur the shield protects the patient. Debris deposited on the output surface of the shield does not endanger the fiber itself.

The ablation process was shown to be quantifiable. Removal of arterial tissue and atheromatous plaque was both consistent and predictable. Under these conditions, an understanding of the ablation process is possible.

Requirements for the successful recanalization of an obstructed vessel were discussed and a multifiber shielded catheter and support system was developed to meet those requirements. The system was shown to be capable of removing large amounts of tissue in a controlled way, making it capable of safely producing a large diameter lumen in an obstructed vessel. Although the laser angiosurgery system developed was relatively complex, operation of the system was made simple through a high degree of computer control and safe through a control system that monitored the system's status, and the behavior of the system was very simple to understand. Ablation progressed at a constant rate which could be predicted based on the power and exposure time selected.

The results of this study provide information about the range of appropriate photon doses over which tissue can be removed using the multifiber shielded catheter described, and

the histological effects of those doses. They also provide insight into the thermal ablation process using this catheter and the argon ion laser that may be valid for other continuous lasers as well.

The constancy of the ablation yield over a wide range of exposure combinations above threshold indicates that if laser light is introduced in a controlled way, and within the exposure ranges investigated, the ablation yield can be assumed to a constant equal to $0.16mm^3/J$, even if the makeup of the target lesion is not completely known. The volume of tissue removed is dependent upon the total energy delivered, and not upon the laser power or exposure time. Only the rate of tissue removal is effected by these parameters. Since the composite hole was consistently fixed at a diameter of 2.5mm, the depth of a hole produced by a given amount of delivered energy (E) can be computed simply by the relation $l = YE/(\pi d^2/4) = (32um/J)E$.

The existence of a power threshold of 1W indicates a minimum rate of energy delivery required to overcome the losses of energy due to thermal diffusion. Ablation may only take place at powers greater than 1W, with a constant ablation yield of $0.16mm^3/J$ for powers greater than 3.5W. The existence of an energy threshold of 0.10J indicates a minimum energy that must be deposited each time a fiber is fired be-

fore ablation can occur. Likewise, a constant ablation yield of $0.16mm^3/J$ was reached for energies greater than 0.17J.

An unavoidable layer of vacuolation and hypereosinophilia approximately 150um thick is produced around each composite hole. However, a layer of collagen alteration beyond that can be reduced by increasing the amount of time between successive fiber firings. This second type of damage appears to be related to thermal heating of the surrounding tissue, decreasing if delay times greater than the characteristic time for thermal relaxation of 1.1s are used. The collagen alteration seen in the second layer did not compromise the structure of the vessel wall, and would probably be repaired by the host without effect.

A simple theoretical model of the thermal ablation process was presented as a tool to understand the ablation process and the important parameters that govern it. Through some simple approximations, equations which predict the ablation velocity and ablation efficiency were developed. These equations illustrate how changes in certain ablation conditions can effect the ablation process. For example, going to larger diameter laser spots increases the ablation velocity and efficiency. Using a laser wavelength more strongly absorbed by the tissue has the same effect. The model was

shown to predict the ablation velocity and ablation efficiency of both single fiber and multifiber devices with some accuracy. However, it was obvious from the inaccuracy of threshold time and damage layer predictions that the model must be developed further. In particular, a better understanding of the penetration depth and how it changes during high power irradiation and ablation, the form of the f(d) efficiency factor, and interaction of adjacent fibers in the multifiber device are necessary. Those efforts are in progress, being undertaken by other members of the Laser Angiosurgery Group.

Successful recanalization of an animal model was demonstrated using the multifiber shield catheter and ablation system. A full in vivo characterization of the laser angiosurgery system is underway at the Cleveland Clinic Foundation in conjunction with this lab. Preliminary findings show that the shielded catheter concept allows for the controlled ablation of obstructions in vivo with a minimization of the complications experienced by other investigators. They also illustrate that the integrated multifiber catheter ablation system is reliable and well suited to an in vivo environment.

The Federal Drug Administration has given approval for the testing of both the 8F (2.5mm) and 4.5F (1.5mm) multifiber catheters, along with the ablation system as described here,

in the coronary arteries of human subjects during internal mammary artery bypass surgery. Although this procedure will not test the usefulness of the system in a percutaneous mode, it will give extremely important information regarding the human host's response to the ablation of atherosclerotic plaques under the controlled conditions afforded by the multifiber laser angiosurgery system. An operating room has been constructed at the Cleveland Clinic Foundation specifically designed to accomodate the angiosurgery system. The complete optical and control systems described in this work have been duplicated there for animal and human trials. Human trials should be beginning soon.

One of the advantages of the multifiber design is that selective removal of tissue is possible. Spectral diagnosis of the tissue in each fiber's field of view using the fluorescence generated by exposure to low level laser light may allow the determination of which fibers should be fired prior to ablation. Incorporation of spectral diagnostics is currently being investigated as a parallel effort by members of the MIT Laser Angiosurgery Group.